

Incremental Nonlinear Dynamic Inversion Controller for a Variable Skew Quad Plane

AE5310: MSc Thesis C&S (2021/22)

Tomaso Maria Luigi De Ponti

Delft University of Technology



TU Delft

MAVLab™

Incremental Nonlinear Dynamic Inversion Controller for a Variable Skew Quad Plane

by

Tomaso Maria Luigi De Ponti

Supervisor: Ewoud Smeur
Co-Supervisor: Bart Remes
Institution: Delft University of Technology
Place: Faculty of Aerospace Engineering, Delft
Project Duration: 11, 2021 - 09, 2022

Preface

The author would like to thank Ewoud Smeur, Bart Remes and Dennis van Wijngaarden for the continuous collaboration, helpful advice and encouragement offered throughout the Research process.

*Tomaso Maria Luigi De Ponti
Delft, August 2022*

Contents

1	Scientific Article	1
2	Literature Study	21

1

Scientific Article

Incremental Nonlinear Dynamic Inversion controller for a Variable Skew Quad Plane

Tomaso Maria Luigi De Ponti
Faculty of Aerospace Engineering
Control & Simulation
TuDelft
Delft, the Netherlands
t.m.l.deponti-1@student.tudelft.nl

Abstract—This paper presents the design of an Incremental Nonlinear Dynamic Inversion (INDI) controller for the novel platform VSQP. Part of the identified challenges is the development of a model for the actuator effectiveness and lift especially as a function of skew, the newly added degree of freedom. In particular it is assumed that the actuator effectiveness changes linearly with actuator state and that aerodynamic forces change quadratically with airspeed and depend mainly on the chordwise component of airspeed. Moreover, the position of the moving actuators is expressed as a function of the corresponding moment arm and the skew angle. The models and assumptions are verified through static and dynamic wind tunnel tests at the OJF of TuDelft. A WLS routine is used to solve the control allocation for the overactuated guidance loop. A lower cost is assigned to the use of the push motor so to steer the control allocation in its favor rather than commanding changes in attitude. A gradual switch of the hover motors in transition is achieved by scheduling $\frac{\partial L}{\partial \theta}$ with airspeed. Therefore, as airspeed increases the outerloop INDI controller evaluates that changing pitch to achieve a certain vertical acceleration set point results in an increasingly cheaper command allocation than changing thrust. An automatic skew controller is designed based on the developed control moment and lift models. The skew angle is scheduled with airspeed so to perform transition while also maximizing control authority. Finally, the controller is validated by performing multiple transitions inside the OJF windtunnel.

Index Terms—incremental nonlinear dynamic inversion, weighted least squares, variable skew quad plane, control moment modelling, lift modelling, transition.

I. INTRODUCTION

Unmanned Air Vehicles (UAVs) have grown in popularity thanks to their ability to perform tasks autonomously without requiring constant intervention of an operator. In addition, the ease of operation achieved by hybrid UAVs in vertical as well as cruising phases offers a cheaper and more straightforward solution compared to user based vehicle operation. Hybrid UAVs embed in their design VTOL capabilities typical of multicopters but are also able to harness the efficiency of a wing in cruise thanks to a transitioning procedure. This transition can simply involve a change in attitude and control or can also require a mutation in the fundamental geometry of the drone.

Applications such as high-rise package delivery, off-shore missions and landings on moving platforms require good wind rejection capabilities and can for example be performed by

both a UAV or a manned helicopter, with the latter leading to obvious higher costs and deployment times. In order to save resources there is the need for a platform able to operate in gusty environments in an autonomous and efficient way using only a very limited input from an operator. The design under development is best described as a Variable Skew Quad Plane (VSQP) and to the best knowledge of the author it is a first in its category.

II. BACKGROUND ON THE PLATFORM

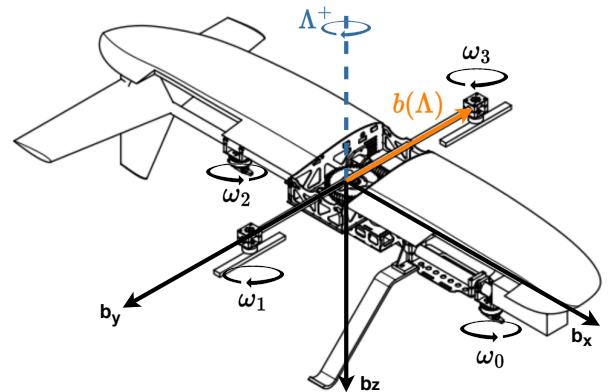


Fig. 1. VSQP

In hover mode, the drone operates as a simple quad-rotor and attitude is controlled through differential thrust. In cruise mode the drone operates as a plane and uses aerodynamic surfaces on the wing as well as tail to achieve attitude control. Similarly to a typical quad-plane, the drone achieves forward speed thanks to a push propeller placed at the tail. In contrast though, the proposed design does not have a fixed wing configuration, but rather implements the rotating concept applied in a OFW as for example the NASA AD-1 prototype plane. A central rotating pivot is used to deploy the wing as the lateral rotors are folded in the fuselage structure. This approach is expected to greatly increase cruise efficiency thanks to the combination of the wings lift generation benefits

as well as drag reduction from the retraction of the unused rotors.

In contrast to the AD-1 OFW, which in the literature is reported to be operated up to a maximum of $60^\circ - 65^\circ$ skew angle [1], the VSQP has an extended range of skew angles from 0° to 90° . Please note that in this paper skew angle is defined to be 0° in Quad mode and 90° in Forward mode with a positive clockwise displacement as shown in Figure 1. Figure 2, Figure 3, Figure 4 and Figure 5 show the geometry of the VSQP at different skew angles Λ . These are renderings from a preliminary CAD assembly of VSQP and lack the fuselage components which are under development. The wing and quad arm are deployed by a servo attached to a gear which hooks onto a centrally located static gear and pivots the top wing box assembly around the rotation point.

Figure 2 shows the VSQP in hover mode. The four motor-props are used to stabilize the drone and the wing is folded in the central body. Figure 3 and Figure 4 show the drone in the transition phase from hover to forward flight. During transition the wing is deployed similarly to a OFW.

Finally, Figure 5 shows the drone in forward flight configuration with fully deployed wing. In VSQP, due to the perpendicular placement of the side rotors with respect to the span axis, as the wing is deployed, the lateral motor-props are folded in the fuselage decreasing their drag contribution. Guidance and stabilisation of the drone is then achieved with the aerodynamic surfaces and the push propeller behind the tail assembly.

III. INDI STABILIZATION BASICS

Classical control theory makes use of PID blocks to enhance robustness and controllability of a given platform. Often, a detailed and expensive gain tuning procedure is needed to achieve the highest performance level. Furthermore, a given gain set cannot optimally serve the full flight envelope due to the platform aerodynamic response continuously changing with the different flight phases. Therefore, gain scheduling is implemented to assure near optimal performance in all flight phases. Logically, such gain set profiling can require substantial time and detailed models of the platform.

NDI was developed as a solution to robust nonlinear control with limited resources and modelling needed. More precisely, NDI aims to linearize a certain nonlinear platform by means of state or outputs feedback [2]. In other words, the aim of NDI is to generate a closed-loop system that behaves as linear system starting from a non-linear open-loop. Therefore, with some modelling knowledge of the forces and dynamics acting upon the drone it is possible to obtain a linear control law for a nonlinear system.

On the other hand, inaccuracies and simplifications introduced in the models can have a detrimental effect on the controller performance [2]. In addition, the development of accurate models of MAV can require expensive resources and is limited by the small sensors which can be carried by a MAV [3]. Therefore, a less model dependent control law is needed for implementation in MAV, leading to the development of

INDI. INDI, has been described since the late 1990s early 2000s to be a less model dependent and more robust solution than NDI [4]. The idea behind INDI is to replace the dynamic model of the platform with data retrieved online by sensor readings.

The basic common assumption in between NDI and INDI, when for example applied to angular accelerations, is that the derivative in time of the angular rates can be represented as a function of state \mathbf{x} and control input \mathbf{u} as in (1).

$$\begin{bmatrix} \dot{p} \\ \dot{q} \\ \dot{r} \end{bmatrix} = \dot{\mathbf{x}} = \mathbf{f}(\mathbf{x}, \mathbf{u}) \quad (1)$$

Equation 1 can be linearized around an initial point, subscripted with "0", by means of a first order Taylor expansion.

$$\begin{aligned} \dot{\mathbf{x}} &\simeq \mathbf{f}(\mathbf{x}_0, \mathbf{u}_0) + \left. \frac{\partial \mathbf{f}(\mathbf{x}, \mathbf{u})}{\partial \mathbf{x}} \right|_{\substack{\mathbf{x}=\mathbf{x}_0 \\ \mathbf{u}=\mathbf{u}_0}} (\mathbf{x} - \mathbf{x}_0) \\ &\quad + \left. \frac{\partial \mathbf{f}(\mathbf{x}, \mathbf{u})}{\partial \mathbf{u}} \right|_{\substack{\mathbf{x}=\mathbf{x}_0 \\ \mathbf{u}=\mathbf{u}_0}} (\mathbf{u} - \mathbf{u}_0) \quad (2) \\ \dot{\mathbf{x}} &\simeq \dot{\mathbf{x}}_0 + \underbrace{\mathbf{F}(\mathbf{x}_0, \mathbf{u}_0)}_{\Delta_x} (\mathbf{x} - \mathbf{x}_0) + \underbrace{\mathbf{G}(\mathbf{x}_0, \mathbf{u}_0)}_{\Delta_u} (\mathbf{u} - \mathbf{u}_0) \end{aligned}$$

Equation 2 can be further simplified by assuming the time-scale separation principle to be valid. This principle states that the contribution to the change in angular acceleration due to the change in angular rates and body speeds is negligible compared to the contribution of changing control inputs [5, 3]. This is because the control elements are assumed to be much more effective and having a faster response than changes in the drone's state. This assumption has been adopted in multiple works in the literature, ranging from drones with fast actuators and high enough sampling rate [3], to nonlinear flight control of helicopters [6].

$$\mathbf{F}(\mathbf{x}_0, \mathbf{u}_0) \Delta \mathbf{x} \ll \mathbf{G}(\mathbf{x}_0, \mathbf{u}_0) \Delta \mathbf{u} \quad (3)$$

Equation 3 reports in mathematical terms the Time-scale separation principle. Equation 4 instead reports the simplified version of Equation 2 using the time-scale separation method.

$$\dot{\mathbf{x}} \simeq \dot{\mathbf{x}}_0 + \mathbf{G}(\mathbf{x}_0, \mathbf{u}_0) (\mathbf{u} - \mathbf{u}_0) \quad (4)$$

Now, by realizing that $\dot{\mathbf{x}}_0$ is nothing other than the current angular acceleration, one can understand how the dynamic model of the drone can be substituted by simple sensor measurements, thus explaining the origin of the labeling of INDI as a sensor-based approach.

Rearranging and using a pseudo-inverse of the effectiveness matrix $\mathbf{G}(\mathbf{x}_0, \mathbf{u}_0)$, it is possible to derive the incremental control law of INDI for a virtual control vector $\boldsymbol{\nu}$ of desired angular accelerations.

$$\Delta \mathbf{u} \simeq (\mathbf{G}(\mathbf{x}_0, \mathbf{u}_0))^+ (\boldsymbol{\nu} - \dot{\mathbf{x}}_0) \quad (5)$$



Fig. 2. VSQP at $\Lambda = 0^\circ$.



Fig. 3. VSQP at $\Lambda = 35^\circ$.



Fig. 4. VSQP at $\Lambda = 65^\circ$.

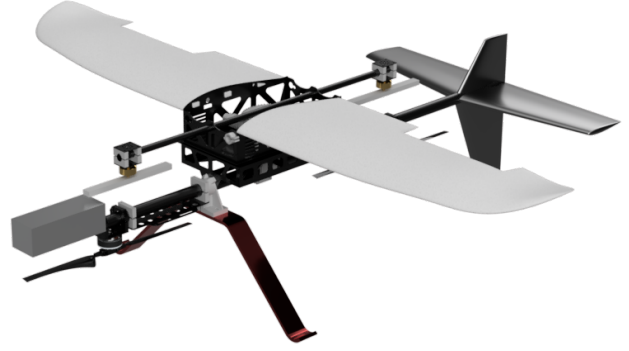


Fig. 5. VSQP at $\Lambda = 90^\circ$.

IV. WLS

Equation 5 presents an overview of how in INDI, control allocation is performed by means of pseudo inverting the effectiveness matrix. This method outputs the smallest two-norm solution which satisfies the desired change in acceleration setpoint.

The first issue that arises from this approach is the lack of knowledge of actuator saturation prior to the computation of the inverse. This occurs when using the pseudo inverse to estimate the control change to achieve the desired change in acceleration and the solution is computed based only on effectiveness and not accounting for the state and possible saturation of the actuators.

Furthermore, it can be argued that this simple approach does not deliver the most optimal solution to the control problem. This occurs when the platform has different actuators with different operational power costs. Therefore, there is a need to prioritize the use of the more power efficient actuators over the others in certain flight phases which cannot be simply encoded in the effectiveness matrix.

Moreover, in the case of saturation, there should be a prioritization of the desired control objective. This makes sure that the most vital control actions for the drone are given priority over secondary ones.

There is the need for a control allocation algorithm which embeds knowledge of prioritization of control objective and of actuator preference to achieve optimal control. Smeur and Höppener [7] propose a WLS algorithm to solve the

control allocation problem specifically for the stabilization innerloop of INDI. More precisely the method solves a least squares problem corresponding to a primary and a secondary objective function. The primary objective is to minimize the error between the desired angular acceleration change and the one produced by the calculated control increment. This is considered the primary objective because it allows the drone to be stabilized. The secondary objective is to achieve the primary objective using the least actuator energy. This objective prevents the control allocation algorithm to converge to a solution where control elements are steered in opposite directions for over-actuated systems. Logically, if there exist only one solution to the primary objective, in other words the effectiveness matrix has full rank, the secondary objective can be disregarded.

The sequential least squares problem aims then to find a solution to the control allocation algorithm which minimizes the cost function $C(u)$ reported in Equation 6.

$$\begin{aligned}
 C(u) &= \underbrace{\|W_u(u - u_d)\|^2}_{\text{Secondary Objective}} + \gamma \underbrace{\|W_v(Gu - v)\|^2}_{\text{Primary Objective}} \\
 &= \left\| \begin{pmatrix} \gamma^{\frac{1}{2}} W_v G \\ W_u \end{pmatrix} u - \begin{pmatrix} \gamma^{\frac{1}{2}} W_v v \\ W_u u_d \end{pmatrix} \right\|^2, \tag{6}
 \end{aligned}$$

W_v is the diagonal weighting matrix of the control objective and it is used to establish a hierarchy. The higher the weights, the larger the cost per control objective error, which will steer the control allocation in favor of its alleviation. W_u is the diagonal weighting matrix of the control input and it is used

to specify a preference between the actuators. The higher the weight, the larger the cost per change in control input, which will steer the control allocation to minimize the usage of the actuator. In systems with different kinds of actuators, higher weights can be assigned to the power hungry control elements to minimize energy usage. The scaling factor γ is used to increase the cost of the primary objective with respect to the secondary objective. It follows that the minimization process will be much more sensitive to errors in the primary objective and therefore it steers the control allocation to alleviate those first.

For convenience the substitutions of Equation 7 are introduced to simplify Equation 6.

$$A = \begin{bmatrix} \gamma^{\frac{1}{2}} W_v (G_1 + G_2) \\ W_u \end{bmatrix} \text{ and } b = \begin{bmatrix} \gamma^{\frac{1}{2}} W_v v \\ W_u u_d \end{bmatrix} \quad (7)$$

Which then leads to .

$$C(u) = \|A u - b\|^2 \quad (8)$$

Now, Equation 8 is the cost function to be minimized in the quadratic programming problem having as bounds the actuator saturation limits. Because INDI is incremental in nature, u_{min} and u_{max} are calculated based on the slack between previous actuator state and saturation limits.

However, it must be realized that VSQP, similarly to a conventional quadplane, is overactuated in both the stabilization innerloop as well as the guidance outerloop. For example, a linear forward acceleration can be achieved by pitching down and using the thrust vector of the lifting motors or by using the pusher motor. The latter though is often preferred because the former could introduce negative lift generated by the wing which could saturate the lifting motors. In contrast, the pusher motor cannot provide negative thrust, meaning that a positive backwards acceleration can only be provided by pitching up the platform. Similarly, during transition, as the airspeed increases, a gradual shift in control allocation from the lifting motors to the wing should occur. This is because VSQP is designed to efficiently sustain its weight in forward flight by exploiting the lift generated by the wing.

As a solution to the INDI control needs of quadplanes, Karssies and de Wagter [8] propose an extension of the WLS method. The main idea is that the control variables of the outerloop are considered as force generating actuators and instead of performing a simple inversion of the outerloop matrix a complete WLS routine is performed. This allows for the prioritization of the control objective, control variables and preferred states also for the outerloop.

Karssies and de Wagter [8] argue that the control variable weighting matrix can be designed to penalize the use of pitch and roll and especially thrust commands compared to using the pusher rotor. This is achieved by assigning lower cost weights to the pusher rotor. In addition, the lower saturation limit of the pusher rotor can be set to 0 to specify the inability of the actuator to provide a positive backwards acceleration.

As for the gradual reduction in the use of lifting motors as the airspeed increases, Karssies and de Wagter [8] argue

that the pitch angle effectiveness with respect to the vertical axis can be scheduled with the square of airspeed. This means that as airspeed increases, the effectiveness of changing θ on vertical accelerations increase, resulting in a cheaper control allocation solution.

V. MODEL OF VSQP

In order to apply the control law defined in (5) and solve the WLS routines as explained in section IV, a precise definition of the effectiveness matrix and how it changes with the state is needed. According to Euler's rotational equations

$$M = I_v \dot{\Omega} + \Omega \times I_v \Omega \quad (9)$$

where: M = Total moment acting on drone
 I_v = Vehicle Inertia Tensor
 Ω = Rotational velocity of vehicle

The total moment acting on the drone can be expressed as the combination of the control moment $M_c(\omega, \delta, \Lambda, v)$, the moment vector generated by the aerodynamic effects $M_a(\Omega, v, \Lambda)$ from which the gyroscopic effect of the motors $M_r(\omega, \dot{\omega}, \Omega)$ is subtracted.

$$I_v \dot{\Omega} + \Omega \times I_v \Omega = M_c(\omega, \delta, \Lambda, v) + M_a(\Omega, v, \Lambda) - M_r(\omega, \dot{\omega}, \Omega) \quad (10)$$

Now differently from previous works [3], the moment exerted by the actuators is further dependent on airspeed and skew angle. This occurs because part of the stabilization is achieved with aerodynamic surfaces, whose effectiveness changes with dynamic pressure. Moreover, some of the actuators change position with respect to the center of gravity as the skew angle is changed. Now rearranging (9) and solving for the angular acceleration leads to:

$$\dot{\Omega} = I_v^{-1} (M_a(\Omega, \Lambda, v) - \Omega \times I_v \Omega) + I_v^{-1} (M_c(\omega, \delta, \Lambda, v) - M_r(\omega, \dot{\omega}, \Omega)) \quad (11)$$

Equation 11 assumes that I_v is constant and not dependent on skew angle. However, works in the literature on OFW aircraft highlight that motions are coupled by inertial moments and as such stabilization becomes a less straight forward task [9, 10]. More precisely, the cross products of inertia I_{xy} and I_{yx} are non-zero in contrast to symmetrical aircraft and change with skew angle [5]. It must be realized that the VSQP differently from a conventional OFW has two side-motors which are mounted perpendicularly to the wing center-line. Therefore, it should be expected that for any skew angle, the mass imbalance in the xy plane from the wing is partially balanced by the side motors. More precisely, by reducing the two half wings and the side motors to point masses at their centroid, it can be estimated that I_{xy} and I_{yx} are reduced by 84.3% compared to the wing only structure. As a consequence, it can be assumed that the changes in inertial tensor with skew and especially the terms I_{xy} and I_{yx} are negligible.

Now, by introducing the substitution

$$F(\Omega, v, \Lambda) = I_v^{-1} (M_a(\Omega, \Lambda, v) - \Omega \times I_v \Omega) \quad (12)$$

which collects all the exerted moments independent of the actuators and

$$G(\omega, \dot{\omega}, \delta, \Lambda, v, \Omega) = I_v^{-1} (M_c(\omega, \delta, \Lambda, v) - M_r(\omega, \dot{\omega}, \Omega)) \quad (13)$$

(11) can be simplified to (14).

$$\dot{\Omega} = F(\Omega, v, \Lambda) + G(\omega, \dot{\omega}, \delta, \Lambda, v, \Omega) \quad (14)$$

As reported in section III, it is now possible to apply a Taylor expansion around the initial point "0" and neglect higher order terms.

$$\begin{aligned} \dot{\Omega} &= F(\Omega_0, v_0, \Lambda_0) + G(\omega_0, \dot{\omega}_0, \delta_0, \Lambda_0, v_0, \Omega_0) \\ &+ \frac{\partial}{\partial \Omega} F(\Omega, v_0, \Lambda_0) + G(\omega_0, \dot{\omega}_0, \delta_0, \Lambda_0, v_0, \Omega) \\ &+ \frac{\partial}{\partial v} F(\Omega_0, v, \Lambda_0) + G(\omega_0, \dot{\omega}_0, \delta_0, \Lambda_0, v, \Omega_0) \\ &+ \frac{\partial}{\partial \Lambda} F(\Omega_0, v_0, \Lambda) + G(\omega_0, \dot{\omega}_0, \delta_0, \Lambda, v_0, \Omega_0) \\ &+ \frac{\partial}{\partial \omega} G(\omega, \dot{\omega}_0, \delta_0, \Lambda_0, v_0, \Omega_0) \\ &+ \frac{\partial}{\partial \dot{\omega}} G(\omega_0, \dot{\omega}, \delta_0, \Lambda_0, v_0, \Omega_0) \\ &+ \frac{\partial}{\partial \delta} G(\omega_0, \dot{\omega}_0, \delta, \Lambda_0, v_0, \Omega_0) \end{aligned} \quad (15)$$

Equation 15 predicts the angular acceleration after an infinitesimal timestep based on the changes in state of the drone and of the actuators. As already highlighted in section III, the first term is no other than the current angular acceleration $\dot{\Omega}_0$ which can be estimated with sensors. Assuming again the time scale separation principle to hold, it is possible to conclude that on a small time scale, changes in angular acceleration are mainly affected by the fast actuators. Therefore the terms partial to Ω , v and Λ are assumed to be much smaller than the terms partial to ω , $\dot{\omega}$ and δ . the partial derivative of Λ is considered small, even though technically skew is changed by an actuator, because the dynamics of this state are much slower than the rest of the actuators. Therefore, it is possible to simplify (15) to (16).

$$\begin{aligned} \dot{\Omega} &= \dot{\Omega}_0 + \frac{\partial}{\partial \omega} G(\omega, \dot{\omega}_0, \delta_0, \Lambda_0, v_0, \Omega_0) \\ &+ \frac{\partial}{\partial \dot{\omega}} G(\omega_0, \dot{\omega}, \delta_0, \Lambda_0, v_0, \Omega_0) + \frac{\partial}{\partial \delta} G(\omega_0, \dot{\omega}_0, \delta, \Lambda_0, v_0, \Omega_0) \end{aligned} \quad (16)$$

section III has explained how (16) can be rearranged to solve for ν and derive the INDI control law. It is now clear that in order to develop a stabilization law for VSQP, models of $M_c(\omega, \delta, \Lambda, v)$ and $M_r(\omega, \dot{\omega}, \Omega)$ are need.

Now, since the rotation plane of the motors is not changed by the actuation of the skew mechanism, no further derivation of $M_r(\omega, \dot{\omega}, \Omega)$ is needed than what is already reported in the literature [3]. In contrast, the novel dependency of the control moment on δ , Λ and v requires for additional insights on the dynamics of the platform. To better tackle the new required derivation let us subdivide M_c into the control

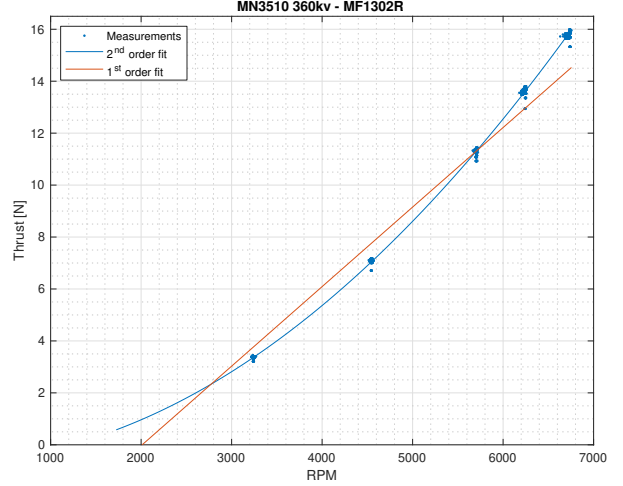


Fig. 6. Thrust force as a function of RPM

moment contribution of the motors $M_{c_{mot}}$ and the one of the aerodynamic surfaces $M_{c_{a.s}}$ so that:

$$M_c(\omega, \delta, \Lambda, v) = M_{c_{mot}}(\omega, \Lambda, v) + M_{c_{a.s}}(\delta, \Lambda, v) \quad (17)$$

A. Control Moment due to the Motors

Figure 6 shows the registered exerted thrust for the motor-prop combination used in VSQP as registered from a motor test bench. Figure 6 describes a quadratic relationship between RPM and Thrust. On the other hand, a linear approximation has the benefit of simplifying the implementation of the thrust curve in the INDI control law while resulting in a RMSE of 0.7 [N], which can be argued is small when compared to the range of registered thrust of 16 [N].

Similarly, for the reactionary torque a motor test bench was used to retrieve the relationship with RPM. A linear approximation of this relationship again simplifies the implementation in the INDI control law while having a contained RMSE of $1.100e - 2 [Nm]$.

Now that the thrust force and reactionary torque have been defined as a function of rpm, it is possible to derive an expression for the exerted moment from a given motor.

$$M_{\text{mot}i}(\omega, \Lambda) = b_i(\Lambda) \times T_i(\omega) + Q_i(\omega) \quad (18)$$

where:

- $M_{\text{mot}i}(\omega, \Lambda)$ = Moment exerted by motor i.
- $b_i(\Lambda)$ = Moment arm vector of motor i
- $T_i(\omega)$ = Thrust vector of motor i
- $Q_i(\omega)$ = Reactionary Torque of motor i

Now, in order to express more in detail $b_i(\Lambda)$, the following definitions for the vector s_{cg} connecting the center of gravity to the rotation point

$$s_{cg} = \begin{bmatrix} x_{rp} - x_{cg} \\ y_{rp} - y_{cg} \\ z_{rp} - z_{cg} \end{bmatrix} \quad (19)$$

and for the vector s_{rp} connecting the rotation point to a given motor i are introduced.

$$s_{rp} = \begin{bmatrix} x_{\text{mot}_i} - x_{rp} \\ y_{\text{mot}_i} - y_{rp} \\ z_{\text{mot}_i} - z_{rp} \end{bmatrix} = \begin{bmatrix} j_{0x} \\ j_{0y} \\ j_{0z} \end{bmatrix} b \quad (20)$$

where: \vec{x}_{cg} = Position of Centre of Gravity in space
 \vec{x}_{rp} = Position of Rotation Point in space
 \vec{x}_{mot_i} = Position of Motor i in space
 \vec{j}_0 = Unit vector of the moment arm
 b = Length of moment arm

It follows then that the moment arm vector at any skew angle in the body reference frame can be described by applying a rotation around the z axis by the additive inverse of the skew angle.

$$\begin{aligned} b(\Lambda) &= \begin{bmatrix} b_x \\ b_y \\ b_z \end{bmatrix} = R_z(-\Lambda) j_0 b + s_{cg} \\ &= \begin{bmatrix} \cos(\Lambda) & -\sin(\Lambda) & 0 \\ \sin(\Lambda) & \cos(\Lambda) & 0 \\ 0 & 0 & 1 \end{bmatrix} \begin{bmatrix} j_{0x} \\ j_{0y} \\ j_{0z} \end{bmatrix} b + \begin{bmatrix} s_{cg_x} \\ s_{cg_y} \\ s_{cg_z} \end{bmatrix} \\ &= \begin{bmatrix} \cos(\Lambda) j_{0x} - \sin(\Lambda) j_{0y} \\ \sin(\Lambda) j_{0x} + \cos(\Lambda) j_{0y} \\ j_{0z} \end{bmatrix} b + \begin{bmatrix} s_{cg_x} \\ s_{cg_y} \\ s_{cg_z} \end{bmatrix} \\ &= \begin{bmatrix} j_x \\ j_y \\ j_z \end{bmatrix} b + \begin{bmatrix} s_{cg_x} \\ s_{cg_y} \\ s_{cg_z} \end{bmatrix} \end{aligned} \quad (21)$$

As for the definition of the thrust vector in 3D, a unit vector i to define the direction of the thrust vector is introduced.

$$T(\omega) = \begin{bmatrix} i_x \\ i_y \\ i_z \end{bmatrix} T(\omega) \quad (22)$$

Now that a definition for both the moment arm and the exerted thrust in 3D space has been defined, it is possible to evaluate (18) for each of the four quad motors. It must also be realized that the longitudinal motors (m_0 and m_2) do not change position as the wing is rotated, thus their skew angle is always

$$M_{c_{as}} = \begin{bmatrix} b_{al} k_{al} v^2 \sin(\Lambda)^3 & -b_{al} k_{ar} v^2 \sin(\Lambda)^3 & 0 & 0 \\ -b_{al} k_{al} v^2 (\cos(\Lambda) - \cos(\Lambda)^3) & b_{al} k_{ar} v^2 (\cos(\Lambda) - \cos(\Lambda)^3) & -b_{el} k_{el} v^2 & 0 \\ 0 & 0 & 0 & -b_{ru} k_{ru} v^2 \end{bmatrix} \begin{bmatrix} \delta_{al} \\ \delta_{ar} \\ \delta_{el} \\ \delta_{ru} \end{bmatrix} \quad (28)$$

Figure 7 reports the evolution of the identified trigonometric relationships of Equation 28 with skew. Figure 7 highlights that as the wing is skewed, the ailerons are expected to exert more moment around the roll axis achieving peak effectiveness

0° . VSQP was designed so to have the C.G. coincident with the rotation point thus leading to negligible s_{cg} .

$$M_{c_{mot}} = \begin{bmatrix} 0 & -b_2 k_{t_2} \cos(\Lambda) & 0 & b_4 k_{t_4} \cos(\Lambda) \\ b_1 k_{t_1} & -b_2 k_{t_2} \sin(\Lambda) & -b_3 k_{t_3} & b_4 k_{t_4} \sin(\Lambda) \\ k_{q_1} & -k_{q_2} & k_{q_3} & -k_{q_4} \end{bmatrix} \vec{\omega} \quad (23)$$

where: k_{x_x} = Linear coefficient of Thrust/Torque curve

Equation 23 highlights that as the wing is deployed, the control moment exerted by the side motors shifts from the roll axis to the pitch axis. The longitudinal motors instead only act around the pitch axis.

B. Control Moment due to the Aerodynamic Surfaces

Forces and moments generated by the aerodynamic surfaces are modeled using simple lifting theory. Lift is assumed to be mainly generated by the chordwise component v_N of the airspeed vector v .

$$v_N = \sin(\Lambda)v \quad (24)$$

The Lift generated by a aerodynamic surface i is then:

$$L_i = C_{L_i}(\alpha) \frac{1}{2} \rho S \sin(\Lambda)^2 v^2 \quad (25)$$

where: L_i = Lift generated by A.S. i
 C_{L_i} = Lift coefficient of A.S. i
 ρ = Air density
 S = Surface area of A.S. i
 v = Airspeed

Now, further assuming that the angle of attack of an aerodynamic surface is equal to its deflection angle δ_{as_i} and that the lift coefficient changes linearly with such angle, it is possible to develop (25) into :

$$L_i = k_{as_i} \delta_{as_i} \frac{1}{2} \rho S \sin(\Lambda)^2 v^2 \quad (26)$$

Where k_{as_i} is a constant coefficient that can be estimated from test flight or wind tunnel experiments. It follows then that the exerted moment of a given aerodynamic surface i is:

$$M_{\text{mot}_i}(\delta, \Lambda, v) = b_i(\Lambda) \times L_i(\delta, \Lambda, v) \quad (27)$$

The moment arm $b_i(\Lambda)$ is defined as in (21). The aerodynamic surfaces on the tail do not change position as the wing is deployed. Therefore their Lift and moment arm is calculated at a constant skew of 0° . Evaluating (27) for each of the four aerodynamic surfaces leads to :

in forward mode. On the contrary, the maximum moment exerted by the ailerons around the y axis is not achieved at either skew extremes but rather at 54.7° . This is the result of the pitch moment arm shortening with skew while

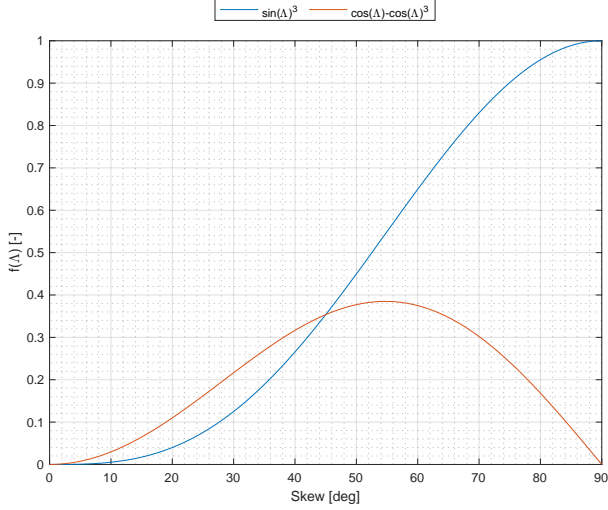


Fig. 7. Evolution of control moment model of the ailerons with skew.

the chordwise component of airspeed increases. The moment exerted by the elevator and by the rudder instead changes only with airspeed and is not expected to be affected by skew.

VI. LIFT MODEL

A precise Lift model has the benefit of providing insight into how guidance and transition should be performed by VSQP. In the guidance outerloop an estimation of $\frac{\partial L}{\partial \theta}$ is used to determine which change in pitch angle is needed to meet a certain linear acceleration reference. A precise Lift model also provides important envelop limits as stall and lift-off conditions. These insights can then be used to schedule the pitch, airspeed and skew profile to safely perform the transition.

Now, the first assumption in the drafting of the lift model is level flight. This allows to approximate the angle of attack with the pitch angle. This assumption simplifies the drafting of the lift model because pitch can be easily measured by the IMU onboard of the drone while a special alpha vane would have to be added to the platform to precisely measure the angle of attack.

Similarly to the aerodynamic surfaces, it can be assumed that most of the lift is generated by the chordwise component of airspeed, leading to an initial lift model similar to (25). However, at the current development stage of VSQP, no fuselage to encompass the wings has been designed yet. Therefore, the wings also have a non negligible cross-section profile which is swept by the airflow also at zero skew. Consequently, it is expected that the wings are able to generate a contained amount of Lift also in Quad mode. Therefore, the relationship between lift and skew can be modeled as a linear function of $\sin(\Lambda)^2$ with a constant offset k_1 .

Lift is also expected to change with angle of attack which, if level flight is assumed, can be approximated by the pitch angle. Again, if well away from stall, it is expected for the

C_L to change linearly with θ and to have an offset k_2 in the case that lift is generated also at 0° pitch angle.

With these insights in mind, it is possible to draft a lift model of VSQP as reported in (29).

$$\begin{aligned} L(\theta, \Lambda, v) &= \frac{1}{2} \rho S v^2 [m_1 \sin(\Lambda)^2 + k_1] [m_2 \theta + k_2] \\ &= \frac{1}{2} \rho S v^2 [m_1 m_2 \theta \sin(\Lambda)^2 + m_1 k_2 \sin(\Lambda)^2 + k_1 m_2 \theta + k_1 k_2] \\ &= \frac{1}{2} \rho S v^2 [\lambda_1 \theta \sin(\Lambda)^2 + \lambda_2 \sin(\Lambda)^2 + \lambda_3 \theta + \lambda_4] \end{aligned} \quad (29)$$

Equation 29 can then be differentiated with respect to θ , as in (30), in order to provide an estimation of $\frac{\partial L}{\partial \theta}(\Lambda, v)$ to be used in the guidance of VSQP.

$$\frac{\partial L}{\partial \theta}(\Lambda, v) = \frac{1}{2} \rho S v^2 [\lambda_1 \sin(\Lambda)^2 + \lambda_3] \quad (30)$$

The coefficients $[\lambda_1, \lambda_2, \lambda_3, \lambda_4]$ of (29) can be estimated by performing a least squares estimation on flight or wind tunnel data having as variables $[\theta \sin(\Lambda)^2, \sin(\Lambda)^2, \theta, 1]$.

VII. VERIFICATION

In order to verify the developed models of $M_c(\omega, \delta, \Lambda, v)$ and $L(\theta, \Lambda, v)$, and estimate the unknown coefficients, static and dynamic tests of VSQP were designed and performed at the Open Jet Facility (OJF) at the aerodynamics department of Faculty of Aerospace Engineering of TuDelft. This facility is best described as a large room with a width of 13[m] and a height of 8[m] in which a large fan driven by a 500[KW] electric engine is able to generate linear controlled flow up to 35[m/s]. The large open test section allows for the assumption of negligible wall interaction effects and a large 350[KW] radiator system is used to compensate for the added heat in the airflow and maintain air density constant.

The OJF External Balance B8604 is used to provide force and moment readings. This is an external 6-component balance manufactured by NLR for TuDelft. The balance is further mounted on a turn table which can rotate the full assembly by 360° .

The readings of the moment balance have been biased before each experiment to remove eventual undesired offsets. Moreover, a test run using only the pole structure and attachments was used to understand their contribution to the balance readings and so remove them from the dataset.

All static tests were automatized in order to increase efficiency and replicability of the experiments. An automatic test procedure was designed to command VSQP specific skew, aerodynamic surface deflection, motor command and pitch combinations in different wind tunnel airspeed settings.

Finally, through translation and rotation transformations of the axes system, the balance readings have been shifted to the C.G. of the drone for better interpretation of the results.

A. Motors

Equation 23 presents a model for the exerted control moment of the motors at different skew. The model predicts that as the wing is deployed, the side motors will shift their

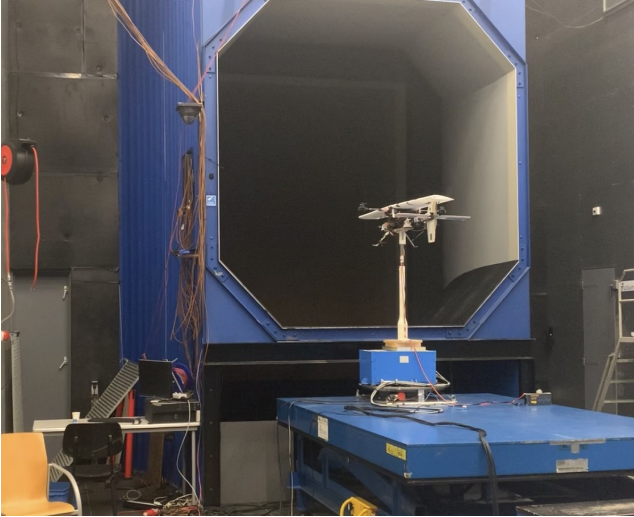


Fig. 8. Static test OJF Setup

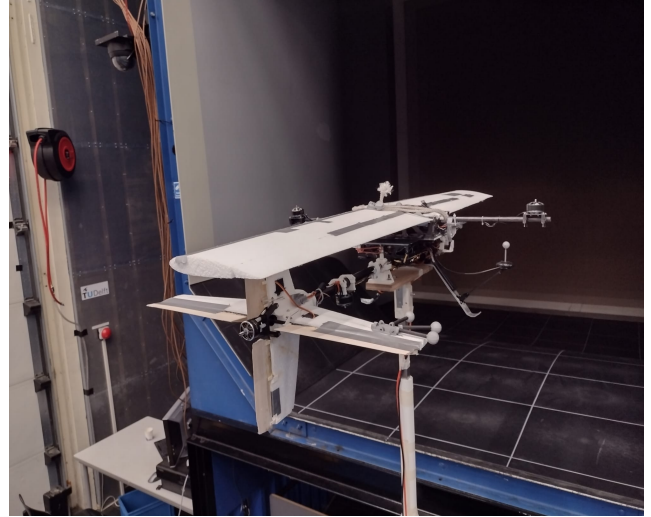


Fig. 9. Pole drone attachment

control action from the roll to the pitch axis. The longitudinal motors instead are expected to only generate pitch control because they are static. In order to validate the developed model, a combination of dynamic and static tests have been developed. Dynamic tests were used to verify the control moment model of the motors due to limited wind tunnel time. It was deemed more resource effective to dedicate most of the limited wind tunnel hours to the study of the aerodynamic surfaces instead, which require precise airspeed measurements for characterization. In the dynamic tests, while VSQP was airborne, a series of doublet signals have been sent to the four hovering motors. During the activation time of the doublet signal, all other actuators received a constant command. This procedure was repeated for all four quad motors and at different skew angles. The angular rates, as recorded by the IMU, are differentiated to obtain an acceleration signal which is then compared to the command received by the actuators. A linear least squares is then used to estimate the effectiveness values of the motors as reported in (5).

Figure 10 and Figure 11 report the estimated roll and pitch effectiveness values of the quad motors at different skew angles up to 60° . It was not possible to obtain data points at higher skew angles as VSQP loses roll control and the safety rope system in place to prevent the drone from crashing interferes with the acceleration readings. Figure 10 highlights that the roll effectiveness of the longitudinal motors (motor 0 and 2) is constant with skew and close to zero. Figure 11 also shows that the pitch effectiveness of the longitudinal motors is constant with skew but non-zero as predicted by (23).

Figure 10 also shows that the side motors lose roll effectiveness as skew is increased. Figure 11 instead shows that the pitch effectiveness of the side motors increases with skew. These conclusions are inline with the predictions from (23). A data fit curve using the trigonometric relationships of the developed model results in a small RMSE of 1.388 and 0.283

$[\frac{rad}{s^2 pprz}]^1$ for roll and pitch effectiveness of the side motors. The contained RMSE suggest that the developed model of (23) can be used to closely describe the control capabilities of the quad motors.

A further static test with a motor test-bench was set up to understand the relationship between thrust and airspeed. In (22) it was indeed assumed that the thrust is simply dependent of ω but a series of works in the literature have highlighted increased thrust capabilities of propellers in crossflow [12, 13, 14]. Figure 12 shows the relationship between thrust and rpm at different crossflow airspeed. It can be understood that for any given ω , the higher the airspeed the higher the thrust. Now, as will be later presented in subsection VII-C, the wing is expected to be able to fully support the weight of the drone from $12[m/s]$ at maximum pitch and skew. This figure is an indication of the expected terminal airspeed of transition. Therefore, after this airspeed the quad motors are expected to be turned off. With such a transition flight envelope in mind and the insights from Figure 12, it can be understood that there is a maximum expected increase in thrust of about $1[N]$ due to crossflow. Furthermore, such increase in thrust is dependent on airspeed which changes at a much slower rate when compared to the controller's update frequency ($500[Hz]$). Therefore, due to the incremental nature of INDI's control law, it is expected that the controller will compensate for such modelling inaccuracy. This conclusion is further supported by the results described in section IX, in which the automatic transition is achieved without any scheduling of thrust with airspeed.

B. Aerodynamic Surfaces

Equation 28 presents a model of the control moment exerted by the aerodynamic surfaces. In the drafting of this model a

¹*pprz* is the basic command unit of Paparazzi UAV [11], the used autopilot firmware on the VSQP.

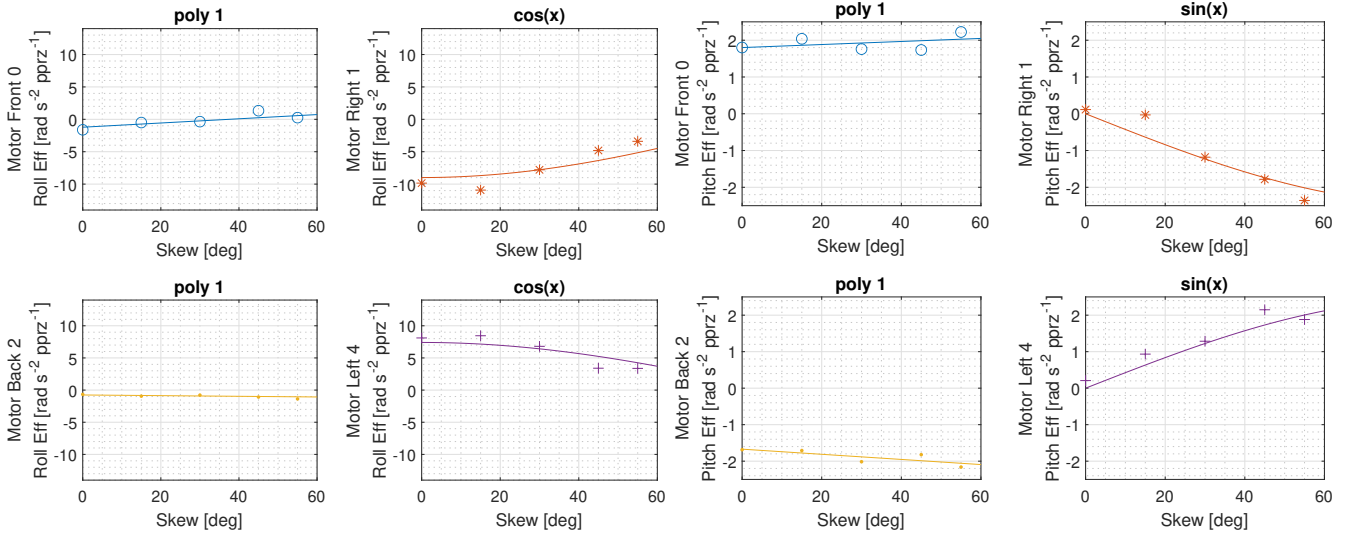


Fig. 10. Evolution of roll effectiveness of quad motors with skew.

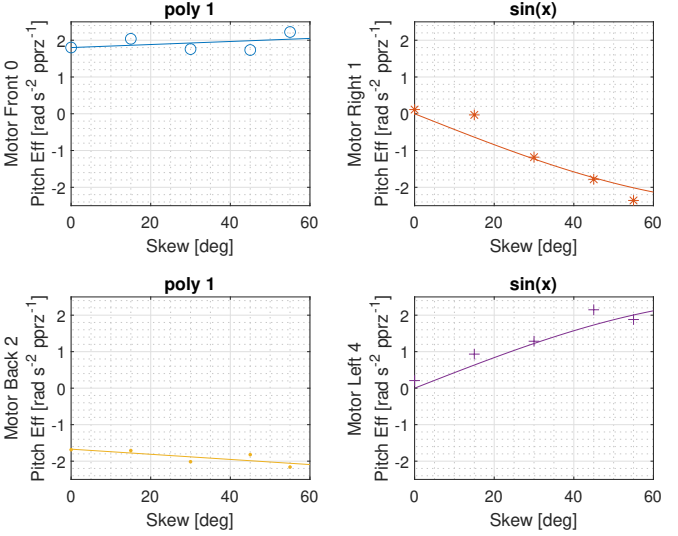


Fig. 11. Evolution of pitch effectiveness of quad motors with skew.

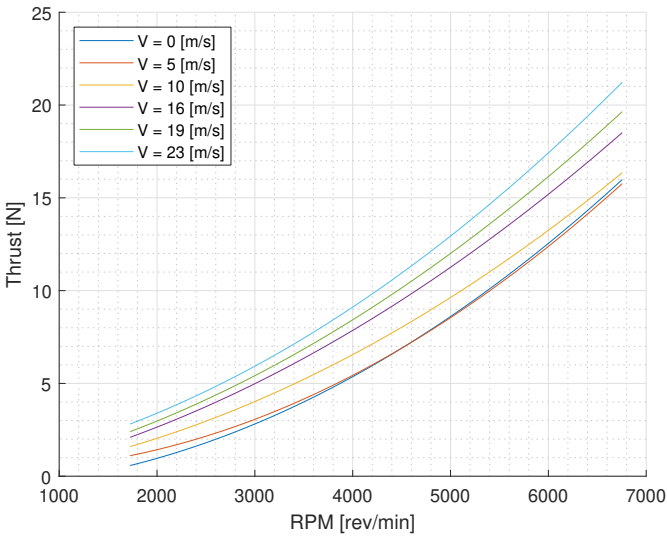


Fig. 12. Thrust level at different wind speeds.

series of assumptions were adopted. First, for all aerodynamic surfaces it was assumed that their exerted moment changes linearly with the commanded deflection angle. Second, the exerted moment is assumed to change with dynamic pressure or in other words with the square of airspeed. Finally, by combining insights on the geometry of the moment arm and

assuming that most of the lift is generated by the chordwise component of airspeed a relationship between exerted moment and skew was developed. Because the tail is not changing position with skew, it was assumed that there is no expected change in exerted moment from the elevator and rudder as the wing is deployed. On the other hand for the ailerons, a trigonometry relationship between skew and exerted moment was identified.

Data from the static test at 0° pitch is used to verify that the assumptions are valid and that the developed model is a truthful representation of the capabilities of the actuators. Figure 18, Figure 19, Figure 24 and Figure 25 show the relationship between the pwm command sent to the ailerons and the registered change in roll and pitch moment with respect to neutral command at different wind speed settings. In order to facilitate interpretation of the results, the data being showed refers to the skew angle of 60° but all conclusions hold also for other states. The specific skew of 60° was chosen because this is the state in which the ailerons are predicted to be effective in both roll and pitch. The plots use pwm as indication of the state of the aerodynamic surfaces as these are deflected by electric servos. The plots identify a linear relationship between the registered moments and the pwm command sent to the ailerons. A similar conclusion can be drawn for the tail aerodynamic surfaces from Figure 30 and Figure 31. The plots highlight again a linear relationship between commanded pwm to the elevator and rudder and change in pitch and yaw moment. These insights verify the

first adopted assumption of linearity between state of the aerodynamic surfaces and respective exerted moments.

Figure 20, Figure 21, Figure 26 and Figure 27 show the relationship between skew angle and registered change in roll and pitch moment at different actuator states for the ailerons. Again, in order to facilitate interpretation of the results only data relative to the wind speed of $9[m/s]$ is shown but the same conclusion holds also for other settings. This specific airspeed is chosen because the drone is expected to be in transition at this stage, thus being in the process of deploying the wing. Figure 20 and Figure 21 show that for all actuator states, the magnitude of exerted roll moment from the ailerons increases with skew angle. More precisely, as expected from (28) a function $k \sin(\Lambda)^3$ results in a fit curve with a contained average RMSE across the dataset of $0.028232[Nm]$ and $0.044506[Nm]$ for the left and right aileron respectively. The small approximation errors are an indication that the developed trigonometric relationship between skew and exerted roll moment models correctly the roll capabilities of the ailerons.

Figure 26 and Figure 27 show that for all actuator states, the magnitude of the pitch moment exerted by the ailerons tends to zero at the two skew extremes of 0° and 90° . Peak pitch moment exerted by the ailerons is instead reached at a skew angle in between 50° and 60° . As predicted by (28) a function $k (\cos(\Lambda) - \cos(\Lambda)^3)$ results in a fit of the data points with a contained average RMSE across the dataset of $0.016485[Nm]$ and $0.032279[Nm]$ for the left and right aileron respectively. This is an indication that the identified trigonometric relationship between skew and exerted pitch moment well models also the pitch capabilities of the ailerons.

As for the tail surfaces, in (28) it was predicted that skew does not affect the control capabilities of the elevator and rudder. Figure 32 and Figure 33 indeed show that for any given actuator state the exerted moment is constant and can be approximated by a linear function.

Figure 22, Figure 23, Figure 28, Figure 29, Figure 34 and Figure 35 show the relationship between wind speed and exerted moment change at different actuator states for all aerodynamic surfaces. In order to facilitate interpretation of the results, the data being showed refers to the skew angle of 60° but all conclusions hold also for other states. The plots highlight that for all actuators the exerted moment changes with the square of airspeed. A function $k v^2$ results in a fit curve with contained RMSE of $0.043762[Nm]$, $0.041204[Nm]$, $0.15119[Nm]$ and $0.01605[Nm]$ for aileron left, aileron right, elevator and rudder respectively.

In conclusion, the static tests verify the proposed model of (28) in each of its adopted assumptions. Therefore, the proposed model is concluded to be a truthful representation of the control capabilities of the aerodynamic surfaces and can be used in the design of a INDI controller for VSQP.

C. Lift Model

Equation 29 presented a modelling structure for the lift generated by the wing at different θ , Λ and airspeed. Level

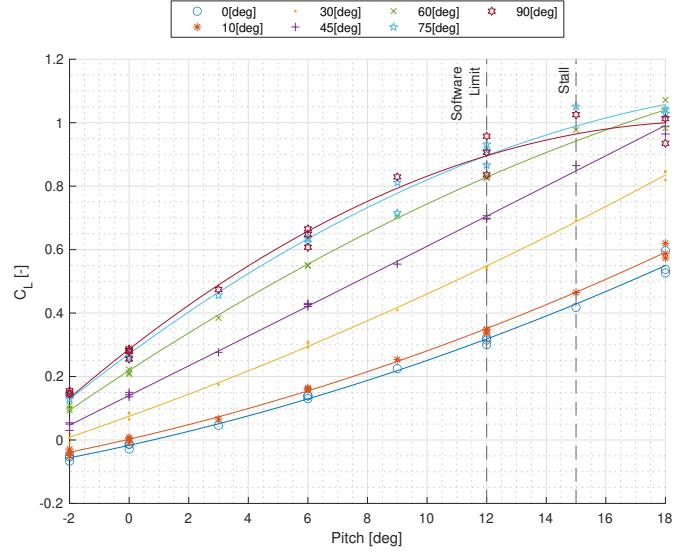


Fig. 13. C_L curve at different airspeed

flight is assumed so to approximate α with θ . The model was derived by simple lift theory and assumed that most of the lift is generated by the chordwise component of airspeed. Furthermore, it was assumed that away from the stall region, lift changes linearly with pitch angle.

A static test with variable pitch provided by the turn table is used to verify the lift model. Figure 13 shows the evolution of the lift coefficient with pitch angle at different skew settings. The lift coefficient was computed according to (31).

$$C_L = \frac{L(\theta, \Lambda, v)}{\frac{1}{2}\rho S v^2} \quad (31)$$

Figure 13 shows that at 90° skew, C_L starts to drop past 12° pitch indicating the beginning of stall. Similar conclusions are achieved through a simulation in XFLR5 for the airfoil MH32 of the wing. A 20% lower softer limit (12°) than the identified stall point is used to assure that VSQP does not enter suddenly in stall. Figure 13 shows that under the software limit C_L changes linearly with pitch for all skew angles. Therefore, the assumption of linearity between Lift and pitch is verified.

Furthermore, Figure 13 shows that the difference between C_L at all pitch angles tends to zero at the skew extremes of 0° and 90° and is largest around 45° . This trend matches the characteristics of the trigonometric function $\sin(\Lambda)^2$ whose derivative is maximized at 45° and then rapidly tends to zero close to 0° and 90° . Moreover, Figure 13 also shows that at 0° skew the wing generates lift, justifying the need to introduce and offset in the lift-skew modelling. A least square approximation of the data points from the static test using the modelling structure of (29) leads to the coefficients of Table I.

Figure 14 shows how the estimated lift model fits the registered data points from the static test. The wind speed displayed well represents the expected flight envelope of the

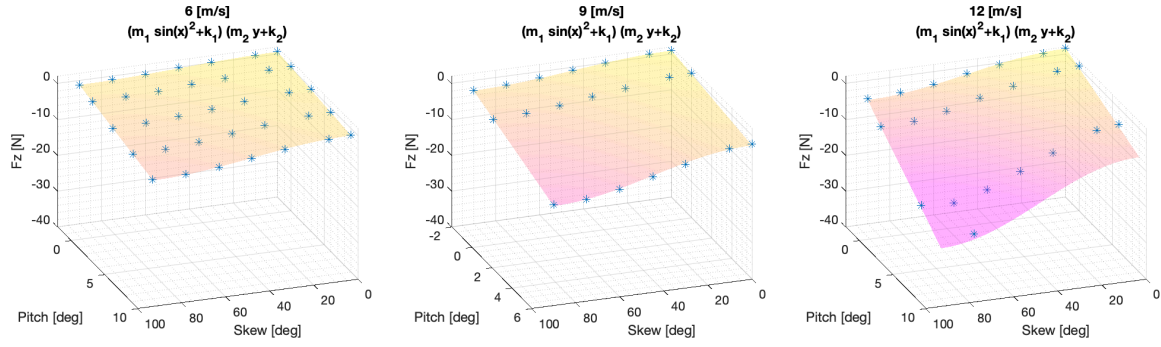


Fig. 14. Lift Model fit of data points

TABLE I
ESTIMATED COEFFICIENT OF LIFT MODEL

λ_1	λ_2	λ_3	λ_4
-1.885	-0.278	-1.504	-0.004

transition of VSQP. The RMSE across the dataset is only $0.4[N]$ indicating that the found model truthfully represents the lift capabilities of the wing at different θ , Λ and airspeed.

VIII. AUTOMATIC SKEW CONTROLLER

The last piece of the controller missing to perform transition autonomously is a skew controller. Now, section V has highlighted that the control moment exerted by the actuators is dependent on skew. Therefore, depending on the airspeed, there exist a skew angle that maximizes the control authority of the drone. Section V further concluded that the lift generated by the drone increases with skew and reached maximum in full forward mode. Section VII presented the verification of the developed models with static and dynamic tests estimating also the unknown coefficients.

These models allow to precisely estimate the Lift and exerted control moment at any given airspeed and skew angle. Therefore, an optimization problem can be defined to evaluate the skew angle that maximizes control and lift at any given airspeed.

First, a mesh of query points spanning the expected airspeed and skew operational ranges is generated. These ranges are $(0, \pi/2)[rad]$ for Λ and $(0, 18)[m/s]$ for airspeed. Secondly, for each of the three stabilization axis two linear programming problems are solved. The variables for all the linear programming problems are the actuators states. The objective function per stabilization axis is defined by the corresponding row in the total exerted control moment model of (17). In a first optimization routine, the objective cost function is minimized. In a second instance, the cost function is maximized. This is done to calculate both the minimum and maximum exerted moment. Subsequently, an average of the absolute optimum points is evaluated to express a general maximum magnitude

control moment that can be exerted at each query point around that specific axis by VSQP.

Each actuator state is constrained to not exceed its minimum and maximum saturation limits. Furthermore, it is expected that the found solutions are maneuvers that can be performed without losing control of other axis. Therefore, the found solution should result in null exerted moment around the remaining stabilization axis. This is ensured by calculating the exerted moment around the remaining axis using (17) and setting it to zero.

Finally, the solution to the optimization problem shall also not cause the drone to lose altitude as this could have catastrophic consequences. Therefore the sum of thrust level as calculated in (22) and Lift (29) are set to be higher or equal than the weight of the drone. A summary of the set up of the linear optimization problem for a sample calculation of the maximum exerted roll moment is presented in algorithm 1. Now, the results of the optimization problems carried out at

Algorithm 1: Maximum Roll Moment Optimization

Optimization variables:

$$\boldsymbol{\omega} = [\omega_0 \ \omega_1 \ \omega_2 \ \omega_3]^T$$

$$\boldsymbol{\delta} = [\delta_{al} \ \delta_{ar} \ \delta_{el} \ \delta_{ru}]^T$$

Cost function:

$$\max_{\boldsymbol{\omega}, \boldsymbol{\delta}} C(\boldsymbol{\omega}, \boldsymbol{\delta}) = M_{c_{mot}}(1, :) \boldsymbol{\omega} + M_{c_{as}}(1, :) \boldsymbol{\delta}$$

Constraints:

$$\omega_{min} \leq \boldsymbol{\omega} \leq \omega_{max}$$

$$\delta_{min} \leq \boldsymbol{\delta} \leq \delta_{max}$$

$$M_{c_{mot}}(2, :) \boldsymbol{\omega} + M_{c_{as}}(2, :) \boldsymbol{\delta} = 0$$

$$M_{c_{mot}}(3, :) \boldsymbol{\omega} + M_{c_{as}}(3, :) \boldsymbol{\delta} = 0$$

$$\sum_{i=0}^3 T_i(\omega_i) + L(\theta, \Lambda, v) \geq m g$$

each query point are three surfaces (S_ϕ, S_θ, S_ψ) indicating the

maximum roll, pitch and yaw moment that the actuators of VSQP can achieve at each skew and airspeed combination. By analyzing these surfaces it is possible to determine which skew angle maximizes the exerted control moment around a specific axis at any given airspeed.

A fourth surface is further introduced to represent the total thrust required at each skew-airspeed combination. This is equal to the amount of thrust that the quad motors have to deliver to maintain altitude and the thrust that the pusher motor has to deliver to maintain a specific airspeed. The quad thrust is approximated to be the force needed on top of the estimated lift to match the weight of the drone. The pusher thrust has been modeled as a linear function of v^2 from preliminary test flight of VSQP in the wind tunnel. The angle of attack is assumed to be small and so approximated to 0° .

$$T_{\text{tot}}(\Lambda, v) = T_{\text{quad}} + T_{\text{push}} = \max(mg - L(\theta, \Lambda, v), 0) + av^2 \quad (32)$$

Now, since the interest is what skew angle minimizes the required thrust level and consequently energy consumption, the actual surface S_T that will be used for further conclusions is the inverse of T_{tot} .

$$S_T(\Lambda, v) = \frac{1}{T_{\text{tot}}(\Lambda, v)} \quad (33)$$

By analyzing S_T it is possible to understand for each airspeed which skew angle results in minimum energy consumption. This surface is needed in addition to the control moment surfaces because it assures that the final skew plan will depict a transition from quad to forward.

In order to compare the surfaces and draw conclusions, each surface is normalized with its maximum as shown in (34).

$$S_{i_{\text{norm}}} = \frac{S_i}{\max(\|S_i\|)} \quad (34)$$

Finally, the surfaces are combined into a general surface S_{tot} through the use of weight coefficients as shown in (35)

$$S_{\text{tot}} = \begin{bmatrix} \gamma_\phi & \gamma_\theta & \gamma_\psi & \gamma_T \end{bmatrix} * \begin{bmatrix} S_\phi \\ S_\theta \\ S_\psi \\ S_T \end{bmatrix} \quad (35)$$

The higher the weight, the more the total surface will resemble the initial one. Therefore, these weights are chosen to establish a wanted hierarchy in-between the transition objectives as shown by Table II.

Now, the primary goal during transition is to change geometry from quad to fixed wing to maximize energy efficiency. As a consequence, the highest weight of 4 is assigned to S_T which is highest when thrust required is lowest. This makes sure that skew is optimized to complete transition as soon as the wing is able to generate enough lift.

Both θ and ϕ can be argued to be crucial toward successful guidance [7]. This is because these two attitude angles determine in which direction the quad thrust and lift vector point. Therefore, achieving precise θ and ϕ reference tracking is crucial towards not losing altitude and avoiding crashes.

It should be noted that there exists a significant difference between the estimated moment of inertia around roll and pitch axes. Through a comparison of the effectiveness of the motors and their thrust results from the motor test bench it is estimated that I_{xx} is 5.79% of I_{yy} . This can also be understood from the fact that most mass is placed along the longitudinal line of the drone. Therefore, maximizing pitch control should have a higher priority, as roll deviations can be corrected less expensively. It follows that that S_θ is assigned a higher weight than S_ϕ . Finally the lowest weight of 1 is then assigned to S_ψ . Evaluating (35) with the weights of Table II leads to S_{tot} as

TABLE II
CHOSEN WEIGHTS FOR (35)

γ_ϕ	γ_θ	γ_ψ	γ_T
2	3	1	4

shown in Figure 15. Now, a straightforward way to schedule Λ with airspeed would be to evaluate which skew setting maximizes S_{tot} at each considered airspeed. This approach results in the red line in Figure 15. The problem with this approach is that moving from a maximum point to the other can involve first sweeping through a dipping region of the surface or in other words a lower control authority state of the drone. The contour plot of Figure 15 particularly highlights this problem when around $8[m/s]$ the preferred skew changes from 0° to 80° . Logically, such behavior is not desired as the drone could lose control and crash. A better solution would be to command skew changes which only increase the control authority of the drone even at the cost of not reaching the maximum as fast. In other words, a modified gradient ascent algorithm can be used to determine a path which changes skew only when the partial derivative $\frac{\partial S_{\text{tot}}}{\partial \Lambda}$ is positive.

$$X_{n+1} = X_n + \alpha \nabla S_{\text{tot}}(X_n) \quad (36)$$

where: $X_n = [\Lambda, v]$ at step n
 α = Learning rate

$$\nabla S_{\text{tot}}(X_n) = \left[\frac{\partial}{\partial \Lambda} S_{\text{tot}}(X) \quad \frac{\partial}{\partial v} S_{\text{tot}}(X) \right] \Big|_{X = X_n} \quad (37)$$

Equation 36 reports the definition of a general gradient ascent method. Equation 37 further defines how the gradient is calculated. Now, in the classical gradient ascent algorithm α is chosen to be a single constant number. Such approach results in path changes which are perpendicular to the isometric lines which cross the points where the gradients are estimated, resulting in the steepest ascent of the curve. On the other hand, it can be argued that such behavior is not wanted in the specific case of the scheduling of Λ with airspeed for VSQP. The wanted airspeed is the output of the guidance module rather than the skew controller. Making the example of VSQP following a ship at sea, the target airspeed is determined by the speed of the moving target. The skew controller should then command a Λ which maximizes control at that specific target airspeed. In a nutshell, two learning rates $[\alpha_\Lambda, \alpha_v]$ can be defined, one for each of the calculated partial derivatives

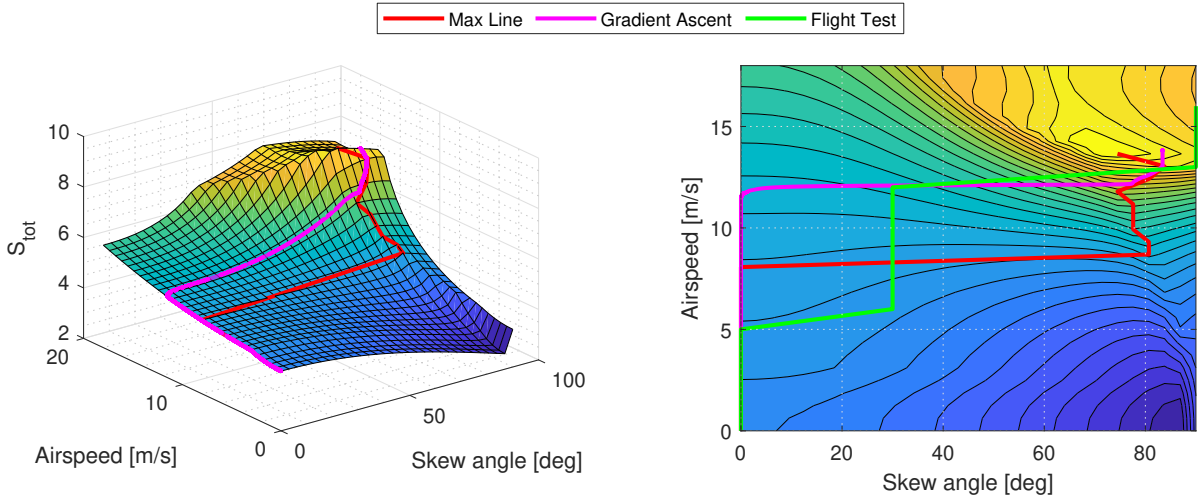


Fig. 15. Skew scheduling with airspeed

of (37). It is then possible to assure an ascent of the curve which encourages changes in Λ by choosing $\alpha_v \ll \alpha_\Lambda$.

The result of this modified gradient ascent is shown in Figure 15. The result indicates that before $12[m/s]$ changing skew angle is not beneficial towards ascending the surface. After $12[m/s]$ the preferred skew is 90° which indicates that all other settings in between are deemed to have less control authority.

This conclusion is also confirmed by multiple flight test performed at the OJF wind tunnel as explained in more detail in section IX. Figure 15 shows that the skew scheduling used in the flight tests well resembles the result of the gradient ascent method. In the flight test, the best configuration is found to be a rapid increase in skew at $12[m/s]$. Differently from the gradient ascent results though, at $5[m/s]$ the preferred skew is 30° . This is the result of an observed reduced stability of VSQP at 0° skew in the airspeed region of $5-8[m/s]$. In this state the drone experiences a heavy pitch up moment which saturates the longitudinal motors. This is thought to be the result of unmodelled aerodynamic interactions in between the wing, horizontal surface and back motor but more scientific insight is needed to further support this conclusion.

IX. VALIDATION

Validation of the developed controller has been performed at the OJF wind tunnel. The large cross sectional area of the facility allowed for the flight test of VSQP. The drone was commanded to maintain its position in space in the wind tunnel autonomously as wind speed was varied. Figure 16 shows VSQP during an autonomous transition at the OJF wind tunnel. A safety rope is used to prevent the drone from crashing in the event of loss of control. This rope is only tensioned enough to not entangle with the propellers and does not sustain the weight of the drone. Figure 17 reports some important states during a transition test available also as a

video ². First, the wind tunnel is activated and set to $18[m/s]$. As airspeed increases, the skew angle controller commands higher setpoints until full forward mode. As the airspeed increases, the effectiveness of changing pitch to control linear accelerations on the z axis increases. Therefore, the outerloop WLS routine evaluates that using pitch instead of the thrust from the quad results in a lower cost function and accordingly a cheaper solution for z control. As a consequence, with the build up of airspeed also pitch increases and the quad motors are gradually turned off. Transition occurs with a remarkable tracking of the target altitude of $3[m]$ without major deviations. The wind speed is maintained constant at $18[m/s]$ for $20[s]$ with VSQP maintaining target position in space in full forward mode as a fixed-wing aircraft. Subsequently, the wind tunnel safety stop is engaged to reduce the wind speed as fast as possible. As soon as the controller senses the slow down in airspeed, maximum pitch is commanded and the quad motors are activated again. With the progressive slow down of airspeed, skew is commanded to return to zero and VSQP completes transition level with the ground and completely reliant on Quad thrust for z control.

The transition was repeated successfully multiple times validating the controller for use in the controlled environment of the wind tunnel. However, outdoor validation is also crucial towards proving the viability of the controller in turbulent gusty environment. Moreover, the controller validated in the wind tunnel does not entirely reflect the final verified design. This has occurred because part of the insights on the dynamics of the drone could only have been developed once the data from the wind tunnel static test were processed. More precisely, the controller validated at the wind tunnel schedules

²<https://1drv.ms/v/s!ApxpUyTQ3WB1gbop5HL-8uViW8yhwx>
(Password: "VSQP").



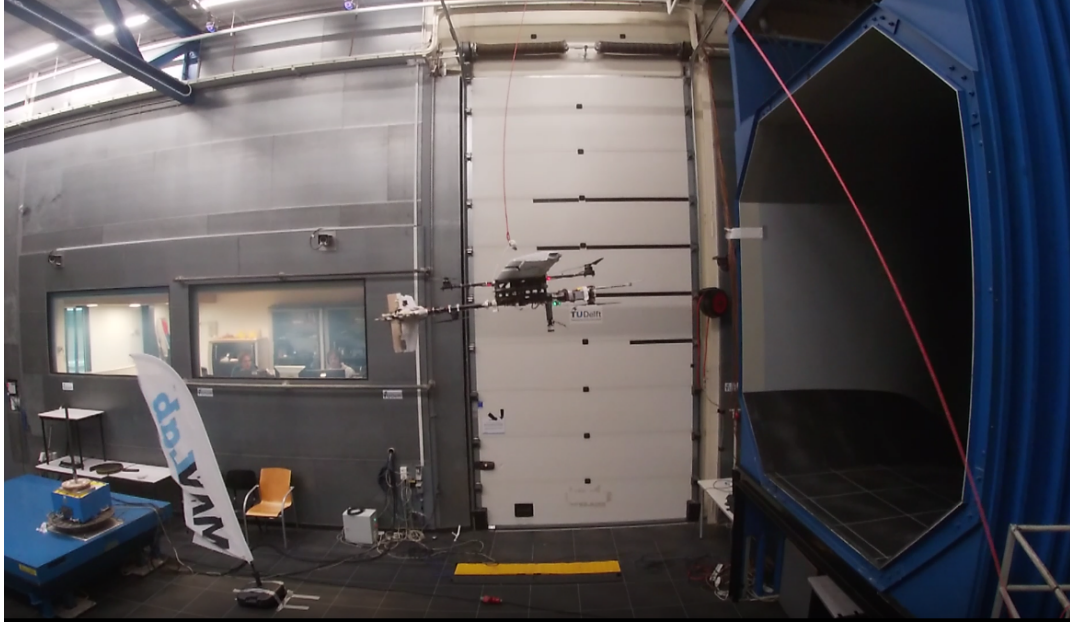


Fig. 16. OJF setup transition test

the effectiveness of the ailerons differently from (28).

$$M_{c_{ail}} = \begin{bmatrix} b_{al} k_{al} v^2 \sin(\Lambda) & -b_{al} k_{ar} v^2 \sin(\Lambda) \\ -b_{al} k_{al} v^2 \cos(\Lambda) & b_{al} k_{ar} v^2 \cos(\Lambda) \\ 0 & 0 \end{bmatrix} \begin{bmatrix} \delta_{al} \\ \delta_{ar} \end{bmatrix} \quad (38)$$

The scheduling used at the wind tunnel, shown in (38), was designed in the field as an initial attempt to express the shift of effectiveness of the ailerons from the pitch to the roll axis similarly to what was done for the side motors. Additionally, the derivative of lift with pitch $\frac{\partial L}{\partial \theta}$ used in the guidance WLS is not based on a precise model of the lift of the wing but was rather tuned in the field and scheduled with $\sin(\Lambda)$.

Outdoor validation of the controller was attempted to validate the entirety of the controller also in a non controlled environment such as the wind tunnel. The outdoor validation started with a series of manual tests which proved that the automatic skew controller works. The controller successfully deployed the wing with increasing airspeed while always allowing successful stabilization of the VSQP. These attempts concluded prematurely due to a catastrophic crash of the platform. Such crash occurred due to a series of unforeseen design flaws of this first prototype of the VSQP.

In particular, the quad motors were heavily undersized for the weight of the drone. The estimated thrust to weight ratio of the VSQP is :

$$\frac{T}{W} = \frac{16 \cdot 4}{4.2 \cdot 9.81} = 1.553 \quad (39)$$

This thrust to weight ratio is calculated using the maximum thrust with full batteries from the motor test bench data. This value is already undesirable as it is lower than the standard of 2 [15, 16] which is generally accepted to be the minimum

limit for acceptable agility. This means that the motors are running at 64.4% in nominal hover instead of having the full 50% of their thrust output available for control corrections.

Furthermore, using the constant velocity (Kv) rating of the motor of 360 and assuming that thrust changes with the square of rotational speed, it is possible to estimate how much reduction in quad thrust is expected at low battery level. Now, the battery pack uses 6 LiPo cells which have nominal voltage of 4.2[V] and empty voltage of 3.5[V]³. Therefore, at low battery level it is expected that the maximum thrust output of one motor is reduced from 16.0[N] to 11.1[N], which in turn reduces $\frac{T}{W}$ to 1.078, leaving next to no thrust slack for control corrections.

The under sizing of the motors manifested in the outdoor test in the form of heavy saturation of all quad motors in the attempt to maintain altitude and correct for gusts and other aerodynamic effects.

While it was not possible to complete the outdoor validation plan, it must be realized that ultimately this was a hardware problem linked to underactuation of the system. It can be further argued that the validation at the wind tunnel also proves the entirety of the controller to be correct. The identified differences between the initial and final controller can be regarded as slight modelling inaccuracies for which INDI has been proved to efficiently correct[8].

X. CONCLUSION

This paper has presented the derivation, verification and validation of an INDI controller which is able to guide and

³A voltage of 3.3[V] can also be achieved by the LiPo cells before a sharp drop off in voltage but a lower safety limit of 3.5[V] was adopted in the flight tests to preserve the batteries.

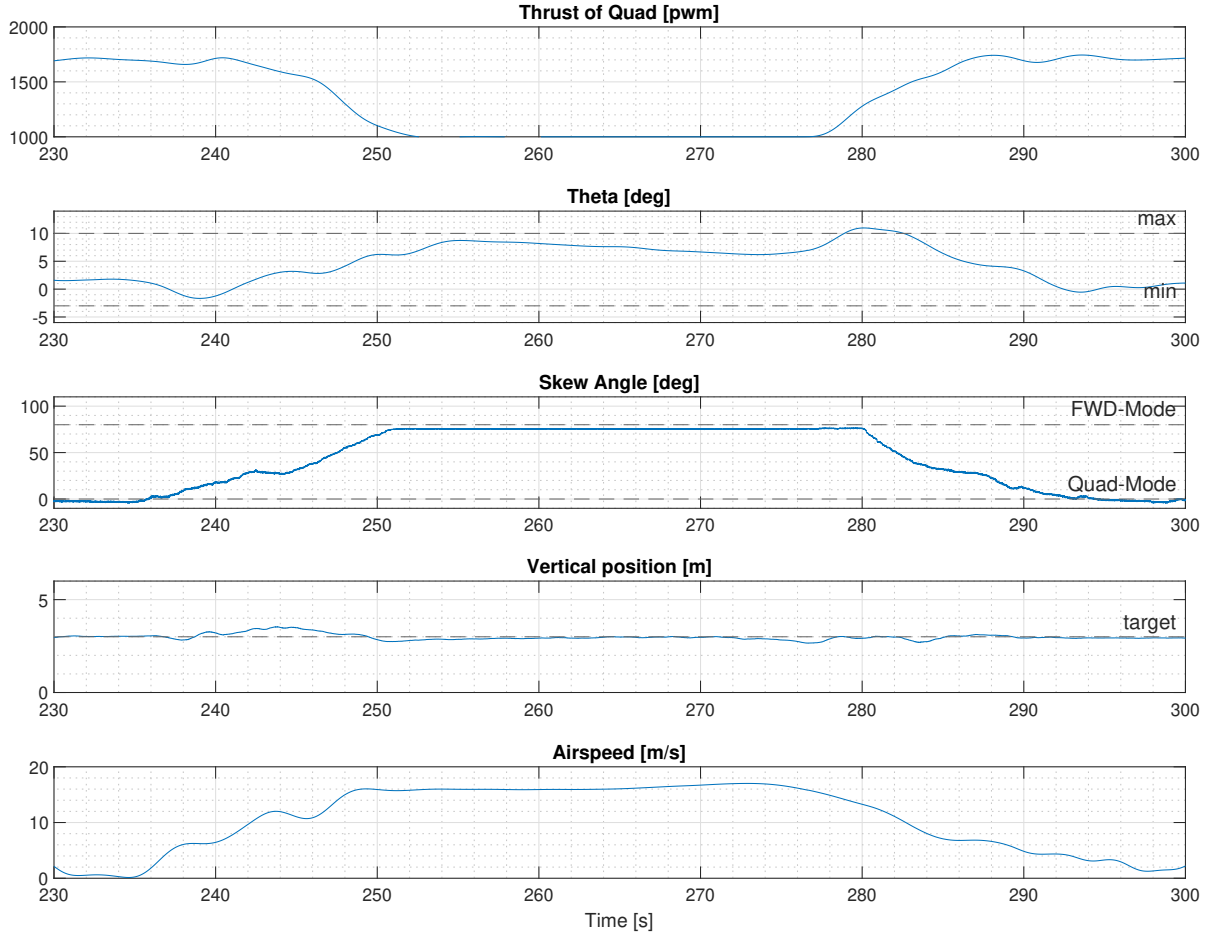


Fig. 17. Transition data

stabilize the VSQP in all of its configurations.

It can be concluded that the main research focus to achieve a functioning controller is the development of a model of the control effectiveness of the actuators and a model of the lifting properties of the wing at any given state of the drone. These models are used by the autopilot to correctly calculate the necessary control allocation to achieve stabilization and guidance.

The multiple successful transitions prove that the models can be based on a few simple but powerful assumptions:

- Control effectiveness changes linearly with actuator state for all actuators.
- Control effectiveness changes quadratically with airspeed for the aerodynamic surfaces.
- Aerodynamic forces generated by the control surfaces and by the wing are mostly dependent on the chordwise component of airspeed which can be expressed in terms of the skew angle.
- The moment arm of the ailerons which affects their control effectiveness is modeled as a vector rotating around the C.G. by an angle equal to the skew.
- Changes in the moments of inertia as skew is adjusted

can be neglected.

Moreover, WLS is proved to be a suitable solution to solve the control allocation problem for the overactuated guidance control loop of the VSQP. Gradual power-on and shutdown of the lifting motors in transition is achieved by tuning the weighting matrices of the WLS routine.

Finally, it is found that an offline optimization routine to maximize control authority can be used to simply but robustly schedule the skew angle command with airspeed. Such solution is validated to always automatically command stable controllable states of the drone throughout the transition envelope.

A. Future Recommendations

The author recommends to complete the validation plan outdoor in its entirety as initially planned. The plan would validate without doubt the correctness of the developed controller also in gusty turbulent environments. Moreover, future developments should be conducted to understand better the interaction between the motors and the lifting surfaces. Flow indicators placed on the horizontal surface have suggested that at low airspeed the back motor generates a negative

angle of attack and in the worst case reverse lift on the horizontal tail. Initial analysis show that this might contribute to the generation of a pitch up moment. Tests without the horizontal tail and with a different tail configuration, as for example a T-tail, should be performed to develop further scientific insights on the phenomenon. With such knowledge better design choices can be developed for the tail-back motor assembly.

Further research should also be conducted to understand the effect of the motors on the control surfaces. Part of the static tests was already designed to gain an initial understanding of the topic. It was proved that the quad motors do not affect the effectiveness of the ailerons. In contrast, the tail surfaces have been shown to change effectiveness especially with push motor command. It must be investigated how the effectiveness of the tail can be modeled with both airspeed and push prop command. Furthermore, it must be evaluated if the increased precision of the model is also reflected by an increase in control performance or if it only adds additional complexity to the controller.

Finally, the development of a model for the exerted moments from aerodynamic effects as reported in (10), can result in a more precise scheduling of skew with airspeed. Including $M_a(\Omega, v, \Lambda)$ in the optimization routine of section VIII can help avoiding regions of severe adverse aerodynamic effects. These would correct the discrepancies identified between the gradient ascent and the actual flight test results.

REFERENCES

- [1] A. R. Seebass. *Oblique Flying Wing Studies*. Sobieczky H. (eds) New Design Concepts for High Speed Air Transport. International Centre for Mechanical Sciences (Courses and Lectures). 1997. DOI: 10.1007/978-3-7091-2658-5_20.
- [2] R. R. da Costa, Q. P. Chu, and J. A. Mulder. "Reentry Flight Controller Design Using Nonlinear Dynamic Inversion". In: *Journal of Spacecraft and Rockets* 40.1 (Jan. 2003), pp. 64–71. DOI: 10.2514/2.3916.
- [3] E. J. J. Smeur, Q. Chu, and G. C. H. E. de Croon. "Adaptive Incremental Nonlinear Dynamic Inversion for Attitude Control of Micro Air Vehicles". In: *Journal of Guidance, Control and Dynamics* 39 (2016), pp. 450–461. ISSN: 1533-3884. DOI: 10.2514/1.g001490.
- [4] Barton Bacon and Aaron Ostroff. "Reconfigurable flight control using nonlinear dynamic inversion with a special accelerometer implementation". In: *AIAA Guidance, Navigation, and Control Conference and Exhibit*. American Institute of Aeronautics and Astronautics, Aug. 2000. DOI: 10.2514/6.2000-4565.
- [5] Lixin Wang, Zijian Xu, and Ting Yue. "Dynamic characteristics analysis and flight control design for oblique wing aircraft". In: *Chinese Journal of Aeronautics* 29.6 (Dec. 2016), pp. 1664–1672. DOI: 10.1016/j.cja.2016.10.010.
- [6] P. Simplício et al. "An acceleration measurements-based approach for helicopter nonlinear flight control using Incremental Nonlinear Dynamic Inversion". In: *Control Engineering Practice* 21 (2013), pp. 1065–1077. ISSN: 0967-0661. DOI: 10.1016/j.conengprac.2013.03.009.
- [7] E. J. J. Smeur and C. Höppener D. andde Wagter. "Prioritized Control Allocation for Quadrotors Subject to Saturation". In: *International Micro Air Vehicle Conference and Flight Competition 2017* (2017), (pp. 37–43). URL: http://www.imavs.org/papers/2017/51_imav2017_proceedings.pdf.
- [8] H.J. Karssies and C. de Wagter. "Extended incremental non-linear control allocation (XINCA) for quadplanes". In: *International Journal of Micro Air Vehicles* 14 (Jan. 2022), p. 175682932110708. DOI: 10.1177/17568293211070825.
- [9] Dr. R.K. Nangia. *Meeting Unmanned Air Vehicle Platform Challenges Using Oblique Wing Aircraft*. Defense Technical Information Center. Nov. 2007.
- [10] W.P. Nelms. *Applications of Oblique-Wing Technology - An overview*. Aircraft Systems and technology Meeting. Sept. 1976.
- [11] Gautier Hattenberger, Bronz Murat, and Gorraz Michel. *Using the Paparazzi Uav System for Scientific Research*. International micro air vehicle conference and competition. 2014.
- [12] B. Theys et al. *Wind tunnel testing of a VTOL MAV propeller in tilted operating mode*. 2014 International Conference on Unmanned Aircraft Systems (ICUAS). pp.1064-1072. 2014. DOI: 10.1109/icuas.2014.6842358.
- [13] B. Theys et al. "Experimental and Numerical Study of Micro-Aerial-Vehicle Propeller Performance in Oblique Flow". In: *Journal of aircraft* 54.3 (May 2017), pp. 1076–1084. ISSN: 0021-8669. DOI: 10.2514/1.c033618.
- [14] Carl Russel et al. *Wind Tunnel and Hover Performance Test Results for Multicopters cUAS Vehicles*. AHS 72nd Annual Forum. May 2016.
- [15] Tony Oliver Mogorosi et al. "Thrust-to-Weight Ratio Optimization for Multi-Rotor Drones Using Neural Network with Six Input Parameters". In: *2021 International Conference on Unmanned Aircraft Systems (ICUAS)*. IEEE, June 2021. DOI: 10.1109/icuas51884.2021.9476744.
- [16] Gordon Ononiwu et al. "Design and Implementation of a Real Time Wireless Quadcopter for Rescue Operations". In: *American Journal of Engineering Research* (2016). DOI: e-ISSN:2320-0847.

Aileron Left

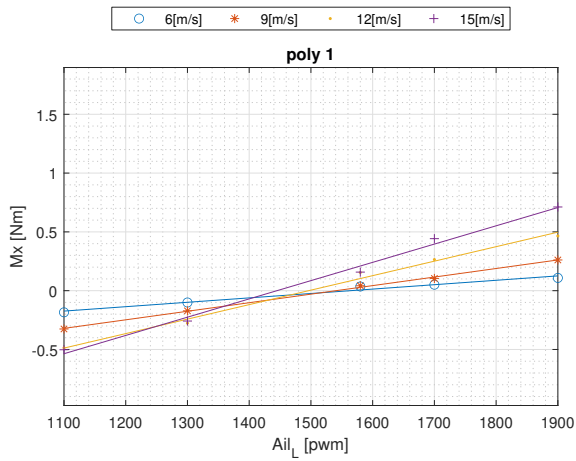


Fig. 18. Linear relation between exerted roll moment and command to the left aileron at different windspeeds

Aileron Right

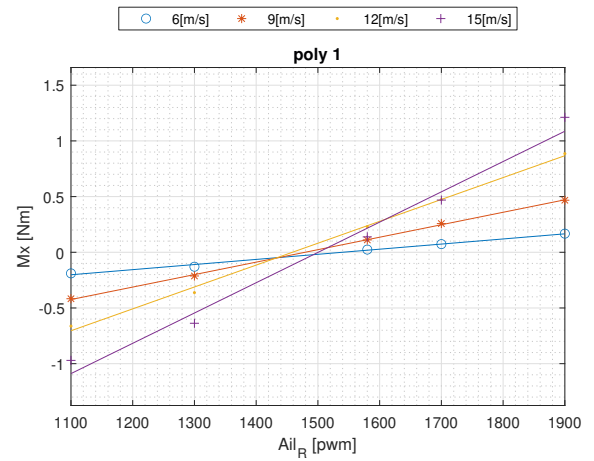


Fig. 19. Linear relation between exerted roll moment and command to the right aileron at different windspeeds

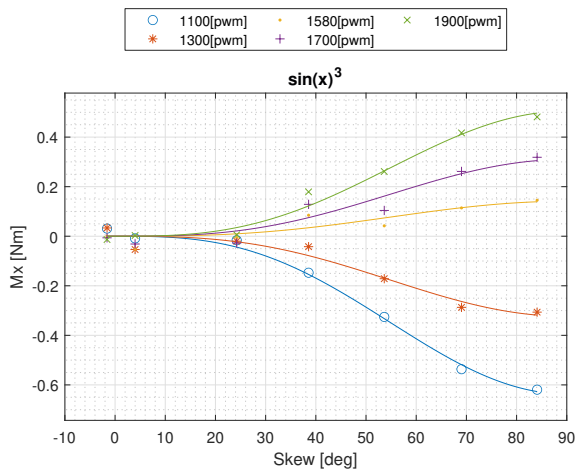


Fig. 20. Trigonometric relation between skew and roll moment exerted by the left aileron at different pwm command values

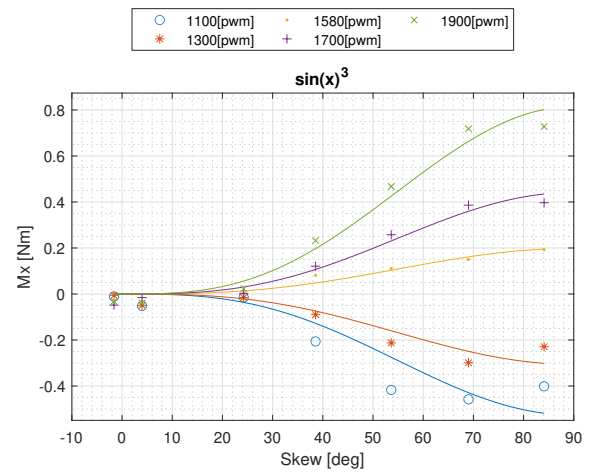


Fig. 21. Trigonometric relation between skew and roll moment exerted by the right aileron at different pwm command values

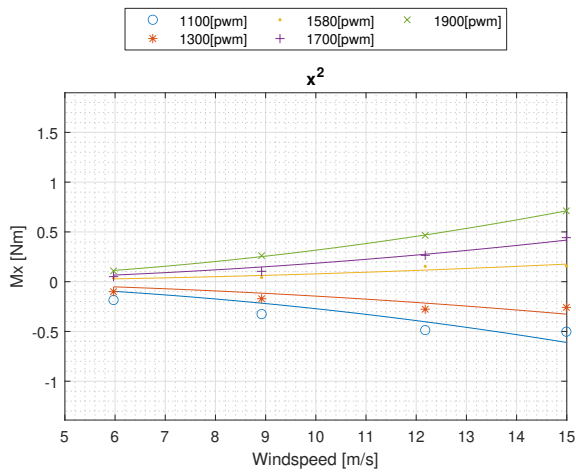


Fig. 22. Quadratic relation between windspeed and roll moment exerted by the left aileron at different pwm command values

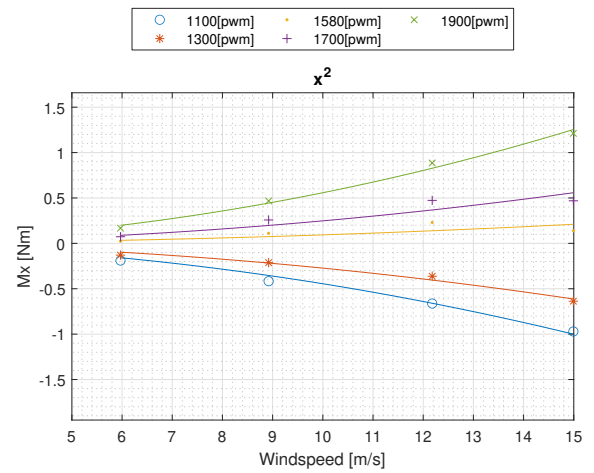


Fig. 23. Quadratic relation between windspeed and roll moment exerted by the right aileron at different pwm command values

Aileron Left

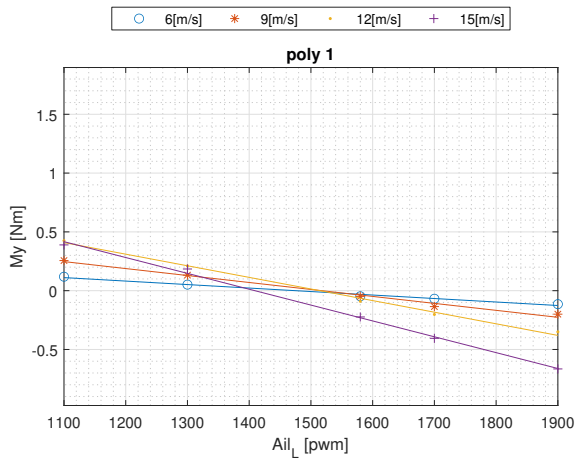


Fig. 24. Linear relation between exerted pitch moment and command to the left aileron at different windspeeds

Aileron Right

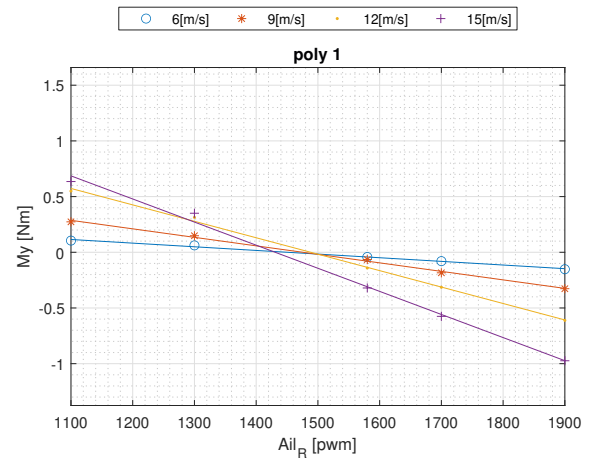


Fig. 25. Linear relation between exerted pitch moment and command to the right aileron at different windspeeds

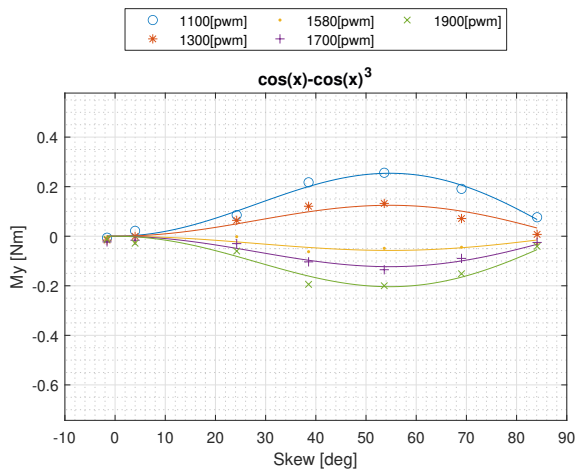


Fig. 26. Trigonometric relation between skew and pitch moment exerted by the left aileron at different pwm command values

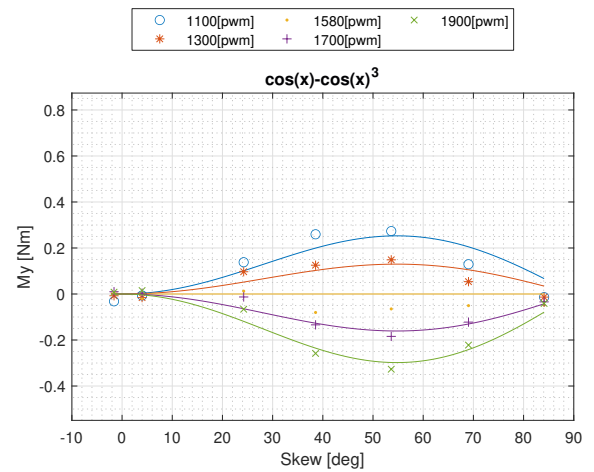


Fig. 27. Trigonometric relation between skew and pitch moment exerted by the right aileron at different pwm command values

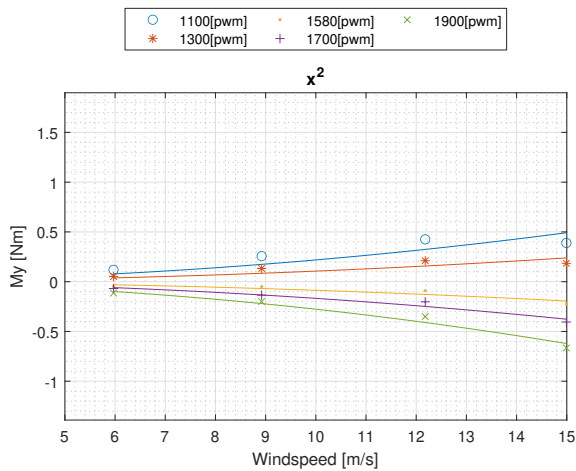


Fig. 28. Quadratic relation between windspeed and pitch moment exerted by the left aileron at different pwm command values

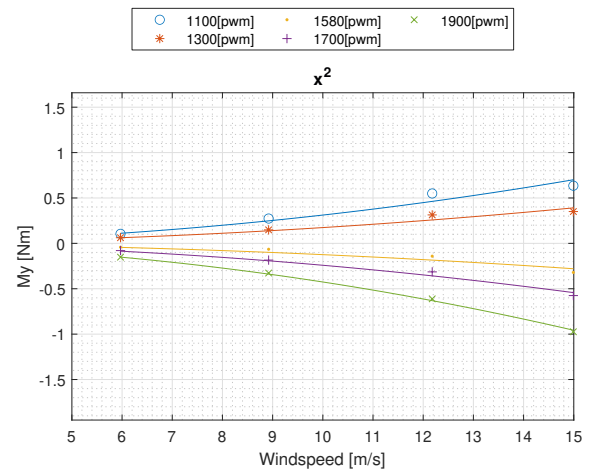


Fig. 29. Quadratic relation between windspeed and pitch moment exerted by the right aileron at different pwm command values

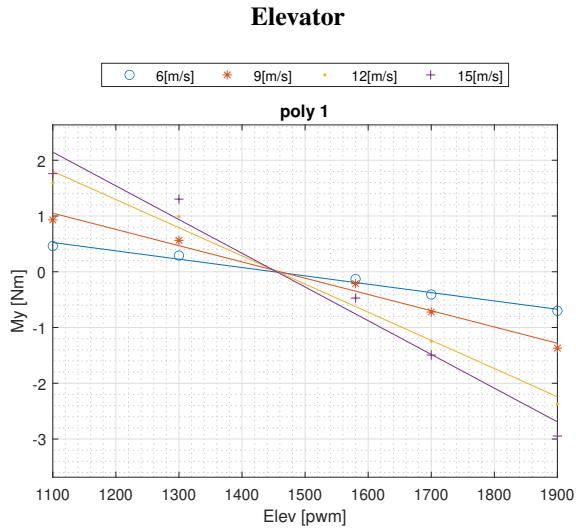


Fig. 30. Linear relation between exerted pitch moment and command to the elevator at different windspeeds

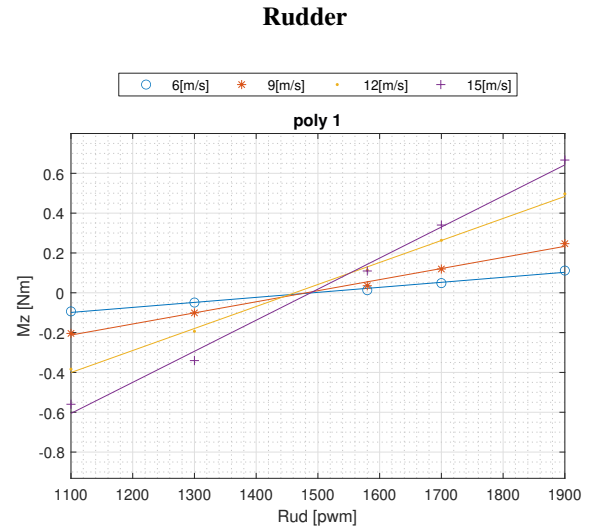


Fig. 31. Linear relation between exerted yaw moment and command to the rudder at different windspeeds

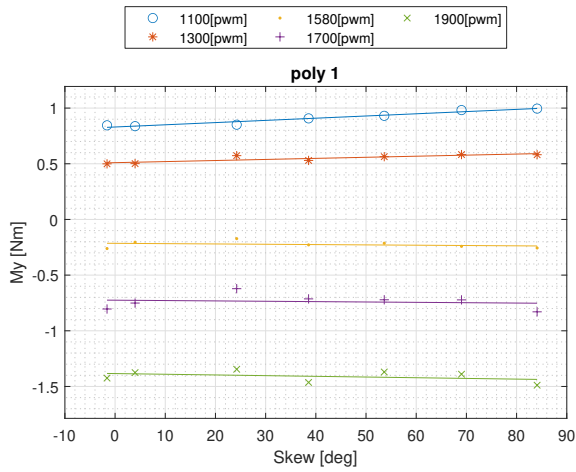


Fig. 32. Trigonometric relation between skew and pitch moment exerted by the elevator at different pwm command values

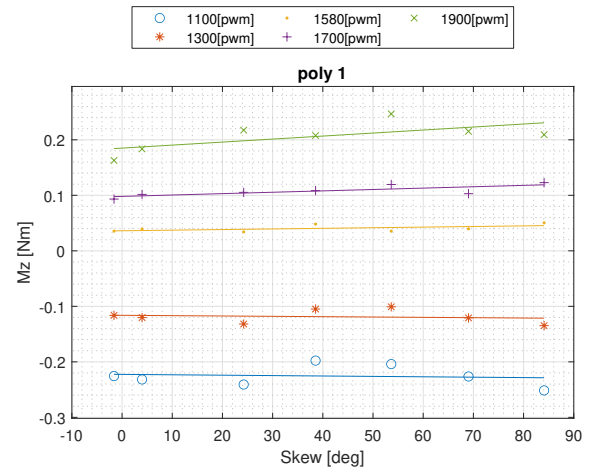


Fig. 33. Trigonometric relation between skew and yaw moment exerted by the rudder at different pwm command values

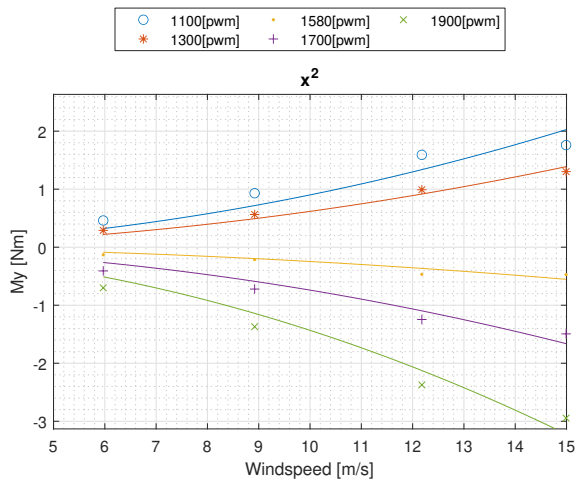


Fig. 34. Quadratic relation between windspeed and pitch moment exerted by the elevator at different pwm command values

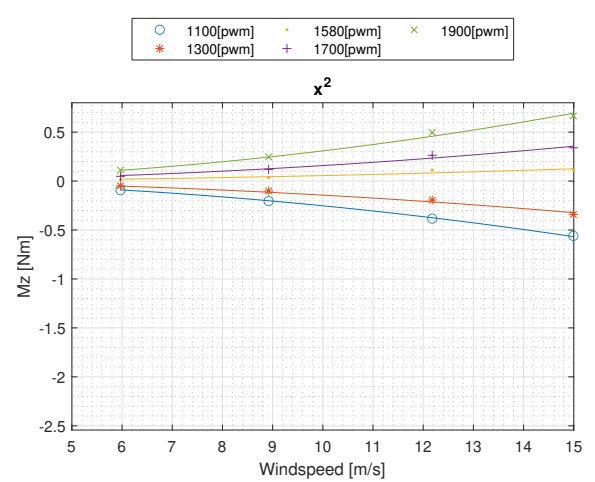


Fig. 35. Quadratic relation between windspeed and yaw moment exerted by the rudder at different pwm command values

2

Literature Study

Executive Summary

Applications such as high-rise package delivery, off-shore missions and landings on moving platforms require good wind rejection capabilities and can for example be performed by both a Unmanned Air Vehicle (UAV) or a manned helicopter, with the latter leading to obvious higher costs and deployment times. In order to save resources there is the need for a platform able to operate in gusty environments in an autonomous and efficient way using only a very limited input from an operator. The design under development is best described as a Variable Skew Quad Plane (VSQP) and to the best knowledge of the author it is a first in its category. In hover mode, the drone operates as a simple quad-rotor and attitude is controlled through differential thrust. On the other hand, in cruise mode the drone operates as a plane and uses aerodynamic surfaces on the wing as well as tail to achieve attitude control. Similarly to a typical quad-plane, the drone achieves forward speed thanks to a push propeller placed at the tail. In contrast though, the proposed design does not have a fixed wing configuration, but rather implements the rotating concept applied in the Oblique Flying Wing (OFW) prototype plane. A central rotating pivot is used to deploy the wing as the lateral rotors are folded in the fuselage structure. VSQP borrows design concepts of OFW to address a number of challenges of hybrid drones. Mainly the ability to fold the wing or in alternative the side rotors in the fuselage allows for respectively better gust rejection in hover [1] and lower drag in cruise [2]. Furthermore, the ability to change the footprint allows for better packability and operation of the platform [3].

On the other hand OFW is a design concept which is famously known for the control complexity. The first goal of the Literature Study logically is to address the following Research Objective:

“What are the control challenges of an OFW? Which solutions are documented in the Literature for the mentioned problems?”.

The most clear disadvantage is the complexity of the control problem of such design. In an OFW motions are coupled by aerodynamic and inertial moments [4] and as such stabilization becomes a less straight forward task [5, 3]. The inertial coupling can be easily understood by analyzing the inertial tensor matrix. The inertial tensor highlights that the cross products of inertia I_{xy} and I_{yx} are non-zero in contrast to symmetrical aircraft [6].

The aerodynamic coupling needs some further insights to be understood, but is well described in the literature [6]. Yue et al. [7] mention that due to the asymmetrical wing layout a non-negligible side force is experienced by the OFW. This occurs because the lateral component of the drag vector for both half wings is in the same direction as opposed to symmetrical wings in which the lateral drag components cancel each other. This means that the OFW generates a side force which is not present in conventional symmetrically swept aircraft. Mcmurtry, Sim, and Andrews [8] argue that pilots in the AD-1 oblique wing program actively used left sideslip or a banking maneuver to compensate for the induced side force. Furthermore, Wang, Xu, and Yue [6] argue that the left swept back wing experiences a higher leading edge suction than the right swept forward one. The authors argue that the higher suction leads to higher generated lift. As a consequence, the left backwards swept wing generates higher lift than the right wing, in turn producing an overall pitch down moment and positive rolling moment.

Moreover, as the skew angle increases, the roll and pitch arm respectively decrease and increase. The reduction in rolling arm leads to lowered roll effectiveness of the ailerons. Therefore, bigger deflections will be required of the ailerons which can lead to saturation. A common solution in OFW designs is to use a differential horizontal surface to help ailerons and rudder to stabilize the aircraft even at high skew angles [6].

In conventional aircraft controller design, models which make use of aerodynamic derivatives are used to simulate the response of the platform. These coefficients are usually extrapolated from flight data.

Often, lateral and longitudinal motion are decoupled and analyzed separately to simplify the control problem. It is clear now though that for OFW such simplification is not possible due to the coupling in inertia and aerodynamic forces. Therefore, a new solution is required to allow for the modelling of the platform.

Maine [9] presents a method to estimate the aerodynamic derivatives from flight data of a OFW through the use of a maximum likelihood estimation. Maine mentions that in theory conventional methods for the estimation of stability and control derivatives can be applied but the computational complexity, the inaccuracy of the linear aerodynamic model and the limited data set make the conventional approach unattractive. Maine proposes to achieve analysis by Separation of Modes, as it is done for conventional aircraft, by eliminating the differential equations of lateral motion from the longitudinal analysis and vice versa. This is achieved by assuming that on-board sensors, which measure the states of interest, have little noise meaning that the measured lateral-directional responses can be used as inputs to the longitudinal equations and vice versa. On the other hand, it can be argued that the assumption of noise-free sensors is not applicable to Micro Air vehicles (MAV) for which airborne equipment is not as accurate as for larger aircraft which can carry larger payloads [10].

Pang, Mei, and Chen [11] further present how a set of conventional aerodynamic derivatives coefficients can be used to create a model for a OFW near space vehicle by simply deriving the equation of motion from Newton's second law for a complete unsimplified inertia tensor.

However, the issue with the methods presented by Maine and by Pang, Mei, and Chen is that the techniques still aim to solve a 39 unknowns problem, being the relevant aerodynamic derivatives, which represents still a complex task to perform accurately. Furthermore, using aerodynamic derivatives to linearize a plant which in reality due to the couplings is nonlinear, introduces discrepancies which can lead to control performance degradation.

There is then the need for a control scheme which is able to deal with nonlinearity and does not depend on an extensive model of the drone. Wang, Xu, and Yue [6] propose to use a Nonlinear Dynamic Inversion (NDI) controller which follows an ideal model reference to provide acceptable handling qualities. On the other hand, inaccuracies and simplifications introduced in the models can have a detrimental effect on the controller performance [12] and are not compensated by the Nonlinear Dynamic Inversion control (NDI). In addition, the development of accurate models of MAV can require expensive resources and is limited by the small sensors which can be carried by a MAV [10]. Therefore, a less model dependent control law is needed for implementation in MAV, leading to the development of Incremental Nonlinear Dynamic Inversion control (INDI). Therefore the second aim of the research plan is to answer:

“What are the fundamental concepts behind INDI control? What are the benefits of INDI over counterparts? Which challenges and solutions does the Literature report for the implementation of INDI on MAV? ”.

The incremental version of nonlinear dynamic inversion control, also known as INDI, has been described since the late 1990s early 2000s to be a less model dependent and more robust solution than NDI [13]. The idea behind INDI is to replace the dynamic model of the platform with data retrieved online by sensor readings. The incremental control law of INDI for a virtual control vector ν of desired angular accelerations, with effectiveness matrix G and current sensed angular acceleration \dot{x}_f is:

$$\Delta u \simeq (G(x_f, u_f))^+ (\nu - \dot{x}_f)$$

Bhardwaj et al. [14] argue that reference models can be used to generate feasible smooth reference trajectories ν directly from the control variables. For the control scheme to work for a system of relative degree r it is important that the reference trajectory is smooth such that the $r - th$ derivative exists. The coefficients \mathbf{k} of the reference model have to be chosen in order to meet the considered platform capabilities. Raab et al. [15] further argue that another important output of the reference model is the reference external state trajectory ξ_{ref} , which collects the lower order derivatives of ν_{ref} . The availability of the reference state trajectory allows for the detection and correction of deviation of the lower level derivatives of the pseudo control vector.

Raab et al. [15] argue that reference model only provides feed-forward control by generating pseudo control vectors which track the reference trajectory. Therefore an error controller is required to adjust the plant external state trajectory to the reference trajectory in case of a deviation. The authors propose to create a feedback loop of the trajectory error χ with Proportional-Integral gains to close the deviation and compensate for steady state errors.

Bhardwaj et al. [14] and Raab et al. [15] discuss an INDI controller structure which makes use of a single dynamics inversion procedure to track a given pseudo control vector by incrementally changing the control input. All things considered, the method is proven to robustly provide control for a hybrid VTOL prototype aircraft. Smeur, Croon, and Chu [16] instead propose a cascaded implementation of INDI for attitude and position control of MAV which embeds the tasks of pseudo control generation and disturbance rejection directly in one single structure. The method makes use of two INDI control loops: inner and outer loop. Inner loop provides stabilisation of the platform while outer loop provides guidance. Two different dynamic inversion routines are performed, one for each loop, therefore needing two different sets of effectiveness matrices.

Wind gust rejection is a critical requirement for a controller implemented in a drone designed to be deployed in outdoor conditions. One of the main advantages of INDI over Proportional Integral and Derivative (PID) in the field of MAV control has been proven to be fast disturbance rejection [16, 17]. This occurs because in an INDI outerloop what is ultimately being tracked is a linear acceleration reference, which is the fastest changing variable. PID instead needs to register an error in velocity tracking before initiating a correcting procedure. In turn this leads to the drone having already accumulated a large position or velocity error before reacting to the disturbance.

Surely, it can be argued that fine tuning of PID, especially the Integral gain, can make a drone perform aggressive corrections. On the other hand, a higher integral gain leads also to overshoot in reference tracking, ultimately generating a trade-off to be evaluated [16]. Additionally, gain tuning can be a resource expensive task which compromises the fast and straightforward application to a drone platform. The trade-off in integral gain tuning between increased offset reduction and corresponding higher overshoot of reference does not apply to INDI. More precisely INDI, due to the incremental nature of its control law, is able to correct for disturbances without having to sacrifice performance. The idea is that any disturbance, even slight model inaccuracies, is registered by the on-board sensors and leads to an increased acceleration error which is then incrementally compensated for. Such assumption is proved to hold in the case in which the control elements can react quick enough and are not saturated.

Pfeifle and Fichter [18] argue that further enhancement of INDI's wind gust rejection on a winged platform could be achieved by using aerodynamic angles instead of Euler angles in the control law. This occurs because the force and torques disturbances from gusts are mostly caused by changes in the aerodynamic angles and therefore would be directly targeted by the attitude control loop. While these considerations might be true in the theoretical sphere, in practice obtaining accurate measurements from angle vane sensors can result to be complex [19].

While INDI promises to bring important benefits over counterparts, a few challenges have been documented in the Literature. First, the basic INDI control law lacks a representation of the actuator dynamics. It is assumed, alike in the work of Sieberling, Chu, and Mulder [20], that the platform uses perfect actuators which respond instantaneously to the commanded input. On the other hand, Li et al. [21] showed in simulation that a real life actuator in response to a chirping reference signal would suffer from lag as well as attenuation of amplitude. Johnson and Kannan [22] argue that Pseudo Control Hedging (PCH) can be used to prevent INDI from adapting to system input characteristics as for example the actuator dynamics. Bhardwaj et al. [14] argue that the hedging effect is incorporated by recalculating the highest order derivative and moving the reference model in the opposite direction (hedge) by an estimate of the amount that the plant did not move due to actuator dynamics.

In an attempt to design a more complete compensation technique for actuator dynamics, Raab et al. [23] suggests to incorporate knowledge of the rate limits of the actuators directly into the control allocation. The idea is then to prioritize faster actuators over slower ones directly at the stage of control allocation.

This is achieved by deriving a new INDI control law which is based on an additional derivative of the system output and so embeds knowledge of the "speed" of the actuators directly in the effectiveness matrix. Therefore, faster actuators will artificially result to be more effective hence will be allocated more increment in control input and vice versa. This method than results to deliver useful results in the case that a drone can use multiple actuators to control coupled axes.

Moving on, regardless of the accuracy level, the output of a sensor is a combination of a measurement signal and a certain amount of noise. Such noise is further amplified in the INDI loop due to the rotational rates being differentiated in time to obtain angular accelerations [10]. Therefore, the signal is usually filtered with second order low pass filters [13] of for example the Butterworth type [24]. As a consequence of filtering, a lag is introduced in the measured signal which if not accounted for can lead to oscillation of the closed loop system [25]. Therefore, these filters have to be applied to both the control objective and control input in order to maintain all signals synchronized.

On the other hand, time delay is also affected by the dynamics of the sensor (Inertial Measurement Unit). Therefore, the synchronization method remains susceptible to unexpected measurement delays [26]. Furthermore, excessive time delays due to the actuator dynamics considerations, noise filtering and sensor dynamics reduce the stability margin of the control system [27]. Hybrid INDI is proposed as a solution for increased robustness and stability margin. Kumtepe, Pollack, and Kampen [26] argue that the general idea is that knowledge of the system can be used in a model to generate fast response to system input, while sensor measurements are used to maintain adequate accuracy in the low-medium frequency range. Therefore, the estimation of the angular acceleration from an On-Board Model (OBM) is fused with measurements from sensors. Kim et al. [27] argue that this is best achieved with a simple proportional gain K_{aug} which defines the proportions of the two signals. In contrast, Kumtepe, Pollack, and Kampen [26] argue that the fusion of the signal is better achieved with a complementary filter.

Ji, Kim, and Kim [28] argue that hybrid INDI together with smartly generated pseudo controls using knowledge of the desired flying dynamics can greatly alleviate the transient response and reduce the workload of the pilot. This is particularly interesting because it candidates hybrid INDI to solve problems in which platforms undergo sudden and complex to model changes in system dynamics, just alike transition for VSQP due to the imbalances generated by the oblique wing.

The Literature further develops on the challenges of drafting of the outerloop effectiveness matrix. The problem with the estimation of the outerloop effectiveness matrix is that it depends on $L(\theta, V)$, $\frac{\partial}{\partial \theta} L(\theta, V)$ and T which are not readily available values. Surely, it can be argued that a model can be created to evaluate the variables value at any considered condition. On the other hand, such process can be tedious and resource expensive. Wijngaarden, Smeur, and Remes [29] and Smeur, Bronz, and Croon [24] propose as an alternative to exploit knowledge of the platform to approximate some of the unknown variables. The authors make the example that for a tail-sitter in forward flight the generated lift is used to compensate the weight of the drone. Therefore, simple substitution for the unknown variables based on the known weight can be introduced. As for $\frac{\partial}{\partial \theta} L(\theta, V)$ Smeur, Bronz, and Croon [24] argue that no simple assumption can be derived and that some sort of data driven aerodynamic model should be used. This occurs because a change in airspeed strongly affects $\frac{\partial}{\partial \theta} L(\theta, V)$ and so no general simplification can be applied. These simplifications are proven to provide precise guidance however, the authors also define the assumptions to be "crude" and "probably inaccurate"[29], hinting to the performance gains which could be achieved with a more accurate model.

The Literature moves on by mentioning that conventional pseudo inversion of the effectiveness matrix to compute control allocation has some drawbacks. This occurs because the solution is computed based only on effectiveness and not accounting for the state and possible saturation of the actuators. Wang, Xu, and Yue [6] propose to scale the actuator inputs with their maximum saturation limit in the control law. Wang, Xu, and Yue argue then that the proposed scaling prevents the single saturation of an actuator when there is another control element which could pick up the control slack. However, it can be argued that this simple approach does not deliver the most optimal solution because it does not take into account the energy consumption of actuators. For example, from a power usage perspective motors have a larger impact than operating aerodynamic surfaces. Therefore, there is a need to priori-

tise the use of some actuators over others in certain flight phases which cannot be simply encoded in the effectiveness matrix. Furthermore, in the case of saturation, there should be a prioritisation of the desired control objective. This makes sure that the most vital control actions for the drone are given priority over secondary ones.

Smear, Höppener, and Wagter [30] proposes a Weighted Least Squares (WLS) algorithm to solve the control allocation problem specifically for the innerloop of INDI. More precisely the method solves a sequential least squares problem corresponding to a primary and a secondary objective function. The primary objective is to minimise the error between the desired angular acceleration change and the one produced by the calculated control increment. The secondary objective is to achieve the primary objective using the least actuator energy. This objective prevents the control allocation algorithm to converge to a solution where control elements are steered in opposite directions for over-actuated systems. The cost function of the quadratic programming problem is constructed by using weighting matrices to establish a hierarchy between control objectives and control inputs while a scaling factor is used to increase the cost of the primary objective.

The next challenge in INDI treated in the Literature is effectiveness estimation, which can result to be a complex error prone process. In order to estimate the effectiveness matrices, flight test data can be used. Multiple authors [10, 16, 24] propose to use a least squares estimation routine to estimate the effectiveness profiles. More precisely, for the inner loop the registered angular acceleration can be compared to the change in actuator inputs while for the outer loop the registered linear acceleration is compared to change in controlled variables. In order to prepare the data for the estimation one has to apply manipulations so to recreate the signals received at the actuator level. This means that filters and actuator dynamics blocks have to be applied where needed.

Furthermore, the system has to be excited in such a way to reveal the underlying dynamics for the least squares to approximate the effectiveness values. In the literature multiple authors [9, 31] propose the use of Doublets. These are identified to better reveal the faster and stronger dynamics of the control elements due to the high frequency and contained deviation from equilibrium. In opposition, Chirps are identified to better reveal the slower state induced dynamics due to the large range of swept frequencies. Smear, Bronz, and Croon [24] further report that non accurate effectiveness estimations for the outerloop can occur if the contribution of the control elements to linear accelerations are not accounted. Therefore, the vertical acceleration due to lift cannot be simply modelled by considering only the pitch angle but also the deflection of the ailerons should be considered.

One of the challenges of an hybrid drone is the development of a control strategy which is able to deal with the numerous nonlinear changes in dynamics during transition. Therefore the last objective of the literature Study is to answer the following question:

“What are the expected changes in vehicle dynamics during transition? What is documented in the literature in regards to INDI control of hybrid drones in transition ?”.

First the changes in effectiveness of the motors in transition due to crossflow and change in moment arm are analyzed. Propeller performance data is crucial for optimal design [32], modelling [33] and for assessing whether stability and controllability is achievable in different flight scenarios. On the other hand, research on performance of UAVs and MAVs propellers in crossflow conditions can result to be complicated due to the low Reynolds number experienced by small propellers, which prevents the use of classical helicopter disk theory [34, 35].

Despite the complexity of the modelling task, there exist a trend in the literature across all proposed model which depicts a positive correlation between crossflow airspeed and propeller performance [36, 37]. In 2017, Theys et al. [38] further develop the research by proposing 3 different modelling techniques to depict the performance of small Propellers at different inflow angles and speeds: Blade Element Momentum Theory (BEMT), Vortex Lattice Method (VLM) and basic conservation of momentum. Theys et al. conclude that while both BEMT and VLM are consistent with each other in thrust estimations, they both overestimate the propeller performance throughout the considered inclination range.

It is further concluded that while both methods correctly predict trends in the propeller performance, accuracy is lost at higher angles of attack. The basic momentum conservation method seems to offer a simple solution to the modelling of the motor/propeller performance, but it heavily depends on test data and uses mechanical power as a control variable which is not straightforward. Pobikrowska and Grabowski [39] present a simplified method which involves the assumption of perfect tangent flow to the blades movement and integration of the lift equation along the radius of the advancing and retreating blade. However, such an approach needs knowledge regarding the lift coefficient of the propeller per cross-section along the radius which could result to be expensive to estimate.

On the other hand, the presented modelling methods all result to be either complex and expensive, or oversimplified and inaccurate. It is then concluded that the most straightforward way to model the performance of the motors is to perform wind-tunnel tests and draw a numerical relation between thrust and RPM.

As for the changes in position of the side motors in transition, Bai and Gururajan [40] argue that a simple model of the changes in geometry can be used to reflect the mutating dynamics of a drone. Therefore, it is concluded that the effectiveness can be scheduled as a trigonometric function of the skew angle.

The next treated topic is that VSQP, similarly to a conventional quadplane, is overactuated in both the inner and outerloop, which becomes particularly evident when a forward acceleration can be obtained by both a pitch down maneuver or by using the push propeller. Furthermore, during transition, as the airspeed increases, a gradual shift in control allocation from the lifting motors to the wing should occur. This is because VSQP is designed to efficiently sustain its weight in forward flight by exploiting the lift generated by the wing. Karssies and Wagter [41] propose Extended Incremental Nonlinear Control Allocation (XINCA) as a single solution to the INDI outerloop control problems. The main idea is that the control variables of the outerloop are considered as force generating actuators and instead of performing a simple inversion of the outerloop matrix a complete WLS routine is carried out. Karssies and Wagter [41] argue that the control variable weighting matrix can be designed to penalize the use of pitch and roll and especially thrust commands compared to using the pusher rotor.

As for the gradual reduction in the use of lifting motors as the airspeed increases, Karssies and Wagter [41] argue that the pitch angle effectiveness with respect to the vertical axis can be augmented by a term representing the contribution of the wing to lift which is assumed to increase with the square of airspeed. Therefore, as airspeed increases, the effectiveness of changing θ on vertical accelerations increases, resulting in a cheaper control allocation solution.

The final topic treated by the Literature Review is the use of knowledge of the plant to enhance control. This is of interest because knowledge of the imbalances of an OFW can be useful in the transition of VSQP to better control performance. Bhardwaj, Raab, and Holzapfel [42] propose to incorporate identifiable disturbances-state dependent damping terms in the feed-forward pseudo control derivative. The authors argue that the control law from the extension of INDI [23] could be further augmented to take into consideration known state dependent influence. It is indeed argued that neglecting state variation terms is not valid for systems with higher damping like winged platforms. The general idea of the proposed method, named Higher Order Reference Model, is to use a feedforward term \dot{v}_{ff} built with plant knowledge which is one derivative level higher than the relative degree of the system.

On the other hand, it could be argued that the whole point of using INDI over NDI is that developing a precise model of the slow state induced effect on the controlled variables can be a complex task given the limited accuracy sensors available to the a MAV. In contrast, Bhardwaj, Raab, and Holzapfel [42] argue that simulation of the presented method proves that the use of model knowledge in the higher order reference model brings the advantage of reducing the feedback control effort even in case of high uncertainties in the design plant model, without introducing any instabilities in the closed loop system. Surely it could be argued that these conclusions are the product of a simulation and not a real life flight test. Nevertheless the proposed method still is a promising candidate to solve the control problem of transition of VSQP.

The concluding chapter of the Literature Review Study is an outlook on the next steps in the thesis project. The main knowledge gap that arises from the literature study is the nonexistence of a INDI controller which can control in a continuous and optimal manner a hybrid drone which suffers from OFW induced moment imbalances alike VSQP. More precisely, there has yet to be defined a way to efficiently model the dynamics of a OFW using only the limited resources available to a small research UAV such as VSQP.

Moreover, there has not yet been documented and verified with real test flights a robust way to implement this knowledge in an extension of an INDI controller to improve performance. There is the need to research how to use the described trimming solutions of an OFW to generate a set of control objectives which provide desirable flying qualities.

Finally, VSQP adds an additional variable to be controlled, being the skew angle of the wing. Therefore, there is the need for a novel controller which uses knowledge of the mutating actuators effectiveness in transition to command optimal skew angles to meet the control objectives. The controller cannot simply decouple wing and quad motors control but has to holistically evaluate the effect of skew angle on both.

The research strategy highlights the methodologies that are expected to be used to answer the research questions. Simulation will be performed with Paparazzi UAV and Matlab-Simulink. The former more suited for online applications while the latter better used for analysis and effectiveness estimations. Verification will be conducted at the Cyberzoo as well as at the Open Jet Wind Tunnel of TuDelft. The former is used for testing in a safe environment the basic parts of the controller while the latter is used to simulate the linear airflow experienced in forward flight. Validation will be performed at the facility of Valkenburgh where the open fields allow for the testing of every flight phase and drone configuration. Finally, a Gantt chart presents how the time thesis budget of 9 months is subdivided into work packages.

In a nutshell, the presented Literature Review Study has addressed the Research Objective by analyzing the benefits, challenges and solutions of both OFW and INDI. A particular focus was centered around what solutions have been documented regarding the use of INDI in the transition of compound-lift, overactuated hybrid drones. Research questions have been drafted to steer the research process to address the knowledge gaps and define the next steps of the thesis project. The research objective of the thesis project is to develop an INDI controller which can stabilize and guide VSQP in all configurations. In this optic, the research will focus on how to augment current INDI solutions to use knowledge from the induced imbalance of OFW and mutating effectiveness of actuators and states. The research will in particular focus on the extension of the actuator allocation methods so to include the wing skew angle as a control variable.

Contents

Preface	i
Executive Summary	ii
List of Symbols	xi
List of Acronyms	xii
List of Figures	xiii
List of Tables	xiv
1 Introduction	1
2 Research Plan Literature Study	3
3 Oblique Flying Wing	4
3.1 Hybrid Drones Benefit and Challenges	4
3.2 Control Challenges of OFW	5
3.3 Modeling of OFW.	6
4 Incremental Nonlinear Dynamic Inversion	8
4.1 Nonlinear Dynamic Inversion	8
4.2 Reduced Model Dependency Control	9
4.3 Pseudo Inverse Control Allocation.	10
4.4 Reference Model	10
4.5 Error Controller	11
4.6 Cascaded INDI	12
4.7 Disturbance Rejection Assessment	16
5 Limitations and Available Solutions of INDI	18
5.1 Actuator Dynamics	18
5.1.1 Pseudo Control Hedging	19
5.1.2 Actuator Dynamics Based Extended INDI.	19
5.2 Time Delay	20
5.2.1 Synchronization Filtering	21
5.2.2 Hybrid INDI	21
5.3 Approximation of Outer Loop Effectiveness.	23
5.4 Control allocation for over-actuated drones	25
5.5 Effectiveness Estimation	28
6 Transition	31
6.1 Motor effectiveness modelling	31
6.1.1 Motor-Prop performance in crossflow	31
6.1.2 Modeling of Moving Rotors.	33
6.2 Extended Incremental Nonlinear Control Allocation	34
6.3 Higher Order Reference Model	35
7 Research Plan for Thesis Project	37
7.1 Knowledge Gap.	37
7.2 Research Objective	37
7.3 Research Questions	38
7.4 Research Strategy	38
7.5 Gantt Chart	39

8 Conclusion	41
References	46
A Attributes and components of VSQP	47

Symbols list

Sign	Description	Unit
$C(u)$	Cost function of Weighted Least Squares problem	-
$G_{1_p}(\Lambda)$	Side motor roll effectiveness	$\text{rad s}^{-2} \text{pprz}^{-1}$
$G_{1_q}(\Lambda)$	Side motor pitch effectiveness	$\text{rad s}^{-2} \text{pprz}^{-1}$
H	Flight altitude.	m
W_u	Diagonal Weighting matrix for the inputs	-
W_v	Diagonal Weighting matrix for the control objective	-
Δ_f	Time lag from filtering	s
Λ	Wing skew Angle	rad
α	Angle of attack.	rad
β	Side slip angle.	rad
D_N	Drag vector in NED	-
G_L	Lift effectiveness matrix	-
G_T	Thrust effectiveness matrix	-
L_N	Lift vector in NED	N
M_{NB}	Transformation matrix from body to NED	-
T_N	Thrust vector in NED	-
\dot{x}_0	Initial time derivative of state	-
\dot{x}_f	Filtered time derivative of state	-
\dot{x}	Time derivative of state	-
η	Attitude vector of the drone	rad
ν	Virtual control vector	-
u	Input vector.	-
ξ	Linear acceleration of drone in NED	m s^{-2}
δ_{aL}	Deflection angle of left aileron.	rad
δ_{aR}	Deflection angle of right aileron.	rad
δ_{eL}	Deflection angle of left elevator.	rad
δ_{eR}	Deflection angle of right elevator.	rad
δ_r	Deflection angle of rudder.	rad
\dot{p}	Time derivative of roll rate.	rad s^{-2}
\dot{q}	Time derivative of pitch rate.	rad s^{-2}
\dot{r}	Time derivative of yaw rate.	rad s^{-2}
γ	Flight path angle.	rad
γ	Scaling factor of primary objective	-
μ	Bank angle.	rad
\bar{x}	State vector.	-
θ	Pitch of attack.	rad
as	Airspeed	m s^{-1}
a	Bandwith of actuator	rad s^{-1}
l_p	Side motor roll arm length	m
l_q	Side motor pitch arm length	m
l	Side motor arm length	m
m	Mass of the drone	kg
p	Roll rate.	rad s^{-1}
q	Pitch rate.	rad s^{-1}
r	Yaw rate.	rad s^{-1}

Acronyms

BEMT Blade Element Momentum Theory.

BET Blade Element Theory.

DOF Degree Of Freedom.

INCA Incremental Nonlinear Control Allocation.

INDI Incremental Nonlinear Dynamic Inversion control.

LMS Least Mean Squares.

MAV Micro Air vehicles.

MAVLab Micro Air Vehicles Laboratory.

NDI Nonlinear Dynamic Inversion control.

NED North East Down reference frame.

OBM On-Board Model.

OFW Oblique Flying Wing.

PCH Pseudo Control Hedging.

PID Proportional Integral and Derivative.

SMC Sliding Mode Control.

TA Transitional Aircraft.

UAV Unmanned Air Vehicle.

VLM Vortex Lattice Method.

VSQP Variable Skew Quad Plane.

WLS Weighted Least Squares.

XINCA Extended Incremental Nonlinear Control Allocation.

List of Figures

1.1	VSQP at $\Lambda = 90^\circ$.	2
1.2	VSQP at $\Lambda = 75^\circ$.	2
1.3	VSQP at $\Lambda = 35^\circ$.	2
1.4	VSQP at $\Lambda = 0^\circ$.	2
3.1	Pressure distribution along chord of OFW [6].	5
3.2	Lift, pitch and roll moment in OFW[6].	5
4.1	Linear reference model of relative degree r [14].	11
4.2	Error controller block diagram [15].	12
4.3	Nested structure of the cascaded INDI controller.	12
4.4	Innerloop INDI	13
4.5	Contents of MAV block	13
4.6	Attitude controller	14
4.7	Outerloop INDI	15
4.8	Simulation of the response of the Drone in the deployment environment.	15
4.9	Position Controller	15
5.1	Linear reference model of relative degree r with PCH [14]	19
5.2	Control structure of hybrid INDI control [28].	22
5.3	Block diagram of complementary filter for angular acceleration estimation [26].	22
5.4	Pitch effectiveness estimation logic diagram	28
6.1	Physical depiction of side-motor arm, wing skew angle and motor numbering in VSQP.	33
6.2	Schematic representation of change in side-motor control arm due to wing skew.	33
6.3	A schematic representation of a XINCA controller [41].	34
6.4	Higher Order Reference Model [42].	36
7.1	Time budget distribution in Gantt chart.	40
A.1	Technical drawing of VSOWQP, dimensions in mm.	48

List of Tables

A.1	Physical characteristics of VSOWQP.	47
A.2	Moments of inertia kg m^2 at different skew angles of VSOWQP.	47
A.3	Components of VSOWQP.	47

Introduction

Unmanned Air Vehicles (UAVs) have grown in popularity thanks to their ability to perform tasks autonomously without requiring constant intervention of an operator. In addition, the ease of operation achieved by hybrid UAVs in vertical as well as cruising phases offers a cheaper and more straightforward solution compared to user based vehicle operation. Hybrid UAVs embed in their design VTOL capabilities typical of multicopters but are also able to harness the efficiency of a wing in cruise thanks to some transitioning procedure. This transition can simply involve a change in attitude or control but can also require a mutation in the fundamental geometry of the drone.

Applications such as high-rise package delivery, off-shore missions and landings on moving platforms require good wind rejection capabilities and can for example be performed by both a UAV or a manned helicopter, with the latter leading to obvious higher costs and deployment times. In order to save resources there is the need for a platform able to operate in gusty environments in an autonomous and efficient way using only a very limited input from an operator. The design under development is best described as a Variable Skew Quad Plane (VSQP) and to the best knowledge of the author it is a first in its category.

In hover mode, the drone operates as a simple quad-rotor and attitude is controlled through differential thrust. In cruise mode the drone operates as a plane and uses aerodynamic surfaces on the wing as well as tail to achieve attitude control. Similarly to a typical quad-plane, the drone achieves forward speed thanks to a push propeller placed at the tail. In contrast though, the proposed design does not have a fixed wing configuration, but rather implements the rotating concept applied in the Oblique Flying Wing (OFW) prototype plane. A central rotating pivot is used to deploy the wing as the lateral rotors are folded in the fuselage structure. This approach is expected to greatly increase cruise efficiency thanks to the combination of the wings lift generation benefits as well as drag reduction from the retraction of the unused rotors while still not affecting VTOL capabilities.

Appendix A reports some fundamental attributes and components of the prototype scaled version of VSQP, which will be used for analysis and tests throughout the thesis project. Contrary to a OFW, which in the literature it is reported to be operated up to a maximum of $60^\circ - 65^\circ$ skew angle [43], the VSQP has an extended range of skew angles from 0° to 90° .

Figure 1.1, Figure 1.2, Figure 1.3 and Figure 1.4 show the geometry of VSQP at different wing skew angles Λ from from 0° to 90° . These are renderings from a preliminary CAD assembly of the VSQP and lack the fuselage components which are under development. The wing is deployed through a servo which rotates a helical screw and so the central pivot gear.

Figure 1.1 shows the VSQP in hover mode. The four motor-props are used to stabilize the drone and the wing is folded in the central body. Figure 1.2 and Figure 1.3 show the drone in the transition phase from hover to forward flight. During transition the wing is deployed similarly to a OFW.



Figure 1.1: VSQP at $\Lambda = 90^\circ$.



Figure 1.2: VSQP at $\Lambda = 75^\circ$.



Figure 1.3: VSQP at $\Lambda = 35^\circ$.

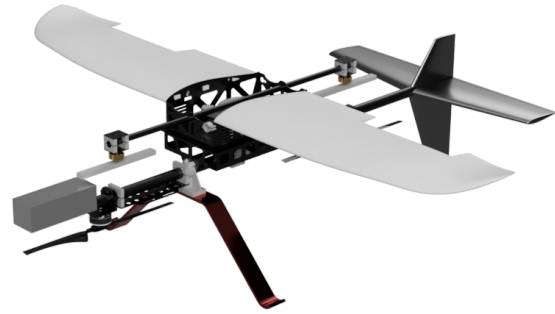


Figure 1.4: VSQP at $\Lambda = 0^\circ$.

Finally Figure 1.4 shows the drone in forward flight configuration with fully deployed wing. In the VSQP, due to the perpendicular placement of the side rotors with respect to the span axis, as the wing is deployed, the lateral motor-props are folded in the fuselage decreasing their drag contribution. Guidance and stabilisation of the drone is then achieved with the aerodynamic surfaces and the push propeller behind the T-tail.

The major challenge of the deployment of such autonomous UAV is the design of a stabilization and guidance control algorithm which can safely operate the drone in a continuous fashion. The very final goal of this research thesis is to apply the developed controller to a scaled prototype of VSQP and achieve safe test flights involving transitions as well as forward and vertical flight maneuvers.

This report starts with an overview of the expected outcomes of the Literature study research in Chapter 2. Chapter 3 aims to report the reasons behind the adoption of a OFW based design as well as the related challenges. In Chapter 4 the general idea behind Incremental Nonlinear Dynamic Inversion control (INDI) is presented. A focus is centered around the additional benefits over Nonlinear Dynamic Inversion control (NDI) and why this control scheme is suitable for non-linear complex systems. In Chapter 5 an analysis is performed of the known limitations of INDI and the solutions presented in the literature are evaluated. Chapter 6 reports an analysis of the expected changes in platform dynamics during transition as well as a review of INDI control solutions to the transition of hybrid drones. Chapter 7 outlines the knowledge gap in the literature which has to be addressed to achieve optimal and safe control of VSQP with INDI. A focus is centered around the drafting of proper research questions which can steer the research project to achieve the final research objective. A Gantt chart is used to subdivide the time budget of the thesis project to different work packages. Finally, Chapter 8 summarizes the most important conclusions from the literature review process, highlighting the contribution to the shared body of knowledge.

2

Research Plan Literature Study

This chapter outlines the driving goals of the Literature study for the Thesis project "Incremental Non-linear Dynamic Inversion Controller for Variable Skew Quad Plane".

As mentioned in Section 3.1, VSQP aims to solve some problems encountered by hybrid drones by employing a central pivot rotating wing alike the one of a OFW. On the other hand OFW is a design concept which is infamously known for the control complexity. The first goal of the Literature Study logically is to address the following Research Objective:

“What are the control challenges of an OFW? Which solutions are documented in the literature for the mentioned problems?”

The answer to the first Research Plan Objective will determine which characteristics are to be expected from a control law that can successfully fly VSQP. As it will be discussed in Chapter 3 and Chapter 4, INDI is found to be the optimal control solution to the problem. Therefore the second aim of the Literature review is to better understand the working mechanism of INDI. In particular it is important to understand the embedded assumptions in the derivation of the fundamental INDI control law and whether they apply to the considered case. Furthermore, in order to develop a fully working controller for VSQP it is crucial to understand from the Literature which challenges have been encountered in the INDI based control of Micro Air vehicles (MAV) and which solutions have already been proven to enhance performance. Therefore the second aim of the research plan is:

“What are the fundamental concepts behind INDI control? What are the benefits of INDI over counterparts? Which challenges and solutions does the Literature report for the implementation of INDI on MAVs? ”

The INDI controller in order to perform transition needs to be complemented with some knowledge regarding the expected dynamics of the platform during the skewing process. Therefore, it is important to understand what has been researched in the literature with regards to the transitional dynamics of UAVs.

“What are the expected changes in vehicle dynamics during transition? What is documented in the literature in regards to INDI control of hybrid drones in transition ?”

In conclusion, answering the Research Plan Objectives of the Literature Study will ideally trace the future steps to be undertaken in the effort to design an INDI controller for VSQP. Another outcome will be the identification of knowledge gaps which will steer the research process to evaluate novel solutions, as a result contributing to the shared body of knowledge.

3

Oblique Flying Wing

This chapter aims to present the reasons behind the adoption of some design characteristics of the OFW. First the challenges of multicopters and conventional hybrid drones are discussed. Subsequently, the novel VSQP design is described with a focus on how it is set to solve the mentioned problems. Finally, the newly introduced challenges of the platform are discussed together with current solutions proposed in the literature.

3.1. Hybrid Drones Benefit and Challenges

Hybrid UAVs, also referred to as Transitional Aircraft (TA), can be regarded as combination of a multicopter and a fixed wing which aims to harness the benefits of both design. Hybrid UAVs embed in their design VTOL capabilities typical of multicopters but are also able to harness the efficiency of a wing in cruise thanks to some transitioning procedure. This transition can simply involve a change in attitude or control but can also require a mutation in the fundamental geometry of the drone. Higher cruise efficiency results in increased range, endurance, payload carrying capacity and maximum forward speed compared to typical rotorcraft, as mentioned by Serrano [44]. Recent survey shows that Hybrid UAV are rapidly growing in popularity and are forecast to successfully conquer the UAV market [45].

The choice of developing the novel VSQP is directed towards improving some challenges common to many hybrid UAV designs such as Tail-sitters and Quad-Planes. Wang, Zhang, and Yang [1] argue that large aerodynamic surfaces add little benefit in hover due to the limited airspeed. Actually, they introduce aerodynamic moments due to wind gusts which are hard to control, especially in the yaw axis. This occurs because when hovering, yawing moments are often mostly generated as a reaction to motor pairs spinning in equal direction that are commanded a higher thrust. This results to be the weakest control action among the controlled axis because it does not directly use the thrust vector to induce a moment but rather only the reactionary torques. Therefore, it can result expensive to generate enough torque to counteract the moments induced by the large aerodynamic surfaces. VSQP by storing the wing in the fuselage greatly decreases the area upon which wind gusts can act, in turn augmenting the disturbance rejection capabilities of the drone.

The second challenge to be addressed is the increased drag in cruise due to the motor-props being over-designed for hover. Vertical flight, as already mentioned, results to be the most power hungry flight phase and so more powerful or numerous motor-props are needed to generate enough lift. Maldonado, Sarker, and Chowdhury [2] make the example of the Panther hybrid drone from the Israel Aerospace Industries which makes use of two tilt rotors on the wing and a stationary rotor in the rear. The rear rotor is designed to provide the extra needed lift in vertical flight. On the other hand, in cruise the rear rotor is deactivated but because exposed to the flow it adds unnecessary drag to the system. VSQP in forward flight stores the unused side rotors in the fuselage, thus not disrupting the flow around the wing and not adding unnecessary drag.

Moreover, the concentration of the majority of the mass moment of inertia along one axis can also intro-

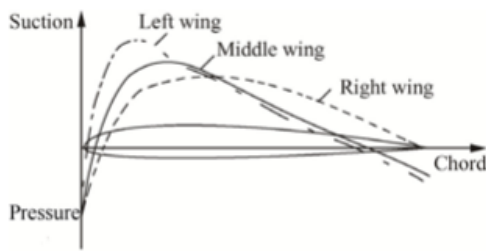


Figure 3.1: Pressure distribution along chord of OFW [6].

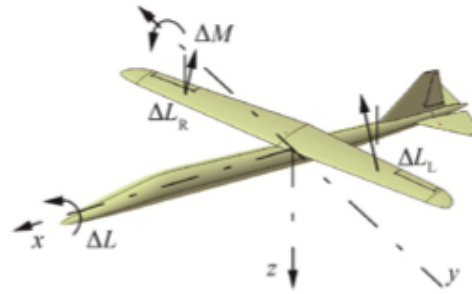


Figure 3.2: Lift, pitch and roll moment in OFW[6].

duce some room for improvement in the platform design. More precisely, in hover the wing is folded in the fuselage, concentrating its mass along the longitudinal axis. In turn, the mass moment of inertia of the roll axis is significantly decreased while along the pitching axis it increases by only a few percentage points due to the already present and fixed longitudinal structure. Therefore, the side rotors compared to the longitudinal motors can be scaled down to smaller, lighter but also more reactive motors. In a nutshell, the exploiting of the favorable mass moment of inertia distribution can lead to a lighter and more aggressive drone.

On the other hand, smaller side rotors, which will most likely run smaller propellers, have lower rotational inertia, meaning that in order to counteract the yawing moment introduced by the longitudinal motors, faster RPM need to be commanded, leading to possible saturation. It can be argued that such problem can be solved for a range of RPM by smartly angulate the side motor thrust vectors to produce a yawing moment. On the other hand, such method adds complexity to the control problem and requires a detailed analysis of which angles produce an optimal control performance. In order to simplify the initial development of the controller of VSQP only a single model of motors is used.

Finally, the ability to change the footprint of the VSQP by rotating the wing can increase the packability of the product, allowing for easier storage and deployment [3].

3.2. Control Challenges of OFW

In contrast to the many benefits discussed, the use of an OFW design also leads to a number of disadvantages. The most clear disadvantage is the complexity of the control problem of such design. Conventional aircraft motion can usually be described by decoupling the longitudinal and lateral modes thanks to the symmetry in the geometry and in the force moment balance. As a result, the task of designing control laws to enhance flying qualities is simplified. In an OFW motions are coupled by aerodynamic and inertial moments [4] and as such stabilisation becomes a less straight forward task[5, 3]. The inertial coupling can be easily understood by analyzing the inertial tensor matrix. The inertial tensor highlights that the cross products of inertia I_{xy} and I_{yx} are non-zero in contrast to symmetrical aircraft [6]. This can be visualized by realizing that at all skew angles, made exception for the fixed wing configuration, the wing creates a mass distribution imbalance with respect to the longitudinal and vertical axis.

The aerodynamic coupling instead needs some further insights to be understood, but is well described in the literature [6]. Consider an OFW with the right wing swept forwards and consequently the left wing swept backwards as shown in Figure 3.1. Yue et al.[7] mentions that due to the asymmetrical wing layout a non-negligible side force is experienced by the OFW. This occurs because the lateral component of the drag vector for both half wings is in the same direction as opposed to symmetrical wings in which the lateral drag components cancel each other. This means that the OFW generates a side force which is not present in conventional symmetrically swept aircraft. This side force also increases with higher skew angles.

Mcmurtry, Sim, and Andrews [8] argue that pilots in the AD-1 oblique wing program actively used left sideslip to compensate for the induced side force. More precisely, the author argues that a sideslip of 1.5° delivered satisfactory lateral control authority up to a skew angle of 60° . Moreover, both Mcmurtry, Sim, and Andrews and Wang, Xu, and Yue argue that a banking maneuver can be performed to use the generated lift vector to compensate for side force. Finally, Mcmurtry, Sim, and Andrews mention that tilting forward the pivot point of the wing would have the effect of banking the wing while leaving the fuselage unbanked. On the other hand, tilting the pivot adds structural complexity and requires strengthening structures and therefore it is not a viable solution for VSQP.

In a nutshell, the side force can be trimmed by either introducing a sideslip angle or a bank angle which can be achieved using many combinations of aileron, rudder and elevator.

Moving on, the pressure distribution along the chord-wise direction is affected by the span-wise component of airspeed as shown by Figure 3.1. Wang, Xu, and Yue [6] argue that the left swept back wing experiences a higher leading edge suction than the right swept forward one. The authors argue that the higher suction leads to higher generated lift. As a consequence, the left backwards swept wing generates higher lift than the right wing, in turn producing an overall pitch down moment and positive rolling moment as shown by Figure 3.2.

Another consequence of the non symmetrical lift distribution is that the left aileron will generate more lift than the right aileron, meaning that they have to be modeled in different fashion.

In the conventional OFW these moments are trimmed through the deployment of both the ailerons as well as the differential horizontal control surfaces [6]. A differential horizontal control surface is often needed because moment balance can easily saturate ailerons at high wing skew angles. One must realize that the ailerons have pitch moment arms in opposite direction with respect to each other. This occurs because the center of gravity can be safely assumed to be around the pivoting point or in other words lying on the longitudinal axis in between the two ailerons. Therefore, the deployment of the ailerons not only generates a rolling moment but also a pitching one. As a consequence the elevators have to work in symbiosis with the ailerons to balance the aerodynamic moments.

Moreover, as the skew angle increases, the roll and pitch arm respectively decrease and increase. The reduction in rolling arm leads to lowered roll effectiveness of the ailerons. Therefore, bigger deflections will be required of the ailerons which can lead to saturation. A common solution in OFW designs is then to implement a differential horizontal surface which can help stabilize the aircraft even at high skew angles [6].

The span-wise component of airspeed also dictates how stall develops along the wing. Logically, the last area of the wing swept by the flow is the one which will experience divergence and so stall sooner. Therefore, the right wing first stalls at the root and later at the right aileron. In contrast, for the left wing stall occurs first at the left aileron and then moves towards the root. This leads to the situation in which the left aileron can be easily stalled at the flight envelope limits, resulting in sudden loss in controllability. It is then crucial for the VSQP not to perform transition at low airspeed or high pitch angles which could lead to hardly recoverable stall.

Final disadvantage of the OFW design is that aereolastic divergence of the forward swept wing has been observed at low airspeed [4, 3]. Although this phenomenon generates instability, complex but possible control laws can be developed to deliver acceptable handling qualities [4].

3.3. Modeling of OFW

In conventional aircraft controller design, models which make use of aerodynamic derivatives are used to simulate the response of the platform. These coefficients are usually extrapolated from flight data. Often, lateral and longitudinal motion are decoupled and analyzed separately to simplify the control problem. It is clear now though that for OFW such simplification is not possible due to the coupling in inertia and aerodynamic forces. Therefore, a new solution is required to allow for the modelling of the platform.

Maine [9] presents a method to estimate the aerodynamic derivatives from flight data of a OFW through the use of a maximum likelihood estimation. Maine mentions that in theory conventional methods for the estimation of stability and control derivatives can be applied to a 5 Degree Of Freedom (DOF) system such as an OFW (the 6th DOF which is velocity can still be ignored). On the other hand, the computational complexity, the inaccuracy of the linear aerodynamic model and the limited data set makes the conventional approach unattractive. Maine proposes to achieve analysis by Separation of Modes, as it is done for conventional aircraft, by eliminating the differential equations of lateral motion from the longitudinal analysis and vice-versa. This is achieved by assuming that on-board sensors, which measure the states of interest, have little noise meaning that the measured lateral-directional responses can be used as inputs to the longitudinal equations and vice-versa.

The proposed modelling technique is concluded to deliver positive results and an unexpected 100% utilization of the data even to the surprise of the author. On the other hand, it can be argued that the assumption of noise-free sensors is not applicable to MAV for which airborne equipment is not as accurate as for larger aircraft which can carry larger payloads [10].

Pang, Mei, and Chen [11] further present how a set of conventional aerodynamic derivatives coefficients can be used to create a model for a OFW near space vehicle by simply deriving the equation of motion from Newton's second law for a complete unsimplified inertia tensor.

However, the issue with the methods presented by Maine and by Pang, Mei, and Chen is that the techniques still aim to solve a 39 unknowns problem, being the relevant aerodynamic derivatives, which represents still a complex task to perform accurately. Furthermore, using aerodynamic derivatives to linearize a plant which in reality due to the couplings is nonlinear, introduces discrepancies which can lead to control performance degradation.

It is then clear that VSQP presents multiple non-linearities due to aerodynamic and inertia coupling which can be complex and expensive to properly model. There is then the need for a control scheme which is able to deal with non-linearity and does not depend on an extensive model of the drone. Wang, Xu, and Yue [6] propose to use a Nonlinear Dynamic Inversion (NDI) controller which follows an ideal model reference to provide acceptable handling qualities. This approach requires to know only the effectiveness profiles of the actuators and the desired response characteristics, drastically reducing the number of unknowns to be estimated. The proposed simulation results depict a flight control which is able to track the reference model and provide acceptable handling qualities. Yue et al. [7] further proposes a Sliding Mode Control (SMC) approach to deal with the changes in inertia, center of gravity position and effectiveness of controls as the wing is being skewed. The sliding mode controller promises to adapt to the parameter changes of the OFW during skewing thanks to appropriately designed sliding functions and approach rates.

On the other hand, in order to define the affine system behind NDI and SMC, some sort of model of the state and control input effects on the dynamics of the platform has to be estimated. Any modelling inaccuracies, which are almost unavoidable on the MAV scale due to limited sensor accuracy and which only affect performance when conducting a real flight test, are not compensated by the NDI control scheme. Therefore, a more robust and less model dependent control law is required. Chapter 4 proposes INDI as a solution focusing on the improvements brought by this control scheme over conventional NDI controllers.



Incremental Nonlinear Dynamic Inversion

This chapter aims to portray the principles and fundamental theories of INDI as reported in the Literature. Section 4.1 briefly explains the principles of NDI, theory from which INDI is further developed. A focus is centered around which challenges of NDI are set to be solved from INDI. Section 4.2 outlines specifically how INDI thanks to reduced model dependency can become a more robust and easier to implement control scheme than NDI. Section 4.3 discusses how the incremental control law is used to obtain control allocation between the control elements. Section 4.4 present how Reference Models can be used to define smooth trajectories to be tracked by the INDI controller. Section 4.5 describes the reason behind the need of an Error Controller in the Reference Model and outlines its structure. Section 4.6 discusses the structure of a cascaded INDI controller explaining the purpose of each control group. Finally, Section 4.7 reports the benefits of INDI in disturbance rejection such as wind gusts.

4.1. Nonlinear Dynamic Inversion

Classical control theory makes use of Proportional Integral and Derivative (PID) blocks to enhance robustness and controllability of a given platform. Often, a detailed and expensive gain tuning procedure is needed to achieve the highest performance level. Furthermore, a given gain set cannot optimally serve the full flight envelope due to the platform aerodynamic response continuously changing with the different flight phases. Therefore, gain scheduling is implemented to assure near optimal performance in all flight phases. Logically, such gain set profiling can require substantial time and detailed models of the platform.

NDI was developed as a solution to robust nonlinear control with limited resources and modelling needed. More precisely, NDI aims to linearize a certain nonlinear platform by means of state or outputs feedback [12]. In other words, the aim of NDI is to generated a closed-loop system that behaves as linear system starting from a non-linear open-loop. The assumption at the base of NDI, reported in mathematical form for a fixed wing aircraft by Equation 4.1, is that a change in angular rates can be expressed as the summation of the influences of state and control input respectively.

$$\begin{bmatrix} \dot{p} \\ \dot{q} \\ \dot{r} \end{bmatrix} = \mathbf{f}_f(\bar{\mathbf{x}}) + \mathbf{g}_f(\bar{\mathbf{x}})\mathbf{u} \quad (4.1)$$

where: $\bar{\mathbf{x}} = [p, q, r, \alpha, \beta, \mu, as, \gamma, H]^T$
 $\mathbf{u} = [\delta_{aL}, \delta_{aR}, \delta_r, \delta_{eL}, \delta_{eR}]^T$

In other words, the change in angular rates is equal to the summation of a function $\mathbf{f}_f(\bar{\mathbf{x}})$ of the state vector and the multiplication of the effectiveness matrix $\mathbf{g}_f(\bar{\mathbf{x}})$ and the control input vector [6]. Therefore, with some limited modelling knowledge of the aerodynamics of the aircraft and effectiveness of the control elements, one can generate a set of first order Taylor expansions centered around the initial

state to estimate $f_f(\bar{x})$ and $g_f(\bar{x})$.

Rearranging Equation 4.1 and using a pseudo-inverse, the optimal control vector u to achieve a wanted change in angular rate can be estimated.

$$u = (g_f(\bar{x}))^+ \left(\begin{bmatrix} \dot{p} \\ \dot{q} \\ \dot{r} \end{bmatrix} - f_f(\bar{x}) \right) \quad (4.2)$$

where: " + " = Pseudo-inverse

Equation 4.2 shows that with some modelling knowledge of the forces and dynamics acting upon the drone it is possible to obtain a linear control law for a nonlinear system.

On the other hand, inaccuracies and simplifications introduced in the models can have a detrimental effect on the controller performance [12]. In addition, the development of accurate models of MAV can require expensive resources and is limited by the small sensors which can be carried by a MAV [10]. Therefore, a less model dependent control law is needed for implementation in MAV, leading to the development of INDI.

4.2. Reduced Model Dependency Control

The incremental version of nonlinear dynamic inversion control, also known as INDI, has been described since the late 1990s early 2000s to be a less model dependent and more robust solution than NDI [13]. The idea behind INDI is to replace the dynamic model of the platform with data retrieved online by sensor readings.

Now, consider a more general expression of Equation 4.1, in which the derivative in time of the angular rates is a function of state and control input.

$$\begin{bmatrix} \dot{p} \\ \dot{q} \\ \dot{r} \end{bmatrix} = \dot{x} = f(x, u) \quad (4.3)$$

Equation 4.3 can be linearized around the initial point, subscripted with "0", by means of a first order Taylor expansion.

$$\begin{aligned} \dot{x} &\simeq f(x_0, u_0) + \left. \frac{\partial f(x, u)}{\partial x} \right|_{x=x_0, u=u_0} (x - x_0) + \left. \frac{\partial f(x, u)}{\partial u} \right|_{x=x_0, u=u_0} (u - u_0) \\ \dot{x} &\simeq \dot{x}_0 + \underbrace{F(x_0, u_0)}_{\Delta_x} (x - x_0) + \underbrace{G(x_0, u_0)}_{\Delta_u} (u - u_0) \end{aligned} \quad (4.4)$$

Equation 4.4 can be further simplified by assuming the time-scale separation principle to be valid. This principle states that the contribution to the change in angular acceleration due to the change in angular rates and body speeds is negligible compared to the contribution of changing control inputs [6, 10]. This is because the control elements are assumed to be much more effective and having a faster response than changes in the drone's state. This assumption has been adopted in multiple works in the literature, ranging from drones with fast actuators and high enough sampling rate [10], to nonlinear flight control of helicopters [46].

$$F(x_0, u_0) \Delta x \ll G(x_0, u_0) \Delta u \quad (4.5)$$

Equation 4.5 reports in mathematical terms the Time-scale separation principle. Equation 4.6 instead reports the simplified version of Equation 4.4 using the time-scale separation method.

$$\dot{x} \simeq \dot{x}_0 + G(x_0, u_0) (u - u_0) \quad (4.6)$$

Now, by realizing that \dot{x}_0 is nothing other than the current angular acceleration, one can understand how the dynamic model of the drone can be substituted by simple sensor measurements, thus explaining the origin of the labeling of INDI as a sensor-based approach.

Rearranging and using a pseudo-inverse of the effectiveness matrix, it is possible to derive the incremental control law of INDI for a virtual control vector ν of desired angular accelerations.

$$\Delta \mathbf{u} \simeq (\mathbf{G}(\mathbf{x}_0, \mathbf{u}_0))^+ (\boldsymbol{\nu} - \dot{\mathbf{x}}_0) \quad (4.7)$$

4.3. Pseudo Inverse Control Allocation

Equation 4.7 shows that the basic principle of INDI is to calculate the required change in control input to close the error to a desired angular acceleration setpoint by knowing the effectiveness values of each actuator over each controlled axis. The effectiveness values are then saved in an effectiveness matrix which is inverted and multiplied with the desired change in angular acceleration to estimate the required change in control input. Similarly, for the outerloop the effectiveness of changes of certain variables as thrust and attitude on linear accelerations are used to calculate the required change in the control variables to achieve a reference signal.

Now, the inversion of the effectiveness matrix in some cases cannot be performed using classical methods. This occurs because in the case of a non-square matrix (e.g. the number of actuators does not equal the number of controlled axes), the standard definition of inverse, shown by Equation 4.8, does not hold. Indeed, the matrix A and its inverse A^{-1} will have respective sizes of $m \times n$ and $n \times m$.

$$AA^{-1} = A^{-1}A = I \quad (4.8)$$

This means that $AA^{-1} \neq A^{-1}A$ with the left hand side of the equation leading to an Identity matrix of size $m \times m$ while the right hand side to an Identity matrix of size $n \times n$.

In order to perform the inversion, the Moore-Penrose algorithm, also known as pseudo inverse, is used. The pseudo inverse returns the minimum Euclidian norm solution to a system of linear equations with multiple solutions. Using the pseudo inverse to calculate the optimal control vector \mathbf{u} , leads to the solution which has the smallest two-norm which should also theoretically lead to the smallest control power [6].

In order to compute the Pseudo inverse first it must be assessed whether the starting effectiveness matrix has linearly dependent columns or rows. It can happen that for certain states the outerloop effectiveness matrix, described in Section 5.3, is greatly simplified and that column or row independence is lost due to the role that the rotation matrix from body frame to North East Down reference frame (NED) plays in its derivation. Applying then the Pseudo Inverse algorithm with the wrong assumption leads to incorrect results and degradation of control for which is difficult to identify the cause in an online application such as drone control.

If the matrix A has linearly independent columns, the Pseudo Inverse is calculated as shown in Equation 4.9.

$$A^+ = (A^T A)^{-1} A^T \quad (4.9)$$

If the matrix has linearly independent rows, the Pseudo Inverse is calculated as shown in Equation 4.10.

$$A^+ = A^T (A A^T)^{-1} \quad (4.10)$$

4.4. Reference Model

Section 4.2 has shown how in INDI only knowledge of the effectiveness matrix of a platform has to be known to compute an incremental control input to achieve a desired pseudo control ν . On the other hand, it has not been discussed yet how ν is computed. Bhardwaj et al. [14] argue that reference models can be used to generate feasible smooth reference trajectories directly from the control variables. Figure 4.1 shows how the schematic inner workings of a linear reference model which produces a pseudo control vector which is the $r - th$ derivative of the control variable.

For the control scheme to work for a system of relative degree r it is important that the reference trajectory is smooth such that the $r - th$ derivative exists. The coefficients \mathbf{k} have to be chosen in order

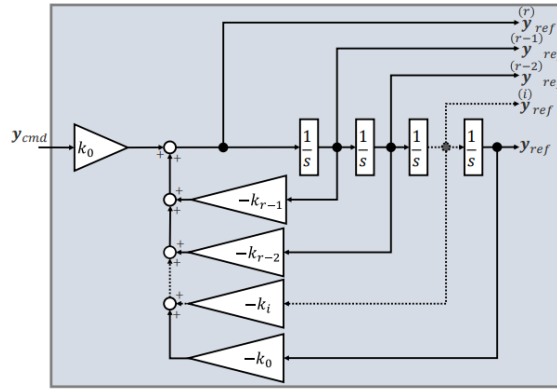


Figure 4.1: Linear reference model of relative degree r [14]

to meet the considered platform capabilities.

It follows that the reference pseudo control vector ν_{ref} generated by the linear reference model of degree r is :

$$\nu_{ref} = \begin{bmatrix} \nu_{1,ref} \\ \vdots \\ \nu_{m,ref} \end{bmatrix} = \begin{bmatrix} y_{1,ref}^{(r_1)} \\ \vdots \\ y_{m,ref}^{(r_m)} \end{bmatrix} \quad (4.11)$$

where: $y_{i,ref}^{(r_i)}$ = r_i - th derivative of $y_{i,cmd}$

Raab et al. [15] further argue that another important output of the reference model is the reference external state trajectory ξ_{ref} , which collects the lower order derivatives of ν_{ref} as depicted by Equation 4.12

$$\xi_{ref} = \begin{bmatrix} \xi_{ref}^1 \\ \xi_{ref}^2 \\ \vdots \\ \xi_{ref}^m \end{bmatrix}, \text{ where } \xi_{ref}^i = \begin{bmatrix} y_{i,ref} \\ \dot{y}_{i,ref} \\ \vdots \\ y_{i,ref}^{(r_i-1)} \end{bmatrix} \text{ and } i = 1, 2, \dots, m \quad (4.12)$$

The availability of the reference state trajectory allows for the detection and correction of deviation of the lower level derivatives of the pseudo control vector as described in Section 4.5.

4.5. Error Controller

Raab et al. [15] argue that reference model only provides feed-forward control by generating pseudo control vectors which track the reference trajectory. Therefore an error controller is required to adjust the plant external state trajectory to the reference trajectory in case of a deviation. The authors propose to create a feedback loop with proper gains of the trajectory error χ defined as:

$$\chi = \xi_{ref} - \hat{\xi} \quad (4.13)$$

where: $\hat{\xi}$ = Estimate of the external state (e.g. from onboard sensors)

Figure 4.2 shows how the calculated trajectory error can be used in a Proportional-Integral loop to close the deviation and compensate for steady state errors.

The output of the error controller, ν_{ec} , can then be added to the pseudo control vector calculated by the reference model ν_{ref} , to generate the input to the INDI control law ν_{des} .

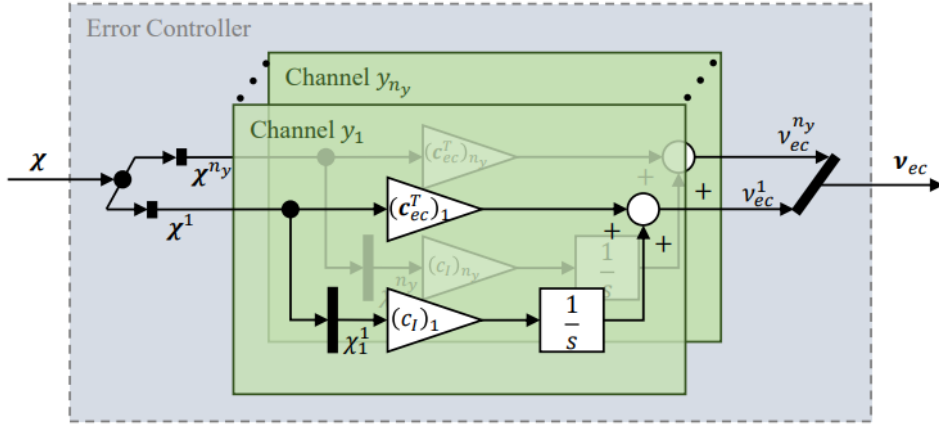


Figure 4.2: Error controller block diagram [15].

4.6. Cascaded INDI

Bhardwaj et al. [14] and Raab et al. [15] discuss an INDI controller structure which makes use of a single dynamics inversion procedure to track a given pseudo control vector by incrementally changing the control input. Section 4.4 and Section 4.5 discussed how for such approach a reference model is needed to generate the pseudo control vector and an additional error controller is needed to provide feedback control on the deviations of the external state trajectory. All things considered, the method is proven to robustly provide control for a hybrid VTOL prototype aircraft.

Smeur, Croon, and Chu [16] instead propose a cascaded implementation of INDI for attitude and position control of MAV which embeds the tasks of pseudo control generation and disturbance rejection directly in one single structure. The method makes use of two INDI control loops: inner and outer loop. Inner loop provides stabilisation of the platform while outer loop provides guidance. Two different dynamic inversion routines are performed, one for each loop, therefore needing two different sets of effectiveness matrices. Figure 4.3 shows a simple representation of the different levels of the cascaded controller.

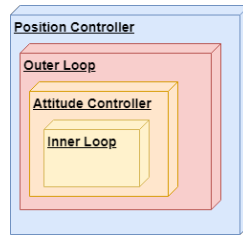


Figure 4.3: Nested structure of the cascaded INDI controller.

Figure 4.3 highlights that the most basic level in the controller is the inner loop. Smeur, Chu, and Croon [10] present the control law of the innerloop for a simple quad-rotor as reported in Equation 4.14.

$$\omega_c = \omega_f + (G_1 + G_2)^+ \left(\nu - \dot{\Omega}_f + G_2 z^{-1} (\omega_c - \omega_f) \right) \quad (4.14)$$

Differently from the general control law of Equation 4.7 where only a single effectiveness matrix G is present, Equation 4.14 makes use of two distinct matrices: G_1 and G_2 .

The first matrix G_1 represent the induced change in rotational acceleration due to a change in actuator input. This matrix has as many columns as the actuators (4 for a quad-rotor) and as many rows as the control objective (4 as $\nu = [\Delta T, \dot{p}, \dot{q}, \dot{r}]^T$).

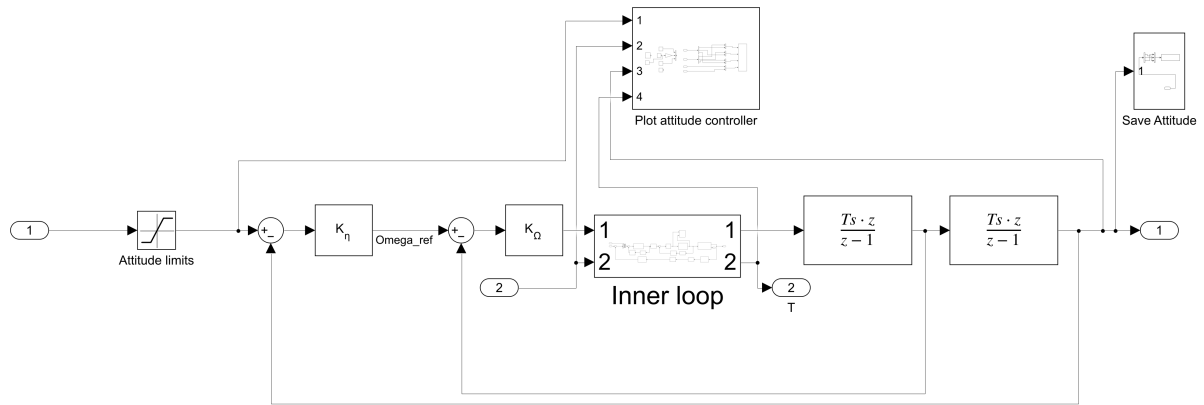


Figure 4.6: Attitude controller

mance of the controller.

The attitude controller is in turn contained in the outerloop controller. The aim of the outerloop controller is to generate a series of thrust increments and attitudes which allow the drone to track a reference linear acceleration signal. Therefore, the input to the outerloop controller is a set of reference linear accelerations in the NED reference frame.

First, the reference linear acceleration setpoint is passed through a saturation limit block. This prevents unachievable accelerations for the platform to be commanded. The specific limits can be evaluated by test flying the platform. Subsequently, the outerloop effectiveness matrix G_n is pseudo inverted and used to calculate the required change in thrust level and attitude. Note that, as explained in Section 5.3, G_n is itself a function of Thrust and attitude, meaning that it has to be re-evaluated at each iteration of the controller.

The outerloop control variables are $[\Delta T, \phi, \theta]^T$ which are passed further to the attitude controller. The heading instead, is not calculated through the inversion of the outerloop effectiveness matrix but rather by the heading controller. The aim of the heading controller is to minimize sideslip β . This is especially important for drones with forward flight capabilities as it assures that the body x axis is aligned with the direction of travel, maximizing the performance of the lifting surfaces. Smeur, Bronz, and Croon [24] and Wijngaarden, Smeur, and Remes [29] all describe the working mechanism of the sideslip controller as reported by Equation 4.15.

$$\dot{\psi}_{\text{ref}} = \underbrace{\frac{g \tan(\phi)}{V}}_{\text{feedforward}} + \underbrace{K_{\beta} \beta}_{\text{feedback}} \quad (4.15)$$

where: $\dot{\psi}_{\text{ref}}$ = Rate of change of reference heading angle
 g = gravitational constant
 ϕ = Roll angle
 V = Airspeed
 K_{β} = Constant gain
 β = Sideslip angle

The rate of change of the reference heading angle is a combination of feed forward and feedback control. The feed forward control describes the rate of change of heading to accomplish a coordinated turn. The feedback control removes sideslip by commanding a heading rate proportional to current β . In simulation the sideslip angle can be simply calculated by comparing the current heading to the direction of the velocity vector. For real life applications, Smeur, Bronz, and Croon [24] suggest to perform an initial test of the platform with a sideslip vane and find a numerical relation between β and the accelerometer registered side specific force f_y . This relation can then be used for other flights to estimate β based on f_y .

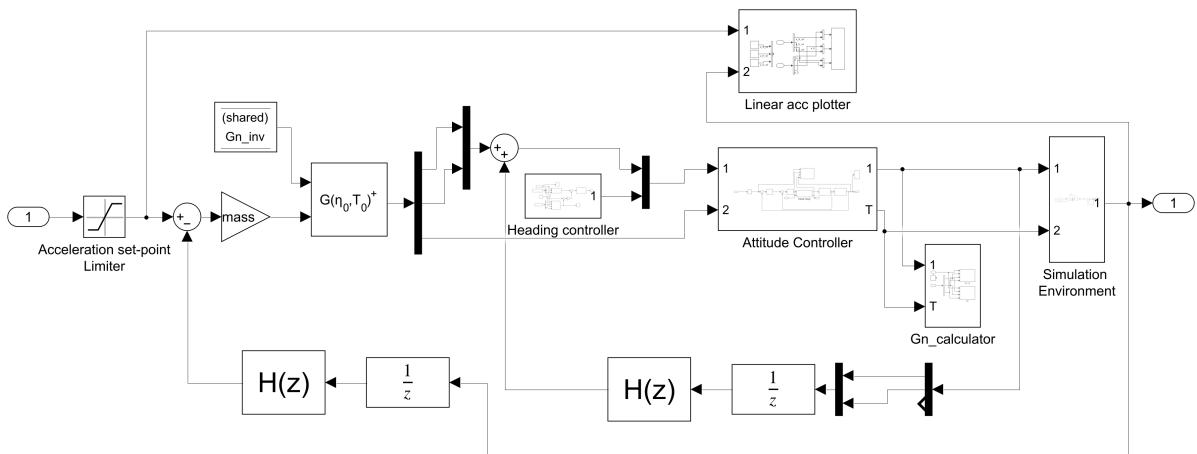


Figure 4.7: Outerloop INDI

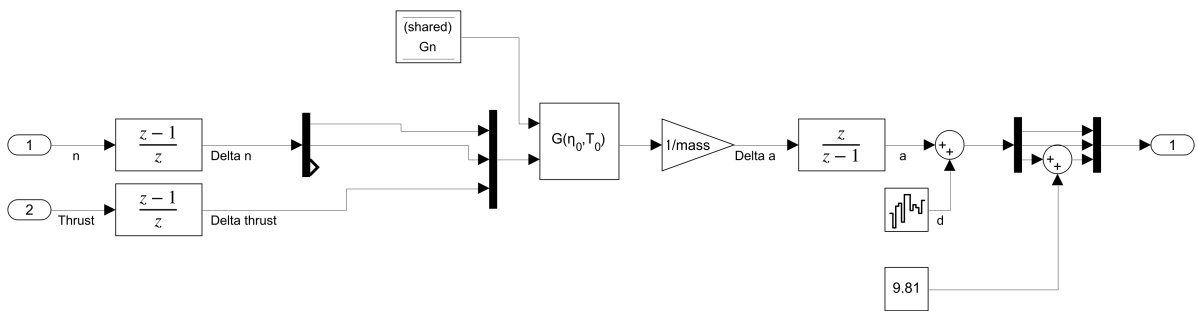


Figure 4.8: Simulation of the response of the Drone in the deployment environment.

Figure 4.8 shows the contents of the block Simulation environment. This block has a similar role to the one the MAV block plays for the innerloop. The aim of the Simulation Environment block is to estimate the achieved linear acceleration given the thrust level and attitude of the drone. This is achieved by using the knowledge carried by the outerloop effectiveness matrix as well as a noise signal to simulate unmodelled influences. In addition, the gravitational acceleration is added to the vertical axis in order to make the outerloop controller command a thrust level able to compensate for the weight of the drone. Further insights in the aerodynamics of the drone as for example Drag estimations can be added in this block.

The final layer of the Flight Control System is the position controller and is shown by Figure 4.9. The input to this layer is a reference position vector in NED and the output is the current position of the Drone. Similarly to the attitude controller, the linear acceleration setpoint is generated by PD gains,

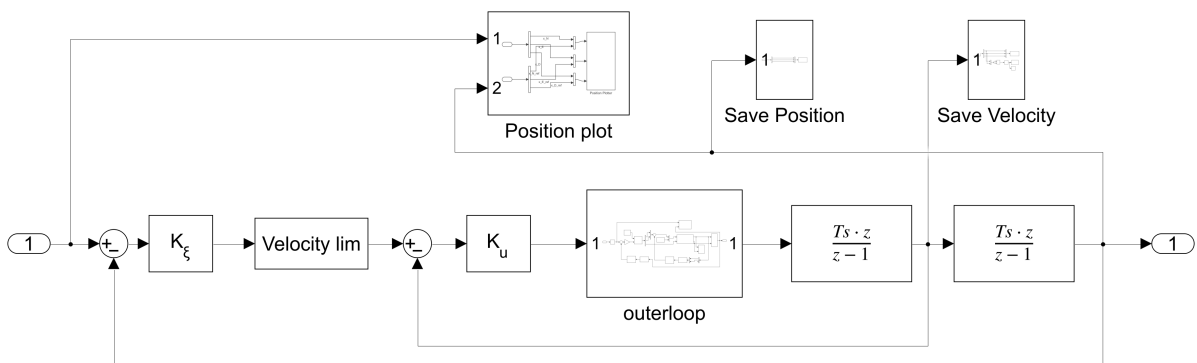


Figure 4.9: Position Controller

respectively K_ξ and K_u . These gains can be tuned by analyzing the tracking performance of the drone of different position setpoints. The reference velocity is limited in order to not command setpoints which exceed the capabilities of the platform. Finally, the output of the outerloop controller is integrated twice in order to estimate the current position of the drone.

4.7. Disturbance Rejection Assessment

Disturbance rejection is a critical requirement for a controller implemented in a drone designed to be deployed in outdoor conditions. This is because disturbances as wind gusts can produce instabilities that if not accounted for can lead to crashes.

One of the main advantages of INDI over PID in the field of MAV control has been proven to be fast disturbance rejection [16, 17]. This occurs for two main reasons. First, in an INDI outerloop what is ultimately being tracked is a linear acceleration reference, in contrast to PID in which the drone reacts to changes in speed and position only. Eventually, this results in the control of the fastest changing variable, which in turn delivers quick control. PID instead needs to register an error in velocity tracking before initiating a correcting procedure. In turn this leads to the drone having already accumulated a large position or velocity error before reacting to the disturbance.

Surely, it can be argued that fine tuning of PID can make a drone both stable and able to make aggressive corrections. In particular, the integral part of the controller can be tuned to aggressively correct for offsets. On the other hand, an higher integral gain leads also to overshoot in reference tracking, ultimately generating a trade-off to be evaluated [16]. Additionally, gain tuning can be a resource expensive task which compromises the fast and straightforward application to a drone platform.

The trade-off in integral gain tuning between increased offset reduction and corresponding higher overshoot of reference does not apply to INDI. More precisely INDI, due to the incremental nature of its control law, is able to correct for disturbances without having to sacrifice performance. The idea is that any disturbance is registered by the on-board sensors and leads to an increased acceleration error which is then incrementally compensated for. Such assumption is proved to hold in the case in which the control elements can react quick enough and are not saturated.

The improvements in gust rejection brought by INDI have been observed by tracking the position error of a small MAV flying in both a wake of a fan [17], as well as in the Open Wind jet facility of TuDelft [16]. Results have proven INDI resulting in up to 7 fold lower position error due to wind gust compared to conventional PID [16].

Pfeifle and Fichter [18] argue that further enhancement of INDI's wind gust rejection on a winged platform could be achieved by using aerodynamic angles instead of Euler angles in the control law. This occurs because the force and torques disturbances from gusts are mostly caused by changes in the aerodynamic angles and therefore would be directly targeted by the attitude control loop. While these considerations might be true in the theoretical sphere, the practical use of aerodynamic angles on a real drone is hindered by a number of problems. First, specifically designed sensors as angle vanes to measure the aerodynamic angles would have to be added to the platform, increasing overall weight. Second, these sensors are not as widely used in the drone industry as for example gyros, therefore resulting to be less robust and optimized. Finally, VSQP due to the VTOL capabilities is expected to experience a large range of inflow angles and occasionally turbulent flow. Therefore, the task of obtaining accurate measurements from the angle vane sensor can result to be complex [19].

Now, it is clear that thanks to the incremental and sensor based nature of the control law, INDI performs well in gust rejection. Therefore, using INDI on a hybrid UAV, which often suffer from gust disturbances due to the large aerodynamic surfaces which are not present in quad-rotors, can lead to great performance benefits especially in the vertical flight phases of take-off and landing.

On the other hand, one must realize that the disturbance rejection capabilities of INDI do not limit to only wind gust. It must be realized that unmodelled effects, such as the neglected influences of state change

on rotational acceleration in Equation 4.4, are picked up by the on-board sensors as disturbances and consequentially compensated for by the controller. Therefore INDI further decreases model dependency as long as update rate and actuator dynamics can deal with the acceleration reference tracking task. Ultimately, this results in the ability to apply certain model simplifications which might not be very accurate but that fast forward the design process and that are dealt with anyways by INDI.

5

Limitations and Available Solutions of INDI

This chapter aims to outline the known limitations of INDI and describe the solutions proposed in the Literature. First, Section 5.1 presents how Pseudo Control Hedging and an extension of INDI can be used to compensate for actuator dynamics. Section 5.2 outlines the problem of time delay and proposes Synchronization Filtering and Hybrid INDI as solutions. Subsequently, Section 5.3 discusses the derivation of the outerloop effectiveness matrix and how simple but powerful assumptions can facilitate its estimation. Section 5.4 presents a Weighted Least Squares algorithm to solve the problem of control allocation for over-actuated drones. Finally, Section 5.5 presents the challenges in effectiveness profiling and how proper estimation processes and excitation techniques can be used to reveal the platform dynamics.

5.1. Actuator Dynamics

The basic INDI control law derived in Section 4.2 lacks a representation of the actuator dynamics. It is assumed, alike the work of Sieberling, Chu, and Mulder [20], that the platform uses perfect actuators which respond instantaneously to the commanded input. On the other hand, real life, actuators do not respond instantaneously due to the fact that they are real physical systems. A motor for example needs some time to increase the angular momentum and converge to the commanded input. Furthermore, actuators have rate and position limits which have to be considered in the controller.

Li et al.[21] showed in simulation what is the difference in reference tracking between a ideal instantaneous and non-ideal actuator dynamics block. For an ideal actuator, tracking a chirping reference signal is possible without generating an error even at high frequencies. This is a wanted behavior because it means that the platform will be able to track closely any reference signal. In contrast, a real life actuator suffer from lag as well as attenuation of the amplitude of the response at high frequencies. In INDI the deviation from the commanded input signal will be compensated for by incrementally commanded corrections which will further augment the discrepancy, ultimately leading to degradation of control performance.

The response of a variety of actuators can be modeled through a first or second order transfer function as explained in multiple works from the literature [10, 17, 16, 24, 25, 29]. For simplicity, let us consider the more straightforward case of a motor which is modeled through a first order dynamics block. Equation 5.1 shows the common form of a first order actuator dynamics block in the S-domain.

$$\begin{aligned} u(s) &= A(s) u_{cmd}(s) \\ \frac{u(s)}{u_{cmd}(s)} &= A(s) = \frac{a}{s+a} \end{aligned} \tag{5.1}$$

Li et al. [21] and Oppenheimer and Doman [47] present a simple gain tuning method to deal with the tracking error due to non-ideal actuator dynamics. More precisely, Oppenheimer and Doman develops

the method in the Z-domain while Li et al. work in the S-domain.

On the other hand, it must be argued that some assumptions in the derivation of the method might hinder its application on a real world platform. First of all, it is assumed that it is possible to accurately model the dynamics of an actuator with a first or second order dynamics block. However, since this is only an approximation of the real world dynamics, there exist inaccuracies, which if not accounted for are augmented by the proportional gain.

Preliminary test of the method on a feedback signal from the actuator with added noise to simulate model inaccuracies show that instability of the system is achieved. In order to assure stability, a gain M of much lower value than the one described by Oppenheimer and Doman is needed. Furthermore, the method does not account for any possible rate limits of the actuator. Similarly to the actuator dynamics block inaccuracy, the discrepancy between the expected and the actual actuator state can lead to instability of the system. Therefore it is clear that other compensation methods have to be researched further.

5.1.1. Pseudo Control Hedging

Johnson and Kannan [22] argue that the idea of Pseudo Control Hedging (PCH) is to prevent INDI from adapting to selected system input characteristics as for example the actuator dynamics. This is achieved by moving the reference model in the opposite direction (hedge) by an estimate of the amount that the plant did not move due to those system characteristics. In other words, by knowing the saturation, rate limits, parameters of the actuator dynamics block $A(s)$ and state of the drone it is possible to calculate what is the expected actual reaction of the plant $\hat{\nu}$ [14].

$$\begin{aligned}\hat{\nu} &= \dot{x}_0 + G(x_0, u_0)\Delta u \\ &= \dot{x}_0 + G(x_0, u_0) A(s) \Delta u_{cmd}\end{aligned}\quad (5.2)$$

Then it is possible to calculate the reaction deficit ν_h by subtracting the expected actual reaction of the plant $\hat{\nu}$ from the desired pseudo control ν_{des} .

$$\nu_h = \nu_{des} - \hat{\nu}\quad (5.3)$$

Bhardwaj et al. [14] argue that, as shown in Figure 5.1, the hedging effect is incorporated in the

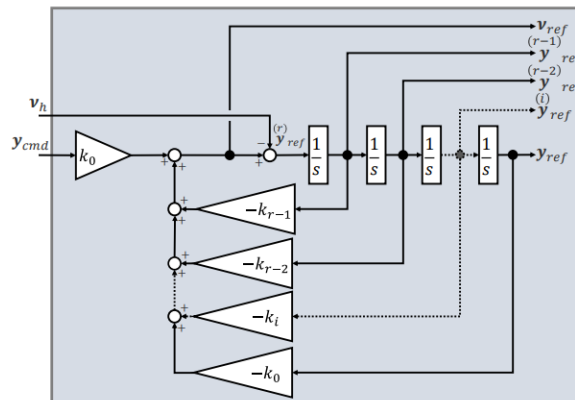


Figure 5.1: Linear reference model of relative degree r with PCH [14]

reference model by recalculating the highest order derivative as :

$$y_{ref}^{(r)} = \nu_{ref} - \nu_h\quad (5.4)$$

5.1.2. Actuator Dynamics Based Extended INDI

Section 5.1.1 has shown how PCH can be used to slow down the reference model dynamics to account for real life actuator dynamics. On the other hand, a more complete method would directly embed knowl-

edge of the actuator dynamics in the generation of the reference pseudo control vector.

Raab et al. [23] suggests to incorporate knowledge of the rate limits of the actuators directly into the control allocation. The idea is then to prioritize faster actuators over slower ones directly at the stage of control allocation. This is achieved by deriving a new INDI control law which is based on an additional derivative of the system output and so embeds knowledge of the "speed" of the actuators.

Raab et al. start by deriving an expression for the true derivative of the pseudo control vector instead of using a Taylor series approximation. Namely for a system defined by $\nu = F(x, u)$:

$$\begin{aligned}\dot{\nu} &= \frac{\partial F(x, u)}{\partial x} \dot{x} + \frac{\partial F(x, u)}{\partial u} \dot{u} \\ &= A \dot{x} + B \dot{u}\end{aligned}\quad (5.5)$$

Now, for simplicity consider a first order dynamics block $A(s)$ as described in Equation 5.1. By realizing that the increment of the command of INDI can be expressed as $\Delta u(s) = u_{cmd}(s) - u(s)$, it is possible to derive that:

$$\begin{aligned}u(s) &= A(s) u_{cmd}(s) \\ u(s) &= A(s) (\Delta u(s) + u(s)) \\ u(s) &= \frac{a}{s+a} (\Delta u(s) + u(s)) \\ s u(s) + a u(s) &= a \Delta u(s) + a u(s) \\ s u(s) &= a \Delta u(s) \\ \dot{u}(s) &= a \Delta u(s) \\ \dot{u}(s) &= K_{act} F_{act}(s) \Delta u(s)\end{aligned}\quad (5.6)$$

where: $K_{act} = a$
 $F_{act}(s) = 1$

What Equation 5.6 shows is that the transfer function $\frac{\dot{u}(s)}{\Delta u(s)}$ can be expressed as the product of a diagonal matrix K_{act} and a diagonal transfer matrix $F_{act}(s)$. Similarly, it is possible to specify a desired behavior of the pseudo control by specifying bandwidth and dynamics.

$$\dot{\nu}(s) = K_v F_v(s) \Delta \nu(s) \quad (5.7)$$

The next step involves performing the Laplace transform of Equation 5.5 by assuming quasi-constant B-matrix, neglecting the state dependent part as per Time Scale Separation principle and substituting it in Equation 5.6.

$$\begin{aligned}\dot{\nu}(s) &= B \dot{u}(s) \\ \dot{\nu}(s) &= B K_{act} F_{act}(s) \Delta u(s)\end{aligned}\quad (5.8)$$

Now it is possible to transform the equation back to the time domain, introduce the substitution $\Delta u_F = F_{act}(s) \Delta u(s)$, perform the pseudo inversion and so obtain the novel control law.

$$\begin{aligned}\Delta u_F &= (B K_{act})^+ \dot{\nu}_{des} \\ &= (B K_{act})^+ K_v F_v(s) \Delta \nu_{des}\end{aligned}\quad (5.9)$$

It is important to realize that now the matrix that is being inverted carries the knowledge of K_{act} or in other words the "speed" of the actuators. Therefore, faster actuators will artificially result to be more effective hence will be allocated more increment in control input and vice versa. This method then results to deliver useful results in the case that a drone can use multiple actuators to control coupled axes.

5.2. Time Delay

As already mentioned in Section 4.2, the control law of INDI makes use of data registered by on-board sensor to approximate the current angular acceleration. More precisely, gyros estimates are used to

measure rotational rates around the 3 body axes. Regardless of the accuracy level, the output of a sensor is a combination of a measurement signal and a certain amount of noise. Such noise is further amplified in the INDI loop due to the rotational rates being differentiated in time to obtain angular accelerations [10]. The noisy angular acceleration measurements can hinder control performance as well as offline effectiveness estimation of the control elements. Therefore, the signal is usually filtered with low pass filters [13] of for example the Butterworth type [24]. The cut-off frequency can be chosen by analyzing which limit allows to obtain a clean signal while still obtaining satisfactory results [10]. Maine [9] in opposition proposes to perform a frequency analysis of the measured vibrations to identify the frequency regions of structural resonance. Subsequently, it is then possible to identify a precise frequency under which the measured noise is minimized.

5.2.1. Synchronization Filtering

As a consequence of filtering, a lag is introduced in the measured signal which if not accounted for can lead to oscillation of the closed loop system [25]. This can be mathematically explained by the fact that in Equation 4.4 all terms with subscript "0" should be synchronized to perform the Taylor expansion [16] and perform the sensor measurement substitution. In mathematical terms indeed a filtered measurement \dot{x}_f will deviate from the initial signal \dot{x}_0 linearly with the introduced lag Δ_f as explained in Equation 5.10

$$\dot{x}_f = \dot{x}_0 + \dot{x}\Delta_f \quad (5.10)$$

By applying the control law depicted in Equation 4.7 to a filtered signal \dot{x}_f one can observe that the achieved state derivative does not track the commanded virtual control vector.

$$\begin{aligned} \Delta u &\simeq (Gx_0, u_0)^+ (\nu - \dot{x}_f) \\ G(x_0, u_0) \Delta u &\simeq G(x_0, u_0) (Gx_0, u_0)^+ (\nu - \dot{x}_f) \\ \dot{x} &\simeq \dot{x}_0 + G(x_0, u_0) G(x_0, u_0)^+ (\nu - \dot{x}_f) \\ \dot{x} &\simeq \nu + \dot{x}_0 - \dot{x}_f \\ \dot{x} &\simeq \nu - \dot{x}\Delta_f \end{aligned} \quad (5.11)$$

In conclusion what Equation 5.11 shows is that the reference virtual control is not tracked but rather deviates by an additional term $-\dot{x}\Delta_f$ which can induce oscillations. The problem is solved and cancellation of the terms is achieved if the Taylor expansion is performed around x_f rather than x_0 , meaning that all signals have been synchronized by applying the same filter everywhere.

5.2.2. Hybrid INDI

Section 5.2.1 has shown why and how filters can be used to keep the acceleration signal and feedback from the actuators synchronized. On the other hand, the only source of time delay considered until now is the introduction of a low pass filter to eliminate high frequency noise in the acceleration signal. In truth, time delay is also affected by the dynamics of the sensor (Inertial Measurement Unit). Therefore, the method remains susceptible to unexpected measurement delays [26]. Furthermore, excessive time delays due to the actuator dynamics considerations, noise filtering and sensor dynamics reduce the stability margin of the control system [27]. Hybrid INDI is proposed as a solution for increased robustness and stability margin.

Hybrid INDI is designed to include characteristics of Model-Based and Sensor-Based INDI. Kumtepe, Pollack, and Kampen [26] argue that the general idea is that knowledge of the system can be used in a model to generate fast response to system input, while sensor measurements are used to maintain adequate accuracy in the low-medium frequency range. Figure 5.2 shows the control structure of the hybrid INDI controller. Knowledge of the vehicle is used to build the On-Board Model (OBM), which outputs an estimation of the angular acceleration based on the commanded actuator states, alike what is done in NDI.

Kumtepe, Pollack, and Kampen [26] as well as Kim et al. [27] explain that the estimation of the angular acceleration can be fused with measurements from the sensor to provide a feedback signal for the

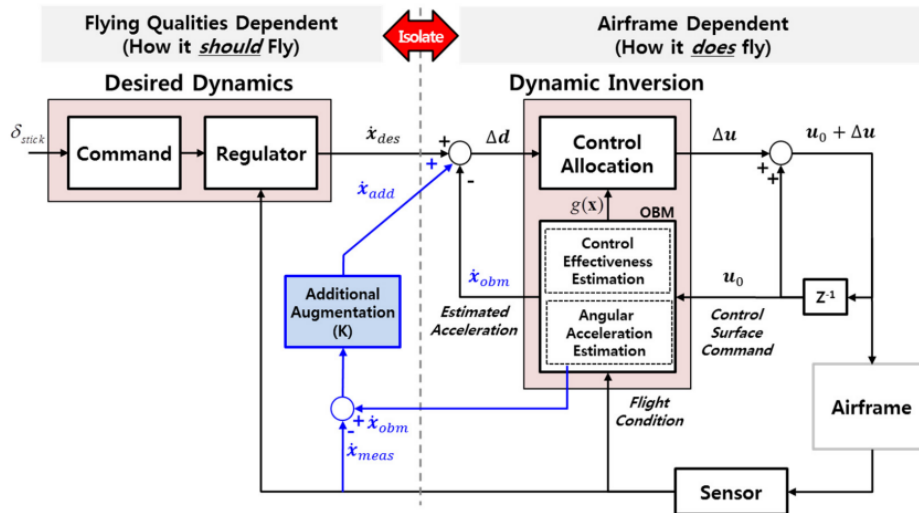


Figure 5.2: Control structure of hybrid INDI control [28].

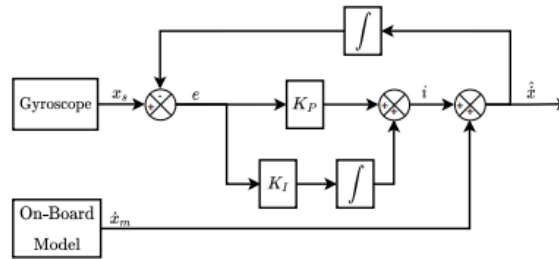


Figure 5.3: Block diagram of complementary filter for angular acceleration estimation [26].

control law. Kim et al. [27] argue that this is best achieved with a simple proportional gain K_{aug} which ranges from 0 to 1. As the gain tends to 1 more and more feedback from the sensor is being used, assuring rejection of possible on-board model inaccuracies. As the gain tends to 0, the control law is more dependent on the OBM and is less susceptible to time delays.

In contrast, Kumtepe, Pollack, and Kampen [26] argue that fusion of the signals is better achieved with a complementary filter as described by Figure 5.3. A complementary filter alleviates noise distortion by combining a high-pass filtered signal with low-frequency noise characteristics and a low-pass filtered signal with high-frequency noise characteristics. In the specific hybrid INDI case the signal with low-frequency noise is the estimation from OBM while the signal with high-frequency noise is the sensor measurement.

Kumtepe, Pollack, and Kampen [26] further state that the novel hybrid INDI control law is found to retain good performance in case of model mismatches and measurements delays in simulations using an F-16 model. The authors further argue that the method can be improved in the future through the use of Kalman filters to exploit both measurement and model simultaneously. Another mentioned recommendation is the future use of angular accelerometer instead of gyroscopes. Logically, using an angular accelerometer to measure and angular acceleration results to be the most straightforward and less noisy method. On the other hand such sensors are not commonly installed in aircraft or UAVs.

Ji, Kim, and Kim [28] in their study propose an hybrid INDI for the control of the transient response of a fighter jet in asymmetric store. Similarly to the VSQP in transition, a fighter jet in asymmetric loading experiences imbalances in the aerodynamic moments and has non negligible cross product terms I_{xy} and I_{yx} . This occurs because, after the rockets have been launched from one single wing, the position

of the center of gravity on the lateral axis is shifted towards the wing still carrying a payload. Furthermore, the wing not carrying the rockets anymore experiences a cleaner flow, in turn producing higher lift and so a rolling moment. Therefore, when the store is launched asymmetrically, a sudden change in lateral-directional axis and trim appears and flying qualities of the aircraft are degraded in proportion to the magnitude of the transient response [28].

Ji, Kim, and Kim [28] argue that hybrid INDI together with smartly generated pseudo controls using knowledge of the desired flying dynamics can greatly alleviate the transient response and reduce the workload of the pilot. This is particularly interesting because it candidates hybrid INDI to solve problems in which platforms undergo sudden and complex to model changes in system dynamics, just alike transition for VSQP due to the imbalances generated by the oblique wing.

However, it must be noted that to the best knowledge of the author research on hybrid INDI is still at an early stage and that there is not yet documentation in Literature of real life applications of the theory.

5.3. Approximation of Outer Loop Effectiveness

Chapter 4 has presented an overview of the structure of an outer-loop INDI controller for guidance. Differently from the innerloop, it is not possible for the outerloop to assume the time scale separation principle because the state dynamics of the drone actually play a crucial role in guidance. For example, a quad-plane uses the lift generated by the wing to perform a number of maneuvers as high speed turns, loitering or simple climbing. Therefore, knowledge of how state dynamics affect linear acceleration is crucial towards assuring proper guidance.

On the other hand, as already mentioned, one of the aims of INDI is to limit model dependency due to the complexity of the development of an accurate enough model from the small sensors which can be carried by a MAV [10]. Therefore, a number of assumptions have to be taken in order for the outerloop controller to provide proper guidance with limited state dynamics knowledge.

Wijngaarden, Smeur, and Remes [29] present a unified approach to INDI outerloop design for a multitude of MAV. The approach starts from the general definition of linear acceleration according to Newton's second law as presented in Equation 5.12 .

$$\ddot{\xi} = \mathbf{g} + \frac{1}{m}\mathbf{L}_N(\boldsymbol{\eta}, V) + \frac{1}{m}\mathbf{D}_N(\boldsymbol{\eta}, V) + \frac{1}{m}\mathbf{T}_N(\boldsymbol{\eta}, T) \quad (5.12)$$

where: $\ddot{\xi}$ = Linear acceleration vector of drone in NED
 \mathbf{L}_N = Lift vector in NED
 \mathbf{D}_N = Drag vector in NED
 \mathbf{T}_N = Thrust vector in NED
 $\boldsymbol{\eta}$ = Attitude of drone

Now using the rotation matrix M_{NB} from body to NED, it is possible to further refine Equation 5.12. The rotation matrix M_{NB} follows the rotation order ZXY ($\boldsymbol{\eta} = [\psi \ \phi \ \theta]$) such that the Euler angle derivatives are well defined at -90° pitch, which is the preferred stated in forward flight for the considered tail sitter.

$$\mathbf{M}_{NB} = \begin{bmatrix} c\theta c\psi - s\phi s\theta s\psi & -c\phi s\psi & s\theta c\psi + s\phi c\theta s\psi \\ c\theta s\psi + s\phi s\theta c\psi & c\phi c\psi & s\theta s\psi - s\phi c\theta c\psi \\ -c\phi s\theta & s\phi & c\phi c\theta \end{bmatrix} \quad (5.13)$$

Please note that in Equation 5.13 for simplicity sine and cosine have been abbreviated to "s" and "c". It follows that the thrust vector can be written as:

$$\mathbf{T}_N = \mathbf{M}_{NB} \begin{bmatrix} 0 \\ 0 \\ T \end{bmatrix} = \begin{bmatrix} (s\theta c\psi + s\phi c\theta s\psi)T \\ (s\theta s\psi - s\phi c\theta c\psi)T \\ c\phi c\theta T \end{bmatrix}, \quad (5.14)$$

and the lift vector as:

$$\mathbf{L}_N = \mathbf{M}_{NB}^{\theta=-\frac{\pi}{2}} \mathbf{L}_B(\theta, V) = \begin{bmatrix} s\phi s\psi L(\theta, V) \\ -s\phi c\psi L(\theta, V) \\ c\phi L(\theta, V) \end{bmatrix} \quad (5.15)$$

Wijngaarden, Smeur, and Remes [29] in the presented derivation consider a tail-sitter as the example platform. Therefore, the Thrust vector has non-zero entries only in the body z axis and the wing generates lift when transition is performed to have $\theta = -\frac{\pi}{2}$. The derivation can be easily modified for different platforms with different geometries and dynamics characteristics.

Wijngaarden, Smeur, and Remes [29] in order to derive Equation 5.15 make use of two assumption. First, it is assumed that the flight path angle is small, hence the lift vector is only rotated from the vertical by the bank angle. Second, it is assumed that the lift is only dependent on airspeed V and pitch angle θ . This assumption, in connection to proper lift curve modelling, is able to describe the lifting properties of most wings. On the other hand, for a wing which is able to change skew angle, Λ must also be considered in the modelling of the lift generation, thus requiring $L(\theta, V, \Lambda)$.

Now, a first order Taylor expansion with respect to the outerloop control variables $\mathbf{v} = [\phi \ \theta \ T]^T$ can be used to derive the control effectiveness matrices for Lift and Thrust, respectively \mathbf{G}_L and \mathbf{G}_T .

$$\begin{aligned} \mathbf{G}_L(\boldsymbol{\eta}, V) &= \begin{bmatrix} \left(\frac{\partial}{\partial \phi} \frac{1}{m} \mathbf{L}_N(\phi, \theta_0, \psi_0, V_0) \Big|_{\phi=\phi_0} \right)^T \\ \left(\frac{\partial}{\partial \theta} \frac{1}{m} \mathbf{L}_N(\phi_0, \theta, \psi_0, V_0) \Big|_{\theta=\theta_0} \right)^T \\ (\mathbf{0})^T \end{bmatrix}^T \\ &= \begin{bmatrix} \mathbf{c}\phi\mathbf{s}\psi L(\theta, V) & \mathbf{s}\phi\mathbf{s}\psi \frac{\partial}{\partial \theta} L(\theta, V) & 0 \\ -\mathbf{c}\phi\mathbf{c}\psi L(\theta, V) & -\mathbf{s}\phi\mathbf{c}\psi \frac{\partial}{\partial \theta} L(\theta, V) & 0 \\ -\mathbf{s}\phi L(\theta, V) & \mathbf{c}\phi \frac{\partial}{\partial \theta} L(\theta, V) & 0 \end{bmatrix} \end{aligned} \quad (5.16)$$

$$\begin{aligned} \mathbf{G}_T(\boldsymbol{\eta}, T) &= \begin{bmatrix} \left(\frac{\partial}{\partial \phi} \frac{1}{m} \mathbf{T}_N(\phi, \theta_0, \psi_0, T_0) \Big|_{\phi=\phi_0} \right)^T \\ \left(\frac{\partial}{\partial \theta} \frac{1}{m} \mathbf{T}_N(\phi_0, \theta, \psi_0, T_0) \Big|_{\theta=\theta_0} \right)^T \\ \left(\frac{\partial}{\partial T} \frac{1}{m} \mathbf{T}_N(\phi_0, \theta_0, \psi_0, T) \Big|_{T=T_0} \right)^T \end{bmatrix}^T \\ &= \begin{bmatrix} \mathbf{c}\phi\mathbf{c}\theta\mathbf{s}\psi T & (\mathbf{c}\theta\mathbf{c}\psi - \mathbf{s}\phi\mathbf{s}\theta\mathbf{s}\psi)T & \mathbf{s}\theta\mathbf{c}\psi + \mathbf{s}\phi\mathbf{c}\theta\mathbf{s}\psi \\ -\mathbf{c}\phi\mathbf{c}\theta\mathbf{c}\psi T & (\mathbf{c}\theta\mathbf{s}\psi + \mathbf{s}\phi\mathbf{s}\theta\mathbf{c}\psi)T & \mathbf{s}\theta\mathbf{s}\psi - \mathbf{s}\phi\mathbf{c}\theta\mathbf{c}\psi \\ -\mathbf{s}\phi\mathbf{c}\theta T & -\mathbf{c}\phi\mathbf{s}\theta T & \mathbf{c}\phi\mathbf{c}\theta \end{bmatrix} \end{aligned} \quad (5.17)$$

Using Equation 5.16 and Equation 5.17 it is possible to derive a INDI incremental control law for the outer loop as shown by Equation 5.18.

$$\ddot{\boldsymbol{\xi}} = \ddot{\boldsymbol{\xi}}_0 + \frac{1}{m} (\mathbf{G}_T(\boldsymbol{\eta}, T) + \mathbf{G}_L(\boldsymbol{\eta}, V)) (\mathbf{v} - \mathbf{v}_0), \quad (5.18)$$

In Equation 5.18 the effect of changes in drag are assumed to occur at a slower rate compared to lift and thrust thus allowing to neglect its effect on the change in linear acceleration. Equation 5.18 can then be rearranged so to describe the required change in control variables to achieve a desired reference acceleration $\ddot{\boldsymbol{\xi}}_{ref}$. It must be remembered that as explained in Section 5.2, $\ddot{\boldsymbol{\xi}}_0$ is a sensor measurement and it must be filtered because of the presence of noise. Therefore, all other related signals must be filtered identically.

$$(\mathbf{v} - \mathbf{v}_f) = m (\mathbf{G}_T(\boldsymbol{\eta}, T) + \mathbf{G}_L(\boldsymbol{\eta}, V))^+ (\ddot{\boldsymbol{\xi}}_{ref} - \ddot{\boldsymbol{\xi}}_f) \quad (5.19)$$

The problem with the estimation of \mathbf{G}_L and \mathbf{G}_T is that $L(\theta, V)$, $\frac{\partial}{\partial \theta} L(\theta, V)$ and T are not readily available values. Surely, it can be argued that a model can be created to evaluate the variables value at any considered condition. On the other hand, such process can be tedious and resource expensive. Wijngaarden, Smeur, and Remes [29] and Smeur, Bronz, and Croon [24] propose as an alternative to exploit knowledge of the platform to approximate some of the unknown variables. Both papers treat at least in part tail-sitter designs in stable forward flight, hence θ between 0° and -90° . It has to be realized that at any airspeed during forward flight, the generated lift is used to compensate the weight of the drone. Therefore, for small flight path angle the generated lift can be approximated to be:

$$L(\theta, V) \approx L(\theta) = -9.81 \sin(-\theta)m \quad (5.20)$$

Similarly, in forward flight for any given airspeed, a tail-sitter uses the thrust vector to compensate for Drag and effect on accelerations other than in the thrust axis is small.

$$T(\theta) = -9.81 \cos(\theta)m \quad (5.21)$$

As for $\frac{\partial}{\partial \theta} L(\theta, V)$ Smeur, Bronz, and Croon [24] argue that no simple assumption can be derived and that some sort of data driven aerodynamic model should be used. This occurs because a change in airspeed strongly affects $\frac{\partial}{\partial \theta} L(\theta, V)$ and so no general simplification can be applied.

Wijngaarden, Smeur, and Remes [29] show that the described assumptions and approximations when used in a outerloop controller can assure precise guidance for the considered platforms. On the other hand, the authors also define the assumptions to be "crude" and "probably inaccurate"[29], hinting to the performance gains which could be achieved with a more accurate model.

5.4. Control allocation for over-actuated drones

Section 4.3 presents an overview of how in INDI control allocation is performed by means of pseudo inverting the effectiveness matrix. This method outputs the smallest two-norm solution which satisfies the desired change in acceleration setpoint.

The first issue that arises from this approach is the lack of knowledge of actuator saturation prior to the computation of the inverse. This occurs because when using the pseudo inverse to estimate the control change to achieve the desired change in acceleration, the solution is computed based only on effectiveness and not accounting for the state and possible saturation of the actuators.

Wang, Xu, and Yue [6] propose a weighting solution of the effectiveness matrix which aims to prevent saturation of actuators in a NDI controller for a OFW. The method involves scaling of the actuator states with their maximum saturation limit. Therefore the control input vector has the form of:

$$\hat{\mathbf{u}} = [\delta_{aL}/\delta_{aLmax}, \delta_{aR}/\delta_{aRmax}, \delta_r/\delta_{rmax}, \delta_{eL}/\delta_{eLmax}, \delta_{eR}/\delta_{eRmax}]^T \quad (5.22)$$

Therefore the NDI control law takes the form of:

$$\mathbf{u} = \Delta (\mathbf{g}_f \Delta)^+ \left(\begin{bmatrix} \dot{p} \\ \dot{q} \\ \dot{r} \end{bmatrix} - \mathbf{f}_f \right) \quad (5.23)$$

where: $\Delta = \text{diag}(\delta_{aLmax}, \delta_{aRmax}, \delta_{rmax}, \delta_{eLmax}, \delta_{eRmax})$
 $\mathbf{g}_f =$ NDI Effectiveness matrix
 $\mathbf{f}_f =$ State induced angular acceleration

Wang, Xu, and Yue argue then that the proposed scaling prevents the single saturation of an actuator when there is another control element which could pick up the control slack.

However, it can be argued that this simple approach does not deliver the most optimal solution to the control problem. This occurs when the platform has different actuators with different operational power costs. For example, consider the case in which both an aerodynamic surface and a motor have the same effectiveness on a specific axis. The commanded solution to an acceleration setpoint will then be to deploy both control elements to the same extent. From a power usage perspective though the motors have a larger impact than operating aerodynamic surfaces. Therefore, there is a need to prioritize the use of some actuators over others in certain flight phases which cannot be simply encoded in the effectiveness matrix.

Furthermore, in the case of saturation, there should be a prioritization of the desired control objective. This makes sure that the most vital control actions for the drone are given priority over secondary ones. Smeur, Höppener, and Wagter [30] make the example of a quad-rotor which is commanded to perform a sudden yaw angle change. The motors can easily saturate to perform the yawing command because of the limited effectiveness on the yaw axis. Therefore, little to no slack is left for tracking of the other

attitude and thrust values. Smeur, Höppener, and Wagter argue that actually for a quad-rotor, control of θ and ϕ is crucial because it directs the thrust vector in the desired direction. Therefore, control of θ and ϕ should be given priority over performing changes in Thrust and ψ .

It is clear then the need for a control allocation algorithm which embeds knowledge of prioritization of control objective and of actuator preference to achieve optimal control. Smeur, Höppener, and Wagter [30] propose a Weighted Least Squares (WLS) algorithm to solve the control allocation problem specifically for the innerloop of INDI.

More precisely the method solves a sequential least squares problem corresponding to a primary and a secondary objective function. The primary objective is to minimize the error between the desired angular acceleration change and the one produced by the calculated control increment. This is considered the primary objective because it allows the drone to be stabilized.

The secondary objective is to achieve the primary objective using the least actuator energy. This objective prevents the control allocation algorithm to converge to a solution where control elements are steered in opposite directions for over-actuated systems. Logically, if there exist only one solution to the primary objective, in other words the effectiveness matrix has full rank, the secondary objective can be disregarded.

The sequential least squares problem aims then to find a solution to the control allocation algorithm which minimizes the cost function $C(u)$ reported in Equation 5.24.

$$\begin{aligned} C(u) &= \underbrace{\|W_u (u - u_d)\|^2}_{\text{Secondary Objective}} + \gamma \underbrace{\|W_v (Gu - v)\|^2}_{\text{Primary Objective}} \\ &= \left\| \begin{pmatrix} \gamma^{\frac{1}{2}} W_v G \\ W_u \end{pmatrix} u - \begin{pmatrix} \gamma^{\frac{1}{2}} W_v v \\ W_u u_d \end{pmatrix} \right\|^2, \end{aligned} \quad (5.24)$$

W_v is the diagonal weighting matrix of the control objective and it is used to establish a hierarchy. The higher the weights, the larger the cost per control objective error, which will steer the control allocation in favor of its alleviation. Smeur, Höppener, and Wagter [30] argue, as already discussed, that for a quad-copter the prioritization of control objectives should be ϕ / θ , then Thrust and finally ψ . Therefore the suggested W_v for the virtual control vector $[\phi \ \theta \ \psi \ T]^T$ is:

$$W_v = \begin{bmatrix} 1000 & 0 & 0 & 0 \\ 0 & 1000 & 0 & 0 \\ 0 & 0 & 1 & 0 \\ 0 & 0 & 0 & 100 \end{bmatrix} \quad (5.25)$$

W_u is the diagonal weighting matrix of the control input and it is used to specify a preference between the actuators. The higher the weight, the larger the cost per change in control input, which will steer the control allocation to minimize the usage of the actuator. For a quad-rotor the choice of weights is trivial because all the actuators are the same motors with same power curves. Therefore, W_u can be set to be the Identity matrix. On the other hand, for systems with different kinds of actuators, higher weights can be assigned to the power hungry control elements to minimize energy usage.

The scaling factor γ is used to increase the cost of the primary objective with respect to the secondary objective. It follows then that the minimization process will be much more sensitive to errors in the primary objective and therefore steer the control allocation to alleviate those first. Smeur, Höppener, and Wagter [30] propose $\gamma^{1/2}$ to be 10000.

For convenience let us introduce the substitutions of Equation 5.26 to simplify Equation 5.24.

$$A = \begin{bmatrix} \gamma^{\frac{1}{2}} W_v (G_1 + G_2) \\ W_u \end{bmatrix} \quad \text{and} \quad b = \begin{bmatrix} \gamma^{\frac{1}{2}} W_v v \\ W_u u_d \end{bmatrix} \quad (5.26)$$

Which then leads to .

$$C(u) = \|A u - b\|^2 \quad (5.27)$$

Now, Equation 5.27 is the cost function to be minimized of a quadratic programming problem having as bounds the actuator saturation limits. Because INDI is incremental in nature, the u_{min} and u_{max} bounds are calculated based on the slack between previous actuator state and saturation limits.

The quadratic programming problem can then be solved with a method of choice as for example the active set method. This algorithm is well described by Smeur, Höppener, and Wagter [30] and is illustrated in algorithm 1. The idea of the algorithm is to divide the input in a free set and an active set, which are respectively the non-saturated and the saturated actuators. The saturation limits inequality constraints of the free set are then dropped while the ones of the active set are transformed in equality constraints. At every iteration of the algorithm, it is made sure that the free and active sets are divided correctly and if needed adjustments are made. Finally, this algorithm stops if the optimal solution is found or if the maximum number of iterations is exceeded.

Algorithm 1: Active set method for WLS problem [30]

Initialization: ;

$$W = \{\emptyset\}, \quad u^0 = (u_{max} - u_{min})/2, \quad d = b - Au^0, S = [\emptyset]$$

for $i = 0, 1, 2, \dots, n_{max}$ **do**

 Determine the free columns in A:

$$A_f = A(:, h), \quad h \notin W$$

 Determine the optimal perturbation by solving the following least squares problem for p_f :

$$d = A_f p_f$$

 Now p is constructed from p_f with zeros for the elements that are in W .

if $u^i + p$ **is feasible then**

$u^{i+1} = u^i + p$ **and:** $d = d - A_f p_f$

 The gradient and Lagrange multipliers are computed with:

$$\nabla = A^T d \text{ and: } \lambda = S \nabla$$

if all $\lambda \geq 0$ **then**

 | The solution u^{i+1} is optimal $u = u^{i+1}$

else

 | The constraint associated with the most negative λ has to be removed from the active set W . Re-iterate with this active set.

end

else

 The current solution violates a constraint which is not in W . Determine the maximum factor α such that αp is a feasible perturbation, with $0 \leq \alpha \leq 1$. Update the residual d and the solution u^{i+1} :

$$u^{i+1} = u^i + \alpha p$$

$$d = d - A_f \alpha p_f$$

 Finally, update the active set and store the sign of the constraint: $S_{jj} = \text{sign}(p_j)$ with j the index of the new active constraint.

end

end

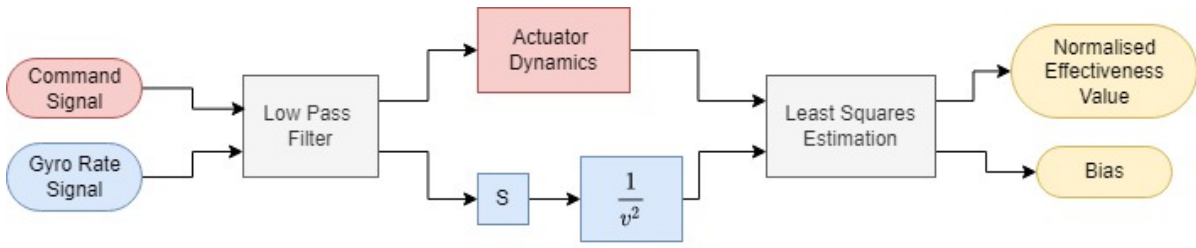


Figure 5.4: Pitch effectiveness estimation logic diagram

5.5. Effectiveness Estimation

Chapter 4 explains how in INDI the modelling effort is contained to the drafting of effectiveness profiles. Section 4.6 further develops by showing that two set of effectiveness matrices have to be estimated, one for the inner loop and one for the outer loop.

The former quantifies the change in angular acceleration across the considered rotational axis per change in control input to the actuators, being this RPM, Paparazzi command unit, deflection angles or any other variable representative of the change in state of the control element. The idea is that by modifying the actuator commands it is possible to achieve stabilisation of the platform.

The latter quantifies the change in linear acceleration across the considered axis per change in controlled variable. These variables usually represent the state of the drone itself and for a quad-rotor are usually the roll angle ϕ , the pitch angle θ and the overall thrust T . As for the heading angle, this is usually controlled by a sideslip controller which is used to align the drone to the flight path and perform coordinated turns. The idea is that by modifying the controlled variables it is possible to achieve guidance of the platform.

In order to estimate the effectiveness matrices, flight test data can be used. Multiple authors [10, 16, 24] propose to use a least squares estimation routine to estimate the effectiveness profiles. More precisely, for the inner loop the registered angular acceleration can be compared to the change in actuator inputs while for the outer loop the registered linear acceleration is compared to change in controlled variables.

$$\text{If system of type: } b = Ax \Rightarrow \hat{x} \text{ which minimizes } \| b - A\hat{x} \|^2 \quad (5.28)$$

Equation 5.28 report the basic working principle of a linear least squares and how its solution is defined. There exist multiple algorithms to find \hat{x} , which depend on the type of input and output being compared. These are not described further because their validity is not the focal point of the research project. Rather, the quality of the registered data plays an important role in the estimation of the effectiveness matrices.

Figure 5.4 shows an high-level block diagram description of the effectiveness estimation process for the innerloop. As shown, the estimation starts from flight data, in particular recorded input commands and angular rates. Pre-processing is extremely important towards achieving a meaningful result. In a typical flight test not all of the considered data can be used, but rather only a portion of it. More precisely, only the data points at timestamps where the studied dynamics are visible should be considered.

Pre-processing also includes filtering noise out of the recorded data. In particular, the IMU angular rates and linear accelerations suffer from high frequency noise due to vibrations of the system. This noise, because it is not carrying any meaningful knowledge towards the effectiveness estimation, should be excluded from further calculations. More precisely, a low pass filter such as a Butterworth filter has to be used. The cut-off frequency should be chosen based upon the highest expected frequency response of the system to excitation inputs.

Filtering of the acceleration introduces a phase shift in the signal thus generating a lag in the time domain. Therefore also the commanded input has to be passed through the same exact filter, as shown in Figure 5.4. Failing to filter the command input signal would mean that any given data point would be

compared to an acceleration which belongs to a different timestamp.

The next step in the manipulation of the angular rate signal is to differentiate it. It needs indeed to be recalled that the definition of effectiveness used in the inner loop is based on angular acceleration and not rate. When estimating the effectiveness of an aerodynamic surface, it is useful to normalize the acceleration signal with the square of airspeed. This because the lift is expected to change with the square of airspeed as described by lifting theory. This trick will allow to estimate a normalized effectiveness value which can be used to predict the true effectiveness at any given airspeed.

Now that the acceleration is ready to be fitted in a least squares approximation, the focus can be shifted to the filtered command signal. As explained in Section 5.1 each control element has actuator dynamics which have to be accounted for. Therefore, the commanded signal is further passed through a first or second order filter corresponding to the type of actuator.

Finally, in order to account for the effect of unconsidered dynamic elements, which are anyways rejected by the incremental structure of the INDI control law as explained in Section 4.7, the commanded input is augmented with a column of ones. This will allow the least squares approximation to extrapolate the bias of the estimation.

Now that the effectiveness estimation process is fully described, the excitation procedure should be further explained. The system indeed has to be excited in such a way to reveal the underlying dynamics for the least squares to approximate the effectiveness values.

$$\text{Doublet}(t) = \begin{cases} 0 & \text{if } t < t_{start} \text{ or } t \geq t_{end} \\ 1 & \text{if } t \geq t_{start} \text{ and } t < \frac{t_{end}-t_{start}}{2} \\ -1 & \text{if } t \geq \frac{t_{end}-t_{start}}{2} \text{ and } t < t_{end} \end{cases} \quad (5.29)$$

In the literature multiple authors [9, 31] propose the use of doublets, as defined in Equation 5.29, to reveal the platform dynamics. Maine [9] uses 87 different combinations of doublets on the elevators, ailerons and rudder to model the dynamics of the OFW in his research. Smeur et al. [31] further develops that doublets have the nice property to contain deviation from equilibrium. This occurs because input is applied symmetrically in both direction and because the maneuver can be designed to take short time spans. Therefore doublets are expected to be very useful in the identification of the inner-loop actuator effectiveness such as motors and aerodynamic surfaces. This occurs because due to time scale separation, it can be assumed that a rapid excitation of the control elements will generate a response which is nearly free of the effect of slowly changing state variables.

$$\text{Chirp}(t) = \begin{cases} 0 & \text{if } t < t_{start} \text{ or } t \geq t_{end} \\ \sin(2\pi t f_0 + \frac{f_1-f_0}{t_{end}-t_{start}} \pi t^2) & \text{if } t \geq t_{start} \text{ and } t < t_{end} \end{cases} \quad (5.30)$$

In order to estimate the outerloop effectiveness, a different excitation method which better reveals the slower dynamics of the control variables of the state should be chosen. Chirps, are sinusoidal signals of sweeping frequency. Equation 5.30 shows the mathematical definition of a linear chirp. Thanks to the large range of spanned frequencies, chirps can be designed to excite the slower state induced dynamics. More precisely, chirping signals can be added on top of the commanded variables as ϕ , θ and Thrust and compared to the registered linear accelerations to extrapolate the outerloop effectiveness.

Smeur, Bronz, and Croon [24] report that non accurate effectiveness estimations for the outerloop can occur if the contribution of the control elements to linear accelerations are not accounted for. Smeur, Bronz, and Croon make the example of the effectiveness of flaps on lift, and so vertical acceleration for a Cyclone drone. It is concluded that the vertical acceleration due to lift cannot be simply modeled by considering only the pitch angle but also the deflection of the ailerons should be considered. This occurs because a positive deflection of the ailerons increases significantly lift and so generates an acceleration. While in the VSQP the control surfaces do not occupy as much wing area as on the Cyclone, it is still good practice to account for their deflection in the estimation of outerloop effectiveness.

In conclusion, the design process will first involve gathering data to develop effectiveness profiles for the INDI inner loop using doublets. Therefore, the platform should be stabilized and further airborne test can be performed. Subsequently, chirps will be used to determine state effectiveness on linear accelerations. Therefore, the outer loop should be able to track autonomously wanted waypoints providing guidance. Finally, validation of the effectiveness profiles should be performed by using a test data set. The test input commanded actuator values and control states should be fed to the developed model and the output should be compared to the registered signals. Accurate model fit proves the estimation process to be successful [24].

The so far described method of effectiveness estimation involves an offline analysis of the recorded data. On the other hand, in order to retrieve this data the drone has to be able to fly which in turn is dependent on the effectiveness matrix provided to the controller. Smeur, Chu, and Croon [10] mention that in order to break the loop an initial crude manual effectiveness tuning procedure or the use of a PID controller can be used to make the platform airborne.

However, any substantial change in the structure (e.g. motors, propellers, Inertia matrix) or flight phase (e.g. airspeed, battery voltage) of the drone requires a re-iteration of the initial effectiveness tuning. As a solution, Smeur, Chu, and Croon [10] propose a method to adaptively change the effectiveness matrix online. This is achieved by extending the conventional innerloop INDI controller with onboard adaptive parameter estimation using a Least Mean Squares (LMS) adaptive filter. Equation 5.31 shows how the effectiveness matrix G , which includes both G_1 and G_2 , is adjusted for the quad-rotor controller using the control law of Equation 4.14.

$$G(k) = G(k-1) - \mu_2 \left(G(k-1) \begin{bmatrix} \Delta\omega_f \\ \Delta\dot{\omega}_f \end{bmatrix} - \Delta\Omega_f \right) \begin{bmatrix} \Delta\omega_f \\ \Delta\dot{\omega}_f \end{bmatrix}^T \mu_1 \quad (5.31)$$

First, the original effectiveness matrix is used to calculate the expected change in angular acceleration for the given inputs. Then, an error signal is computed by comparing the expected and measured angular acceleration. Finally, the error signal is used to increment the effectiveness matrix. The constants μ_1 and μ_2 define the stability and rate of convergence of the algorithm. Higher gains lead to faster convergence but can also have detrimental effects on stability [10].

The presented adaptive algorithm promises to provide accurate online tuning of effectiveness values by requiring only an initial crude estimation. On the other hand, there exist a number of concerns with its implementation. First of all, as hopefully clear by now, effectiveness estimation is not a trivial task. Data quality and pre-processing is crucial towards obtaining meaningful results. Obvious measurement outliers to the human eye might still steer the algorithm in the wrong direction.

Furthermore, the robustness of the method can be limited by bad convergence or bad learning. The former meaning that as any other convergence algorithm instabilities or slow rate of convergence can occur. This is of particular concern for such a critical and high frequency task as the stabilisation routine. The latter refers to the drone wrongly learning effectiveness values as for example while being on the ground and having weight supported with no thrust. Moreover, higher number and different actuators increase the complexity of the effectiveness estimation process, hence making less forward the application of adaptive INDI on a platform such as VSQP.

While it can be argued that all the mentioned problems can be solved with a careful choice of filtering parameters, algorithm convergence constants and effectiveness bounds, the resilient problem with adaptive INDI on VSQP remains the potential risks. Due to the online nature of the algorithm, any problems in the convergence routine can result in loss of control of the platform, hence potentially generating catastrophic consequences. Therefore, a more conservative approach would be to use adaptive INDI as a monitoring tool during the preliminary flight test, steering the manual tuning in the right direction and leaving the final effectiveness estimation to a more robust offline analysis.

6

Transition

One of the challenges of an hybrid drone is the development of a control strategy which is able to deal with the numerous nonlinear changes in dynamics during transition. This chapter proposes some of the modelling and control solutions reported in the Literature which target the expected transitional dynamics of VSQP. Section 6.1 presents a review of the expected changes in effectiveness during transition of the motors and how to model them. Section 6.2 discusses the implementation of a WLS routine also in the outerloop to provide pusher prop control and gradual switch from hover to cruise mode. Finally, Section 6.3 reports how the Reference Model can be extended to include knowledge of state dependent dynamics thus enhancing control.

6.1. Motor effectiveness modelling

Section 4.7 highlights the capability of INDI to deal with model inaccuracies thanks to the incremental nature of its control law. On the other hand, large inaccuracies in effectiveness profiling can degrade the control performance and even lead to instability. For example, Smeur, Chu, and Croon [10] have shown that the addition of bumpers to a Bebop2 without a re-evaluation of the effectiveness matrix leads to fast oscillations which hinder the control performance. Similarly, large inaccuracies in motor effectiveness estimation can be expected to have detrimental effects on stability.

Therefore, it is important to understand how the effectiveness of motors is expected to change during transition. A modelling technique allows to embed knowledge of the expected changes in the effectiveness directly in the INDI controller.

6.1.1. Motor-Prop performance in crossflow

Propeller performance data is crucial for optimal design [32], modelling [33] and for assessing whether stability and controllability is achievable in different flight scenarios. Furthermore, propellers in VTOL rotorcraft experience a larger range of inflow angles compared to helicopters in forward flight ($80^\circ - 90^\circ$) and fixed-wing aircraft ($0^\circ - 10^\circ$) [48]. In vertical maneuvers propellers experience axial flow while during level cruise inflow angles depict more of a crossflow airfield. There exist plenty of literature on modelling of propellers in axial flow, often performed as a result of wind tunnel experiments [49, 50, 51, 52], simulation [53, 54] or a mix of the two [55].

On the other hand, research on performance of UAVs and MAVs propellers in crossflow conditions can result to be complicated due to the low Reynolds number experienced by small propellers, which prevents the use of classical helicopter disk theory [34, 35].

Despite the complexity of the modelling task, there exist a trend in the literature across all proposed models which depicts a positive correlation between crossflow airspeed and propeller performance. Theys et al. [36] investigated in 2014 the effect of different angles of attack (0° up to -180°) and different airspeed (0-6-9 m/s) on the propeller performance. The experiment data was recorded from a

6-axis force/moment sensor placed on a turning table inside the subsonic wind tunnel of the University of Liege. Unfortunately errors and saturation of the setup sensor exclude the use of the 9m/s data batch from further analysis.

The study concludes that at 6m/s, the same mechanical power level generates more thrust at 90° angle of attack (crossflow) rather than in pure axial flow. However, the percentage difference in thrust level decreases as the mechanical power required increases. Other useful conclusions from a modelling perspective are that hub forces result to be 2 order of magnitude lower than the thrust force, meaning that in comparison they can be neglected. In contrast, the torque exerted by the motor results to be in the same order of magnitude as the pitching and rolling moment produced by the rotating propeller in crossflow. Therefore, these moments cannot be neglected in the modelling of the drone. It can though be assumed that, given a strong enough structure, these moments will balance out at the CG. This occurs because in a symmetrical structure with opposite motors spinning in opposite directions, the hub forces will have equal magnitude but reverse direction. Therefore, given a strong enough structure, the hub forces will propagate and cancel each other out at the center of gravity. Further confirmation of the findings from Theys et al. [36] is found also by Russel et al. [37], who conclude that for a given RPM and airspeed the considered propeller outputs more thrust in crossflow compared to axial flow.

In 2017, Theys et al. [38] further develop the research by proposing 3 different modelling techniques to depict the performance of small Propellers at different inflow angles and speeds. The proposed methods are benchmarked against test results from the subsonic wind tunnel at angles of attack varying from 0° to 90° at the single airspeed of 6m/s. Wind tunnel data again shows that at equal mechanical power required, more thrust is generated in crossflow compared to purely axial flow.

The first modelling method proposed is Blade Element Momentum Theory (BEMT). BEMT is a well known modelling technique based on Blade Element Theory (BET) and momentum conservation. BET is widely used to model the basic aerodynamics of helicopter rotor blades, however Kuitche et al.[56] for example has also proven its relevance for propeller based applications.

On the negative side, BEMT requires a precise model of the propeller geometry at all radius position of relevance. This would require to be known how the airfoil and twist change across the radius. Crude assumptions of the geometry generate inaccuracies which propagate in the calculations. Logically meaningful results require expensive resources, which could be better employed for different tasks, especially given that modelling of the propeller performance is not the main focus of the research.

The second method presented by Theys et al. is the Vortex Lattice Method (VLM) which is extensively described by Katz and Plotkin [57]. VLM is a numerical method based on boundary elements that can represent both steady and unsteady attached flows. VLM uses theory of potential flow to model lifting surfaces as a series of discrete vortices. Theys et al. conclude that while both BEMT and VLM are consistent with each other in thrust estimations, they both overestimate the propeller performance throughout the considered inclination range. It is further concluded that while both methods correctly predict trends in the propeller performance, accuracy is lost at higher angles of attack. It can then be concluded that both methods are not suitable for the considered research topic due to their complexity and inaccuracy at the analysed crossflow conditions.

Finally the last method presented by Theys et al. is based on conservation of momentum and aims to reduce modelling cost by only needing the diameter of the propeller to perform calculations as described by Glauert [58]. Solving the momentum conservation equations for some data points from test flights or wind tunnel tests allows for the calculation of the propeller efficiency defined as the ratio between induced power and mechanical power. The propeller efficiency can then be used to estimate the required mechanical power in order to generate a desired thrust in a given crossflow condition.

While such method seems to offer a simple solution to the modelling of the motor/propeller performance, it is also true that the use of mechanical power as a control variable is not straightforward. A more straightforward modelling method would rather correlate PWM or RPM to generated thrust so to allow for the drafting of effectiveness profiles of the motors in different airspeed. It is then clear that the

conservation of momentum approach does not serve well to the desired purpose.

Pobikrowska and Grabowski [39] present a simplified method to analyze crossflow effect on propeller performance. This involves the assumption of perfect tangent flow to the blades movement and integration of the lift equation along the radius of the advancing and retreating blade. Again though, such an approach needs knowledge regarding the lift coefficient of the propeller per crosssection along the radius. This information is not readily available from the manufacturer and the resource cost needed to extrapolate it would be high. The use of flight test data to develop an approximation resulted in inaccuracies especially at high wind speeds and RPM.

All the presented modelling techniques result to be either complex and expensive, or oversimplified and inaccurate. Given the purpose application of the model findings, it is deemed that the most straightforward way to model the performance of the motor-propeller combination is to perform wind tunnel tests in increasingly higher crossflow. A polynomial relation between RPM (or PWM), airspeed and thrust is then drafted from the recorded data. In such manner, the effectiveness of the motor-propellers can be easily estimated and implemented in the INDI controller.

6.1.2. Modeling of Moving Rotors

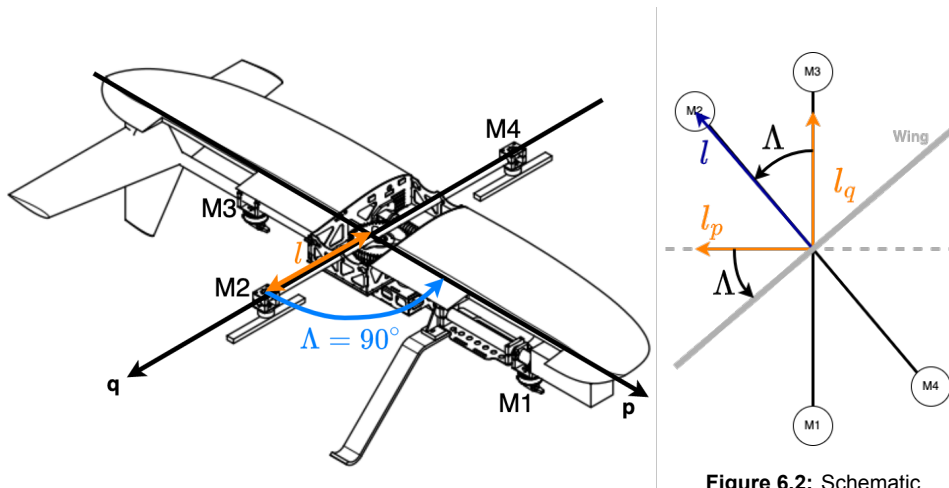


Figure 6.1: Physical depiction of side-motor arm, wing skew angle and motor numbering in VSQP.

Figure 6.2: Schematic representation of change in side-motor control arm due to wing skew.

Section 3.2 has mentioned that during transition as the skew angle increases, the ailerons experience a reduction of the roll arm and an increment in the pitch arm. Therefore, it is mentioned the need for a OFW at high skew angles to use a differential horizontal surface to help the ailerons achieve roll control. In contrast as shown by Figure 6.1 and Figure 6.2, for the side motors as the skew angle increases the roll arm l_p increments while the pitch arm l_q decreases. Therefore, at high skew angles the side motors have a significant effectiveness on the roll axis. It is then clear that during transition the motors experience a change in effectiveness, interchanging between the roll and pitch axis.

Bai and Gururajan [40] argue that a model of a morphing geometry quadcopter can be simply obtained by analyzing the changes in the moving structure. The considered quadcopter has a central hub which allows for the change of the incidence angle of the arms. Bai and Gururajan argue that a simple model of the changed dynamics can be achieved by calculating the inertial tensor as a trigonometric function of the incidence angle in-between the arms. On the other hand, in INDI the inertial matrix is not directly used in the control law, rather its knowledge is embedded in the effectiveness matrix. Therefore, in the case of VSQP the effectiveness values can be scheduled as trigonometric functions of the wing skew angle to achieve a similar result.

Now, assuming that the rotation center is close to the center of gravity, it can be assumed that the change in arm length can be scheduled with the skew angle Λ as shown in Equation 6.1.

$$\begin{aligned} l_p &= \sin(\Lambda) l \\ l_q &= \cos(\Lambda) l \end{aligned} \quad (6.1)$$

The effectiveness of the side motors is directly dependent on the relative moment arm. Therefore, Equation 6.1 can be used to derive an approximation for the change in effectiveness during transition. This is achieved by scheduling the roll effectiveness in hover ($\Lambda = 90^\circ$) and the pitch effectiveness in forward flight ($\Lambda = 0^\circ$) as shown in Equation 6.2.

$$\begin{aligned} G1_p(\Lambda) &= \sin(\Lambda) G1_{p90^\circ} \\ G1_q(\Lambda) &= \cos(\Lambda) G1_{q0^\circ} \end{aligned} \quad (6.2)$$

6.2. Extended Incremental Nonlinear Control Allocation

Section 5.4 has discussed how the control allocation problem for an overactuated drone can be solved through the design of a minimization routine which is solved with the active set method. The weighing matrices used in the cost functions are designed to reflect a desired prioritization in control objective and commanded input. Section 4.6 has introduced the idea of cascaded INDI in which two inversion routines are used to control the considered platform. More precisely, it was introduced the idea of developing an outerloop controller which uses an INDI control law to achieve guidance through the inversion of a "Outerloop Effectiveness Matrix" containing information of the effectiveness on linear acceleration of the control variables. Section 5.3 further discussed that the outerloop effectiveness matrix is depended on the state of the drone and as such it needs to be re-evaluated at every iteration of the control algorithm. It was also mentioned how knowledge of the platform and its transitional dynamics can be used to introduce some simple but powerful assumptions that facilitate the evaluation of the outerloop effectiveness matrix.

On the other hand, it must be realized that VSQP, similarly to a conventional quadplane, is overactuated in both the inner and outerloop. For example, a linear forward acceleration can be achieved by pitching down and using the thrust vector of the lifting motors or by using the pusher motor. The latter though is often preferred because the former could introduce negative lift which could saturate the lifting motors. In contrast, the pusher motor cannot provide negative thrust, meaning that a positive backwards acceleration can only be provided by pitching up the platform. Similarly, during transition, as the airspeed increases, a gradual shift in control allocation from the lifting motors to the wing should occur. This is because VSQP is designed to efficiently sustain its weight in forward flight by exploiting the lift generated by the wing.

Karssies and Wagter [41] propose Extended Incremental Nonlinear Control Allocation (XINCA) as a single solution to the INDI outerloop control needs of quadplanes. XINCA is an extension of the WLS method presented in Section 5.3 also referred to by the authors as Incremental Nonlinear Control Allocation (INCA). The main idea is that the control variables of the outerloop are considered as force generating actuators and instead of performing a simple inversion of the outerloop matrix a complete WLS routine is carried out. This allows for the prioritization of the control objective, control variables and a specification of preferred states also for the outerloop. Figure 6.3 shows that the output of the

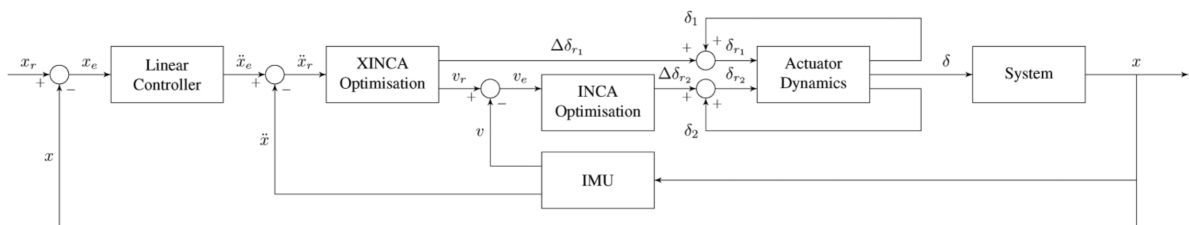


Figure 6.3: A schematic representation of a XINCA controller [41].

XINCA optimization is the required change in command to the pusher prop which is directly sent to the

actuator and the virtual control input to the innerloop. Karssies and Wagter [41] argue that the control variable weighting matrix can be designed to penalize the use of pitch and roll and especially thrust commands compared to using the pusher rotor. This is achieved by assigning lower cost weights to the pusher rotor. In addition, the lower saturation limit of the pusher rotor can be set to 0 to specify the inability of the actuator to provide a positive backwards acceleration.

As for the gradual reduction in the use of lifting motors as the airspeed increases, Karssies and Wagter [41] argue that the pitch angle effectiveness with respect to the vertical axis can be augmented by a term representing the contribution of the wing to lift. Equation 6.3 reports the proposed structure of the augmentation term.

$$\frac{\partial L}{\partial \theta} = -\frac{C_{L\alpha}\rho u^2}{2S} \quad (6.3)$$

where: $C_{L\alpha}$ = Change in lift per change in angle of attack
 ρ = Air density
 u = True airspeed
 S = Wing surface area
 m = Platform's mass

Equation 6.3 highlights a few interesting aspect of the proposed approach. First, the effectiveness of the wing is assumed to increase with the square of airspeed, as expected from basic lift theory. This means that as airspeed increases, the effectiveness of changing θ on vertical accelerations increase, resulting in a cheaper control allocation solution. It can then also be concluded that a similar assumption can be implemented in the modelling of the effectiveness of the aerodynamics surfaces in the innerloop. Secondly, it is assumed that $\alpha \approx \theta$, which holds for small path angles.

It could be argued that the proposed method requires some sort of aerodynamic model of the platform to extrapolate $C_{L\alpha}$ which could result to be resource expensive to perform accurately. On the other hand, Karssies and Wagter [41] argue that, as already discussed in Section 4.7, model inaccuracies are compensated for by the incremental nature of INDI. Therefore, it could also be concluded that an accurate but expensive aerodynamic model is not needed, freeing resources for other tasks.

6.3. Higher Order Reference Model

Section 3.1 has hinted to the possibility of generating a control objective which is a combination of measurements readings and OBM output, hence directly employing knowledge of the plant into the control loop. This methodology is particularly interesting because it could be implemented in the transition of VSQP to use knowledge of the imbalances of an OFW to enhance control performance.

Bhardwaj, Raab, and Holzapfel [42] also propose to incorporate identifiable disturbances state-dependent damping terms in the feed-forward pseudo control derivative. The authors argue that the control law from the extension of INDI [23] which was discussed in Section 5.1.2, could be further augmented to take into consideration known state dependent influence. It is indeed argued that neglecting state variation terms is not valid for systems with higher damping like winged platforms. The general idea of the proposed method, named Higher Order Reference Model, is to use a feedforward term $\dot{\nu}_{ff}$ built with plant knowledge which is one derivative level higher than the relative degree of the system so that it can be used in the extended INDI control law described in Section 5.1.2.

Now consider again the system from Equation 5.5. The control law for this continuous system for a given commanded pseudo control derivative $\dot{\nu}_{cmd}$ can be derived by performing an inversion. In contrast to Section 5.1.2, this derivation shall not neglect the state dependent terms.

$$\begin{aligned} \dot{\nu} &= \mathbf{A} \dot{\mathbf{x}} + \mathbf{B} \dot{\mathbf{u}} \\ \dot{\mathbf{u}}_{cmd} &= \mathbf{B}^{-1} (\dot{\nu}_{cmd} - \mathbf{A} \dot{\mathbf{x}}) \\ \dot{\mathbf{u}}_{cmd} &= \mathbf{B}^{-1} \dot{\nu}_{ff} \end{aligned} \quad (6.4)$$

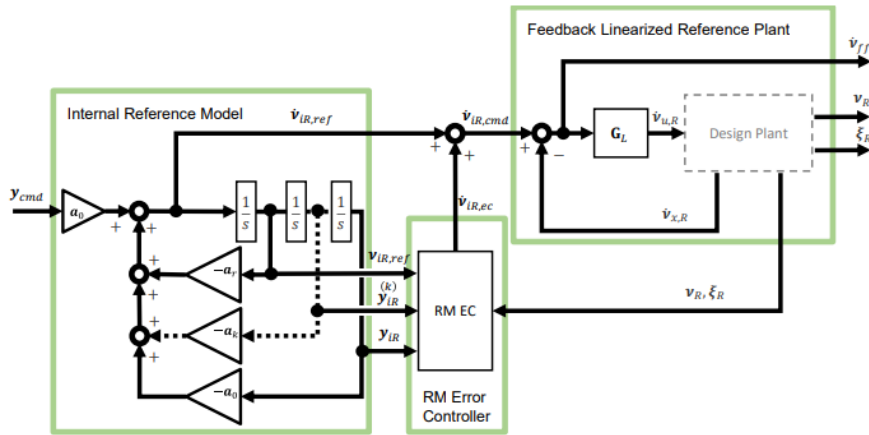


Figure 6.4: Higher Order Reference Model [42].

Equation 6.4 shows that \dot{v}_{ff} can be calculated by subtracting state derivative influence from the commanded signal of the reference model. The state derivative influence can be modeled as the product of a matrix \hat{A} , being the Jacobian of the nonlinear reference system with respect to the reference states, and the derivatives themselves. The closed loop reference dynamics can be obtained by substituting Equation 6.4 back into the system definition of Equation 5.5.

$$\begin{aligned}
 \dot{v} &= A \dot{x} + B \dot{u} \\
 &= A \dot{x} + B B^{-1} (\dot{v}_{cmd} - \hat{A} \dot{x}) \\
 &= \underbrace{A \dot{x}}_{\dot{v}_x} + \underbrace{(B B^{-1} (\dot{v}_{cmd} - \hat{A} \dot{x}))}_{\dot{v}_{ff}}
 \end{aligned} \tag{6.5}$$

This substitution proves that by using a perfect model of the state influence ($\hat{A} = A$), using the feedforward term \dot{v}_{ff} in the control law of Equation 5.9 leads to the perfected tracking of \dot{v}_{cmd} . On the other hand, a model by its nature is a simplification of the real dynamics, hence $\hat{A} \simeq A$ introducing some inaccuracies in the estimation of the state induced influence. Therefore, as shown by Figure 6.4, an Error Controller is added internally in the Reference Model to compensate for deviation of the reference states outputted by the Feedback Linearized Reference Plant from the ones generated by the Internal Reference Model¹.

Now, the use of an Higher Order Reference Model or the idea of a Hybrid INDI as presented in Section 3.1, could represent an interesting solution to the problem of transition of OFW, for which some state induced imbalances are predicted to challenge the control of the drone. Therefore, investigating further these ideas and extending them where needed could lead to meaningful results.

On the other hand, it could be argued that the whole point of using INDI over NDI is that developing a precise model of the slow state induced effect on the controlled variables can be a complex task given the limited accuracy sensors available to the a MAV. Even though the presented Higher Order Reference Model has an internal Error Controller, it could be argued that stability of the whole system could be hindered as a result of the introduced model inaccuracies.

Bhardwaj, Raab, and Holzapfel [42] argue that simulation of the presented method proves that the use of model knowledge in the higher order reference model brings the advantage of reducing the feedback control effort even in case of high uncertainties in the design plant model, without introducing any instabilities in the closed loop system. Surely it could be argued that these conclusions are the product of a simulation and not a real life flight test. Nevertheless the proposed method still is a promising candidate to solve the control problem of transition of VSQP.

¹Please note that in Figure 6.4 some signals have subscript "iR" which is dropped for simplicity in the presented explanation.

Research Plan for Thesis Project

The aim of this section is to identify the knowledge gap in the literature which prevents the straightforward implementation of a INDI controller in the VSQP. The identified knowledge gaps are used to produce research questions which can help steer the research process to achieve the final objective. Finally, a Gantt chart is used to subdivide the available time-budget in different work packages.

7.1. Knowledge Gap

The presented review of the literature has revealed a continuous effort in the scientific community to improve upon the challenges experienced by both OFW based designs as well as by INDI controlled platforms. On the other hand, a number of knowledge gaps prevent the straightforward use of an INDI controller on VSQP.

The main knowledge gap that arises from the literature study is the nonexistence of a INDI controller which can control in a continuous and optimal manner a hybrid drone which suffers from OFW induced moment imbalances alike VSQP. More precisely, there has yet to be defined a way to efficiently model the dynamics of a OFW using only the limited resources available to a small research UAV such as VSQP.

Moreover, there has not yet been documented and verified with real test flights a robust way to implement this knowledge in an extension of an INDI controller to improve performance. There is the need to research how to use the described trimming solutions of an OFW to generate a set of control objectives which provide desirable flying qualities.

Finally, VSQP adds an additional variable to be controlled, being the skew angle of the wing. Therefore, there is the need for a novel controller which uses knowledge of the mutating actuators effectiveness in transition to command optimal skew angles to meet the control objectives. The controller cannot simply decouple wing and quad motors control but has to holistically evaluate the effect of skew angle on both.

7.2. Research Objective

The research objective represents the main goal of the research activity. A detailed definition of the research goal can help in the scheduling of work packages. The main research objective of this thesis is:

“To achieve stable controlled flight of the novel hybrid Variable Skew Quad-Plane Drone by means of INDI stabilization and guidance based on parameters estimation from data driven modelling”.

The research objective together with the knowledge gap can be used to redact scientific research questions which will be addressed during the thesis project.

7.3. Research Questions

In order to provide proper steering of the research process and proof of fulfillment of the research objective, a set of research questions and sub-question has been developed to address the identified knowledge gaps.

Q1 How can knowledge from the induced imbalances of the OFW be used to enhance the performance of the INDI controller?

Q1.1 How can the imbalances of the OFW be corrected for using the actuators available to the platform?

Q1.2 How can the desired flying dynamics of VSQP be modeled using data available to the autopilot?

Q2 How can knowledge from the mutating effectiveness of the actuators and states be used to design an INDI controller which is able to control the skew angle?

Q2.1 How can the effectiveness of the actuators and state be modeled with respect to the skew angle?

Q2.2 What defines optimal control in the specific case of VSQP?

Q2.3 How can optimal control be related to the platform state and skew angle?

7.4. Research Strategy

During the research process three main test environments will be used : Simulation, Controlled Environments for Verification and Outdoor testing for Validation.

As for simulation, scripts will be run in two environments: Paparazzi UAV [59] and Matlab-Simulink. Paparazzi UAV is an autopilot software platform which is used to implement the developed control strategies in C and C++, which can then be flashed directly onto the drone. Paparazzi is also used to run simulations of the response of the chosen drone to the stabilization and guidance scripts. Paparazzi UAV is chosen over other counterparts due the fact that it is open-source, and so easily modifiable, and due to the extensive contribution and experience of the MavLab in its development. Unfortunately, the ease of use of the simulations comes at the price of lower accuracy, which can generate a reality gap that has to be accounted for in real flight tests.

Matlab-Simulink is instead used to build a model of the drone and perform analysis on the control performance. Furthermore, Matlab is used to implement the least squares estimations of the effectiveness values. Matlab-Simulink is chosen over other counter-parts due to the extensive engineering extension packs and functions, as for example the signal processing toolbox, which allows the user to focus on the implementation rather than the development in code of basic theories. On the other hand, the Matlab-Simulink experience is limited to offline applications due to the hungry computational requirements thus excluding real time applications on processing limited platforms such as drone autopilots.

Verification is conducted in two controlled environments: Cyberzoo and Open Jet Wind Tunnel at the Faculty of Aerospace Engineering of TuDelft. The Cyberzoo is a drone cage which allows for the testing of contained procedures. These are for example gain tuning or excitation maneuvers. Forward flight is not possible due to the contained footprint. Advantages of the Cyberzoo are the extensive availability, safe environment, Optitrack near perfect state estimation and safety rope system. On the other hand, GPS signals cannot be properly used due to the shielding of the surrounding metal structure, leading to a reality gap that has to be accounted for in real test flights.

The Open Jet Facility has a large cross sectional area and is used to test the drone in linear airflow and estimate effectiveness values at different airspeed. Alike the Cyberzoo, the OJF uses Optitrack for state estimation and has a safety rope system. On the negative side the OJF requires to be booked well in advance and needs some training to be operated safely.

Finally, validation is performed at the drone testing facility of Valkenburgh. The facility consists of open wide fields which are dedicated to testing of new drone platforms providing all the necessary freedom of movement required by the full flight envelope. The test flight set up usually requires a safety pilot with a transmitter and a ground station operator that instructs the autopilot through the Ground Station Interface on Paparazzi UAV.

7.5. Gantt Chart

The research plan described is aimed to the initiation of a master thesis at the faculty of Aerospace Engineering of TuDelft. Therefore, the structure the project abides the well defined MSc academic level standards.

- **Problem** The definition of the problem to be addressed by the novel research.
- **Literature Review** Academic literature and frameworks are used to identify the specific knowledge gap to be addressed.
- **Model/Test** The insights from the literature review are used to develop a model and/or tests procedure aimed to research the defined knowledge gap.
- **Verification and Validation** The novel technology is applied to industry standards to check the correctness and is applied to the initial problem to check if it offers a viable solution.
- **Iteration and recommendations** Where necessary, the technology is adjusted and re-tested. Recommendations are provided to help peers reproduce and improve on the contents of the research.

The end result of the research is an extension of the body of knowledge which is well validated and replicable. The time budget for the master thesis is 9 months, of which 2 are dedicated to the literature review process. The remaining time is dedicated to the development of the novel technology as well as its verification and validation. The research process can be considered terminated when the knowledge gap has been fully addressed, therefore contributing to the general body of science.

The detailed schedule of the planned activities is presented in a Gantt chart Figure 7.1.

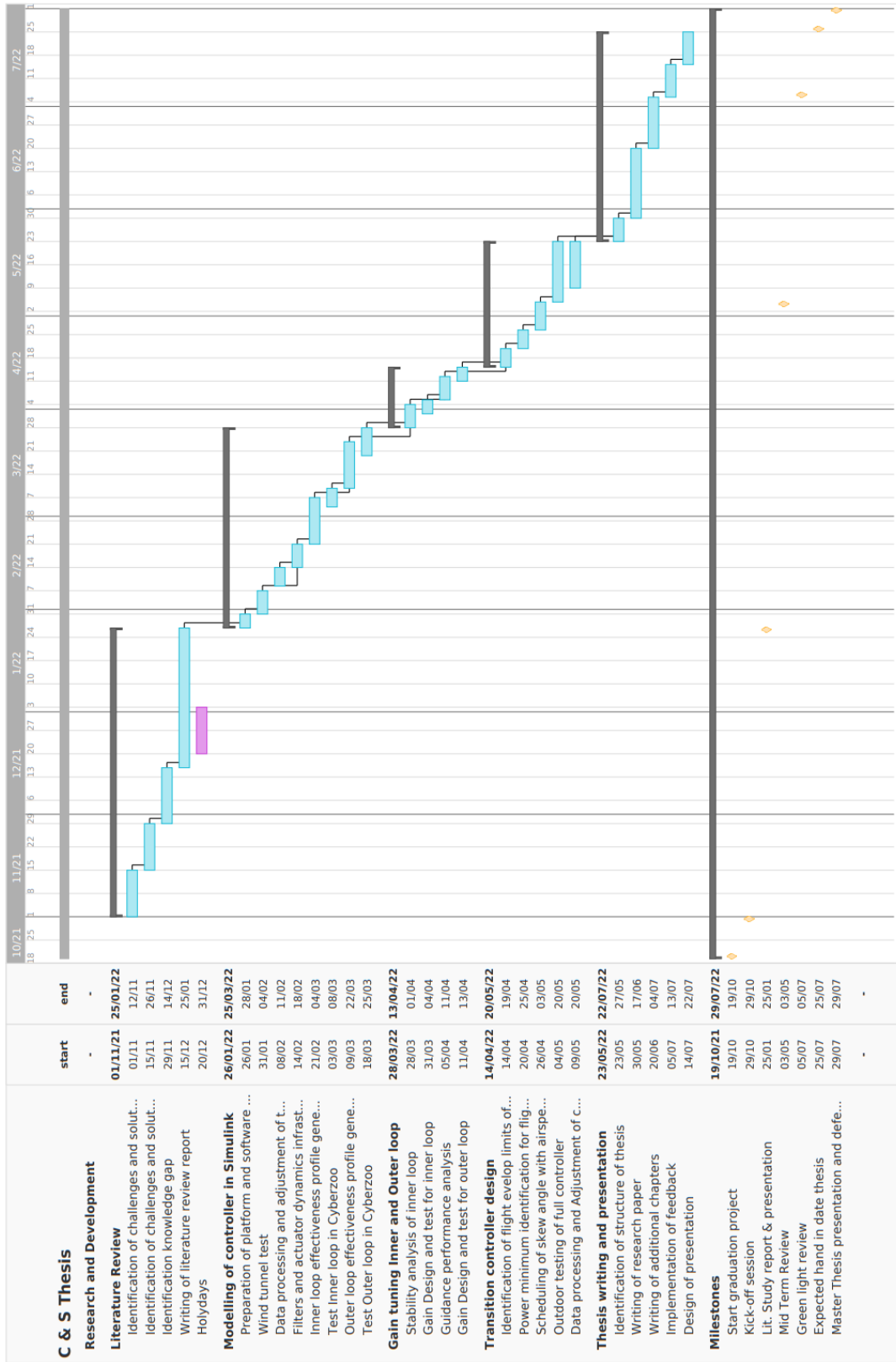
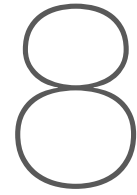


Figure 7.1: Time budget distribution in Gantt chart.



Conclusion

This report presented the Literature Review Study for the thesis topic "Incremental Nonlinear Dynamic Inversion Controller for Variable Skew Quad Plane". VSQP is a novel design which in vertical flight resembles a quad-rotor, in forward flight a fixed wing and in transition it deploys the wing similarly to a OFW.

The main challenge of a OFW is identified to be the complex control due to the numerous couplings in the Inertia matrix as well as in the aerodynamics. Performing a combination of sideslip and banking maneuvers as well as deploying ailerons and elevators in a coordinated way can offer limited control of the OFW. Decoupling of lateral and longitudinal motion is complex and conventional aerodynamic models result inaccurate and expensive to develop. Therefore, there is the need for a control scheme which is not heavily dependent on accurate models of the platform and which can deal with the nonlinearity of the couplings.

INDI has contained model dependency, applicability to nonlinear cases and increased robustness through the use of sensor based measurements feedback. Reference models in combination to error controllers are used to generate pseudo control inputs to the INDI controller. Alternatively, cascaded INDI can be used to decouple guidance and stabilization control. Finally the Literature highlights the better disturbance rejection capabilities of INDI compared to classical control methods such as PID.

Actuator dynamics cause delay and attenuate the response of control elements to the commanded input. Therefore, it is concluded that Pseudo Control Hedging can be used to prevent INDI from adapting incrementally to the slow actuator dynamics. Furthermore, by extending the basic control law of INDI to artificially incorporate the "speed" of the actuators in the effectiveness matrix it is possible to prioritize fast control elements. Time delay due to noise filtering and sensor dynamics can hinder control performance. Synchronization filtering together with an on-board model extension of INDI can be used to mitigate for unexpected measurements delays. Control allocation for over-actuated drones can be solved by solving a Weighted Least Squares sequential problem which aims to achieve the control objective at the least power consumption. Weighting matrices are used to prioritize control objective and control inputs while deviations from the preferred states are penalized. As for effectiveness profiling, Doublets are used to reveal the control elements dynamics due to the high frequency and contained deviation from equilibrium while Chirps are used for the slower state induced dynamics due to the large range of swept frequencies.

It is further concluded that changes in effectiveness play a key role in the transition of VSQP. The literature highlights that an increase in motor effectiveness is expected with higher speed cross-flows. Wind-tunnel tests to draw a numerical relation between thrust, RPM and cross-flow airspeed have to be performed because the modelling methods in the Literature result to be either complex and expensive, or oversimplified and inaccurate. Changes in effectiveness due to the moving side arms of VSQP are concluded to be modeled as a trigonometric function of the skew angle. Extended Incremental Nonlinear Control Allocation is used to provide pusher prop control and gradual switch from the quad-

motors to wing lift generation. Finally, knowledge of state dynamics can be implemented in a Higher Order Reference Model which is proved in simulation to reduce the control effort even in case of high uncertainties in the design plant model.

In a nutshell, the presented Literature Review Study has addressed the Research Objective by analyzing the benefits, challenges and solutions of both OFW and INDI. A particular focus was centered around what solutions have been documented regarding the use of INDI in the transition of compound-lift, overactuated hybrid drones. Research questions have been drafted to steer the research process to address the knowledge gaps and define the next steps of the thesis project. The research objective of the thesis project is to develop an INDI controller which can stabilize and guide VSQP in all configurations. In this optic, the research will focus on how to augment current INDI solutions to use knowledge from the induced imbalance of OFW and mutating effectiveness of actuators and states. The research will in particular focus on the extension of the actuator allocation methods so to include the wing skew angle as a control variable.

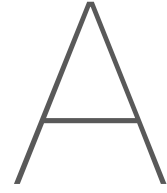
References

- [1] Shuyang Wang, Jing Zhang, and Lingyu Yang. "Wind Disturbance Rejection Control Law Based on AESO for a Hybrid Tail-Sitter UAV". In: *2020 39th Chinese Control Conference (CCC)*. IEEE, July 2020. DOI: [10.23919/ccc50068.2020.9189580](https://doi.org/10.23919/ccc50068.2020.9189580).
- [2] Victor Maldonado, Prithviraj Sarker, and Souma Chowdhury. *A Modular Design Approach to A Reconfigurable Unmanned Aerial Vehicle*. 2017. DOI: [10.2514/6.2017-0224](https://doi.org/10.2514/6.2017-0224).
- [3] W.P. Nelms. *Applications of Oblique-Wing Technology - An overview*. Aircraft Systems and technology Meeting. Sept. 1976.
- [4] I. Kroo. *The aerodynamic design of oblique wing aircraft*. AIAA Aircraft Systems, Design and Technology Meeting. Oct. 1986. DOI: [10.2514/6.1986-2624](https://doi.org/10.2514/6.1986-2624).
- [5] Dr. R.K. Nangia. *Meeting Unmanned Air Vehicle Platform Challenges Using Oblique Wing Aircraft*. Defense Technical Information Center. Nov. 2007.
- [6] Lixin Wang, Zijian Xu, and Ting Yue. "Dynamic characteristics analysis and flight control design for oblique wing aircraft". In: *Chinese Journal of Aeronautics* 29.6 (Dec. 2016), pp. 1664–1672. DOI: [10.1016/j.cja.2016.10.010](https://doi.org/10.1016/j.cja.2016.10.010).
- [7] Ting Yue et al. "Sliding mode control design for oblique wing aircraft in wing skewing process". In: *Chinese Journal of Aeronautics* 32 (2019), pp. 263–271. ISSN: 1000-9361. DOI: [10.1016/j.cja.2018.11.002](https://doi.org/10.1016/j.cja.2018.11.002).
- [8] T Mcmurtry, A Sim, and W Andrews. "AD-1 oblique wing aircraft program". In: *1st Flight Test Conference*. 1981.
- [9] R. Maine. *Maximum likelihood estimation of aerodynamic derivatives for an oblique wing aircraft from flight data*. Guidance and Control Conference. Aug. 1977. DOI: [10.2514/6.1977-1135](https://doi.org/10.2514/6.1977-1135).
- [10] E. J. J. Smeur, Q. Chu, and G. C. H. E. de Croon. "Adaptive Incremental Nonlinear Dynamic Inversion for Attitude Control of Micro Air Vehicles". In: *Journal of Guidance, Control and Dynamics* 39 (2016), pp. 450–461. ISSN: 1533-3884. DOI: [10.2514/1.g001490](https://doi.org/10.2514/1.g001490).
- [11] Jie Pang, Rong Mei, and Mou Chen. *Modeling and control for near-space vehicles with oblique wing*. 10th World Congress on Intelligent Control and Automation. 2012. DOI: [10.1109/wcica.2012.6358164](https://doi.org/10.1109/wcica.2012.6358164).
- [12] R. R. da Costa, Q. P. Chu, and J. A. Mulder. "Reentry Flight Controller Design Using Nonlinear Dynamic Inversion". In: *Journal of Spacecraft and Rockets* 40.1 (Jan. 2003), pp. 64–71. DOI: [10.2514/2.3916](https://doi.org/10.2514/2.3916).
- [13] Barton Bacon and Aaron Ostroff. "Reconfigurable flight control using nonlinear dynamic inversion with a special accelerometer implementation". In: *AIAA Guidance, Navigation, and Control Conference and Exhibit*. American Institute of Aeronautics and Astronautics, Aug. 2000. DOI: [10.2514/6.2000-4565](https://doi.org/10.2514/6.2000-4565).
- [14] Pranav Bhardwaj et al. "Integrated Reference Model for a Tilt-rotor Vertical Take-off and Landing Transition UAV". In: *2018 Applied Aerodynamics Conference*. American Institute of Aeronautics and Astronautics, June 2018. DOI: [10.2514/6.2018-3479](https://doi.org/10.2514/6.2018-3479).
- [15] Stefan A. Raab et al. "Proposal of a Unified Control Strategy for Vertical Take-off and Landing Transition Aircraft Configurations". In: *2018 Applied Aerodynamics Conference*. American Institute of Aeronautics and Astronautics, June 2018. DOI: [10.2514/6.2018-3478](https://doi.org/10.2514/6.2018-3478).
- [16] E.J.J. Smeur, G.C.H.E. de Croon, and Q. Chu. "Cascaded incremental nonlinear dynamic inversion for MAV disturbance rejection". In: *Control Engineering Practice* 73 (Apr. 2018), pp. 79–90. DOI: [10.1016/j.conengprac.2018.01.003](https://doi.org/10.1016/j.conengprac.2018.01.003).

- [17] E.J.J. Smeur, G.C.H.E. de Croon, and Q. Chu. *Gust disturbance alleviation with Incremental Nonlinear Dynamic Inversion*. 2016 IEEE/RSJ International Conference on Intelligent Robots and Systems (IROS). 2016. DOI: [10.1109/iros.2016.7759827](https://doi.org/10.1109/iros.2016.7759827).
- [18] Ole Pfeifle and Walter Fichter. "Cascaded Incremental Nonlinear Dynamic Inversion for Three-Dimensional Spline-Tracking with Wind Compensation". In: *Journal of Guidance, Control, and Dynamics* 44.8 (Aug. 2021), pp. 1559–1571. DOI: [10.2514/1.g005785](https://doi.org/10.2514/1.g005785).
- [19] Pengzhi Tian et al. "UAV Flight Test Evaluation of Fusion Algorithms for Estimation of Angle of Attack and Sideslip Angle". In: *AIAA Guidance, Navigation, and Control Conference*. American Institute of Aeronautics and Astronautics, Jan. 2016. DOI: [10.2514/6.2016-0645](https://doi.org/10.2514/6.2016-0645).
- [20] S. Sieberling, Q. P. Chu, and J. A. Mulder. "Robust Flight Control Using Incremental Nonlinear Dynamic Inversion and Angular Acceleration Prediction". In: *Journal of Guidance, Control, and Dynamics* 33.6 (Nov. 2010), pp. 1732–1742. DOI: [10.2514/1.49978](https://doi.org/10.2514/1.49978).
- [21] Xiang Li et al. "A Method to Compensate Interaction between Actuator Dynamics and Control Allocator under Incremental Nonlinear Dynamic Inversion Controller". In: *IOP Conference Series: Materials Science and Engineering* 428 (Oct. 2018), p. 012048. DOI: [10.1088/1757-899x/428/1/012048](https://doi.org/10.1088/1757-899x/428/1/012048).
- [22] Eric Johnson and Suresh Kannan. "Adaptive Flight Control for an Autonomous Unmanned Helicopter". In: *AIAA Guidance, Navigation, and Control Conference and Exhibit*. American Institute of Aeronautics and Astronautics, June 2002. DOI: [10.2514/6.2002-4439](https://doi.org/10.2514/6.2002-4439).
- [23] Stefan A. Raab et al. "Consideration of Control Effector Dynamics and Saturations in an Extended INDI Approach". In: *AIAA Aviation 2019 Forum*. American Institute of Aeronautics and Astronautics, June 2019. DOI: [10.2514/6.2019-3267](https://doi.org/10.2514/6.2019-3267).
- [24] E. J. J. Smeur, M. Bronz, and G. C. H. E. de Croon. "Incremental Control and Guidance of Hybrid Aircraft Applied to a Tailsitter Unmanned Air Vehicle". In: *Journal of Guidance, Control, and Dynamics* 43.2 (Feb. 2020), pp. 274–287. DOI: [10.2514/1.g004520](https://doi.org/10.2514/1.g004520).
- [25] Zexin WANG et al. "Onboard actuator model-based Incremental Nonlinear Dynamic Inversion for quadrotor attitude control: Method and application". In: *Chinese Journal of Aeronautics* 34.11 (Nov. 2021), pp. 216–227. DOI: [10.1016/j.cja.2021.03.018](https://doi.org/10.1016/j.cja.2021.03.018).
- [26] Yagiz Kumtepe, Tijmen Pollack, and Erik-Jan Van Kampen. "Flight Control Law Design using Hybrid Incremental Nonlinear Dynamic Inversion". In: *AIAA SCITECH 2022 Forum*. American Institute of Aeronautics and Astronautics, Jan. 2022. DOI: [10.2514/6.2022-1597](https://doi.org/10.2514/6.2022-1597).
- [27] Chong-Sup Kim et al. "Stability Margin and Structural Coupling Analysis of a Hybrid INDI Control for the Fighter Aircraft". In: *International Journal of Aeronautical and Space Sciences* 22.5 (July 2021), pp. 1154–1169. DOI: [10.1007/s42405-021-00394-8](https://doi.org/10.1007/s42405-021-00394-8).
- [28] Chang-ho Ji, Chong-sup Kim, and Byoung-Soo Kim. "A Hybrid Incremental Nonlinear Dynamic Inversion Control for Improving Flying Qualities of Asymmetric Store Configuration Aircraft". In: *Aerospace* 8.5 (May 2021), p. 126. DOI: [10.3390/aerospace8050126](https://doi.org/10.3390/aerospace8050126).
- [29] D.C. van Wijngaarden, E.J.J. Smeur, and B.W.D. Remes. "Flight Code Convergence: Fixedwing, Rotorcraft, Hybrid". In: *IMAV 2021* (2021).
- [30] E. J. J. Smeur, D. Höppener, and C. de Wagter. "Prioritized Control Allocation for Quadrotors Subject to Saturation". In: *International Micro Air Vehicle Conference and Flight Competition 2017* (2017), (pp. 37–43). URL: http://www.imavs.org/papers/2017/51_imav2017_proceedings.pdf.
- [31] E. J. J. Smeur et al. "Modelling of a Hybrid UAV Using Test Flight Data". In: *IMAV2014* (2014).
- [32] Ohad Gur and Aviv Rosen. "Optimizing Electric Propulsion Systems for Unmanned Aerial Vehicles". In: *Journal of Aircraft* 46 (2009), pp. 1340–1353. ISSN: 0021-8669. DOI: [10.2514/1.41027](https://doi.org/10.2514/1.41027).
- [33] Pierre-Jean Bristeau et al. *The role of propeller aerodynamics in the model of a quadrotor UAV*. 2009 European Control Conference (ECC). pp. 683-688. 2009. DOI: [10.23919/ecc.2009.7074482](https://doi.org/10.23919/ecc.2009.7074482).
- [34] P.B.S. Lissaman. "Low-Reynolds-Number Airfoils". In: *Ann. Rev. Fluid Mech.* 15.1 (1983), pp. 223–239. DOI: <https://doi.org/10.1146/annurev.fl.15.010183.001255>.

- [35] Herbert S. Ribner. *Propellers in yaw*. Wartime report L-219. Originally issued December 1943 as Advance restricted report 3L09. Washington, DC: National Advisory Committee for Aeronautics, 1943. 60 S., [12] Bl.
- [36] B. Theys et al. *Wind tunnel testing of a VTOL MAV propeller in tilted operating mode*. 2014 International Conference on Unmanned Aircraft Systems (ICUAS). pp.1064-1072. 2014. DOI: [10.1109/icuas.2014.6842358](https://doi.org/10.1109/icuas.2014.6842358).
- [37] Carl Russel et al. *Wind Tunnel and Hover Performance Test Results for Multicopters cUAS Vehicles*. AHS 72nd Annual Forum. May 2016.
- [38] B. Theys et al. "Experimental and Numerical Study of Micro-Aerial-Vehicle Propeller Performance in Oblique Flow". In: *Journal of aircraft* 54.3 (May 2017), pp. 1076–1084. ISSN: 0021-8669. DOI: [10.2514/1.c033618](https://doi.org/10.2514/1.c033618).
- [39] Katarzyna Pobikrowska and Tomasz Goetzendorf-Grabowski. *Wind tunnel tests of hovering propellers in the transition state of Quad-Plane*. Buletin of the Polish Academy of Sciences. 2021. DOI: [10.24425/BPASTS.2021.138821](https://doi.org/10.24425/BPASTS.2021.138821).
- [40] Ye Bai and Srikanth Gururajan. "Evaluation of a Baseline Controller for Autonomous "Figure-8" Flights of a Morphing Geometry Quadcopter: Flight Performance". In: *Drones* 3.3 (Aug. 2019), p. 70. DOI: [10.3390/drones3030070](https://doi.org/10.3390/drones3030070).
- [41] H.J. Karssies and C. De Wagter. "Extended incremental non-linear control allocation (XINCA) for quadplanes". In: *International Journal of Micro Air Vehicles* 14 (Jan. 2022), p. 175682932110708. DOI: [10.1177/17568293211070825](https://doi.org/10.1177/17568293211070825).
- [42] Pranav Bhardwaj, Stefan A. Raab, and Florian Holzapfel. "Higher Order Reference Model for Continuous Dynamic Inversion Control". In: *AIAA Scitech 2021 Forum*. American Institute of Aeronautics and Astronautics, Jan. 2021. DOI: [10.2514/6.2021-1130](https://doi.org/10.2514/6.2021-1130).
- [43] A. R. Seebass. *Oblique Flying Wing Studies*. Sobieczky H. (eds) New Design Concepts for High Speed Air Transport. International Centre for Mechanical Sciences (Courses and Lectures). 1997. DOI: [10.1007/978-3-7091-2658-5_20](https://doi.org/10.1007/978-3-7091-2658-5_20).
- [44] Alex Ramirez Serrano. "Design methodology for hybrid (VTOL + Fixed Wing) unmanned aerial vehicles". In: *Aeronautics and Aerospace Open Access Journal* 2 (June 2018). ISSN: 2576-4500. DOI: [10.15406/aaobj.2018.02.00047](https://doi.org/10.15406/aaobj.2018.02.00047).
- [45] Adnan S. Saeed et al. "A survey of hybrid Unmanned Aerial Vehicles". In: *Progress in Aerospace Sciences* 98 (Apr. 2018), pp. 91–105. DOI: [10.1016/j.paerosci.2018.03.007](https://doi.org/10.1016/j.paerosci.2018.03.007). URL: <https://ui.adsabs.harvard.edu/abs/2018PrAeS..98...91S>.
- [46] P. Simplício et al. "An acceleration measurements-based approach for helicopter nonlinear flight control using Incremental Nonlinear Dynamic Inversion". In: *Control Engineering Practice* 21 (2013), pp. 1065–1077. ISSN: 0967-0661. DOI: [10.1016/j.conengprac.2013.03.009](https://doi.org/10.1016/j.conengprac.2013.03.009).
- [47] Michael W. Oppenheimer and David B. Doman. "Methods for Compensating for Control Allocator and Actuator Interactions". In: *Journal of Guidance, Control, and Dynamics* 27.5 (Sept. 2004), pp. 922–927. DOI: [10.2514/1.7004](https://doi.org/10.2514/1.7004).
- [48] David Serrano et al. "Effect of disk angle-of-attack on aerodynamic performance of small propellers". In: *Aerospace Science and Technology* 92 (2019), pp. 901–914. ISSN: 1270-9638. DOI: [10.1016/j.ast.2019.07.022](https://doi.org/10.1016/j.ast.2019.07.022).
- [49] John Brandt and Michael Selig. "Propeller Performance Data at Low Reynolds Numbers". In: *49th AIAA Aerospace Sciences Meeting including the New Horizons Forum and Aerospace Exposition*. American Institute of Aeronautics and Astronautics, Jan. 2011. DOI: [10.2514/6.2011-1255](https://doi.org/10.2514/6.2011-1255).
- [50] Roberto Fabela et al. *Experimental characterization of a small and micro unmanned aerial vehicle propulsion systems*. AIAA Atmospheric Flight Mechanics Conference. Jan. 2016. DOI: [10.2514/6.2016-1530](https://doi.org/10.2514/6.2016-1530).
- [51] M. Raju Hossain and Nicholas Krouglicof. *Propeller dynamometer for small Unmanned Aerial Vehicle*. CCECE 2010. 2010. DOI: [10.1109/ccece.2010.5575152](https://doi.org/10.1109/ccece.2010.5575152).

- [52] Kenneth M. Asson and Patrick F. Dunn. "Compact dynamometer system that can accurately determine propeller performance". In: *Journal of Aircraft* 29 (Jan. 1992), pp. 8–9. ISSN: 0021-8669. DOI: [10.2514/3.46118](https://doi.org/10.2514/3.46118).
- [53] Robert W. Deters, Gavin Kumar Ananda Krishnan, and Michael S. Selig. "Reynolds Number Effects on the Performance of Small-Scale Propellers". In: *32nd AIAA Applied Aerodynamics Conference*. American Institute of Aeronautics and Astronautics, June 2014. DOI: [10.2514/6.2014-2151](https://doi.org/10.2514/6.2014-2151).
- [54] Michael Ol, Cale Zeune, and Michael Logan. "Analytical/Experimental Comparison for Small Electric Unmanned Air Vehicle Propellers". In: *26th AIAA Applied Aerodynamics Conference*. American Institute of Aeronautics and Astronautics, June 2008. DOI: [10.2514/6.2008-7345](https://doi.org/10.2514/6.2008-7345).
- [55] Mohsen Rostami and Amir hamzeh Farajollahi. "Aerodynamic performance of mutual interaction tandem propellers with ducted UAV". In: *Aerospace Science and Technology* 108 (2021), p. 106399. ISSN: 1270-9638. DOI: [10.1016/j.ast.2020.106399](https://doi.org/10.1016/j.ast.2020.106399).
- [56] Maxime Alex Junior Kuitche et al. "Blade element momentum new methodology and wind tunnel test performance evaluation for the UAS-S45 Balaam propeller". In: *CEAS Aeronautical Journal* 11 (2020), pp. 937–953. ISSN: 1869-5582. DOI: [10.1007/s13272-020-00462-x](https://doi.org/10.1007/s13272-020-00462-x).
- [57] Joseph Katz and Allen Plotkin. *Low-Speed Aerodynamics*. Cambridge University Press, 2001. DOI: [10.1017/cbo9780511810329](https://doi.org/10.1017/cbo9780511810329).
- [58] H. Glauert. *Airplane Propellers*. Springer Berlin Heidelberg, 1935, pp. 169–360. DOI: [10.1007/978-3-642-91487-4_3](https://doi.org/10.1007/978-3-642-91487-4_3).
- [59] Gautier Hattenberger, Bronz Murat, and Gorraz Michel. *Using the Paparazzi Uav System for Scientific Research*. International micro air vehicle conference and competition. 2014.



Attributes and components of VSQP

Table A.1: Physical characteristics of VSOWQP.

Attribute	Value	Unit
Mass (to be verified)	3.00	kg
C.G. longitudinal position from nose	518	mm

Table A.2: Moments of inertia kg m^2 at different skew angles of VSOWQP.

Attribute	$\Lambda = 90^\circ$	$\Lambda = 45^\circ$	$\Lambda = 0^\circ$
I_{xx}	2.049e-2	2.394e-2	2.862e-2
I_{xy}	2.593e-4	4.258e-3	1.113e-4
I_{yx}	2.593e-4	4.258e-3	1.113e-4
I_{yy}	2.065e-1	2.028e-1	1.979e-1
I_{xz}	8.238e-3	8.079e-3	7.977e-3
I_{yz}	-2.422e-4	-2.005e-4	-2.7692e-5
I_{zx}	8.238e-3	8.079e-3	7.977e-3
I_{zy}	-2.422e-4	-2.005e-4	-2.7692e-5
I_{zz}	2.164e-1	2.161e-1	2.158e-1

Table A.3: Components of VSOWQP.

Component	Model	Number of Units
Lifting motors	T-motor MN3510-25	4
Pusher motor	Brother hobby 2812 900kv	1
Aerodynamic surfaces servos	MG90s	4
Autopilot	Pixhawk 4	1
GPS	HolyBro Pixhawk 4	1
Powerboard	Holybro Pixhawk 4 Power Module (PM07)	1
ESC	f35A blheli ESC	5
Receiver	TBS crossfire micro receiver	1
Lifting propellers	T-motor 13" folding propellers	4
Pusher propeller	APC 8x6	1
Central Pivot Servo	Savox HV servo	1
Pitot tube	MS45XX	1
Batteries	Turnigy 8000 mAh 4S	2

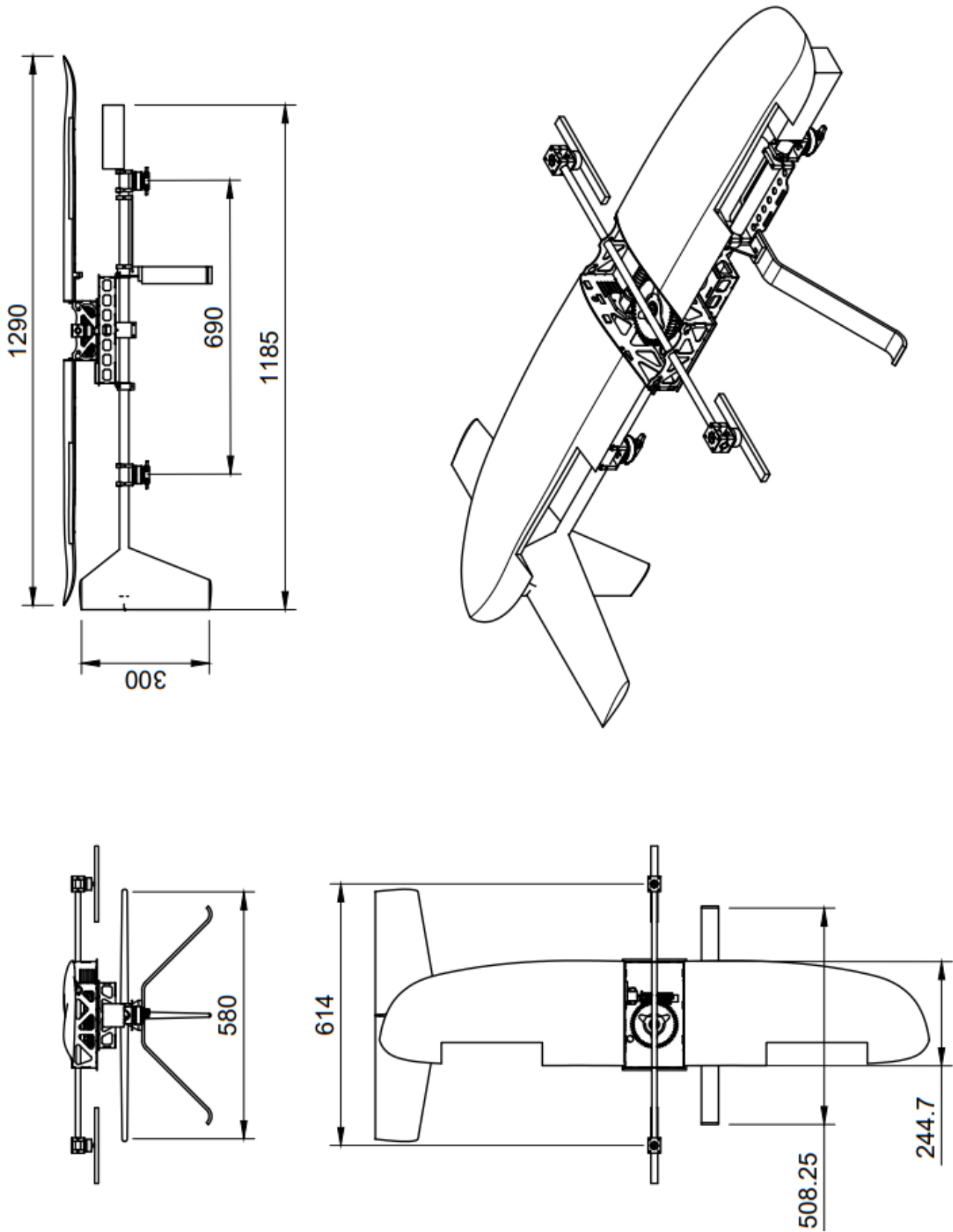


Figure A.1: Technical drawing of VSOWQP, dimensions in mm.